

UNIVERSITEIT ANTWERPEN

Faculteit Wetenschappen

Departement Scheikunde

Modelling of methane, acetylene and silane plasmas:
study of the plasma chemistry

Modelleren van methaan, acetyleen en silaan plasma's:
studie van de plasma chemie

Proefschrift voorgelegd tot het behalen van de graad van doctor
in de Wetenschappen aan de Universiteit Antwerpen,
te verdedigen door

Dieter Herrebout

Promotor: Prof. Dr. R. Gijbels UA

Co-Promotor: Prof. Dr. A. Bogaerts UA

Co-Promotor: Dr. A. Vanhulsel VITO

Antwerpen

2003

*So.. Finally,...we meet **again** Mister Woudloper!*

Dankwoord

Met het voltooien van het doctoraatswerk, zou ik nu even volgende mensen willen bedanken die me de voorbije jaren geholpen en gesteund hebben.

In eerste instantie wil ik mijn ouders bedanken. Zij hebben mij de kans geboden om dit eindwerk aan te vatten. Op elk moment stonden ze klaar en toonden ze interesse in het onderzoek waar ik mee bezig was. Ook van mijn broer heb ik veel hulp gehad de voorbije jaren.

Mijn promotoren Prof. R Gijbels en Prof. A. Bogaerts wil ik bedanken voor de steun die ik heb mogen ontvangen tijdens het doctoraat, de vele discussies, het naleeswerk...

Ook mijn co-promotor Annick Vanhulsel en Eric Dekempeneer van VITO wens ik te bedanken voor de samenwerking, de discussies, de suggesties... En uiteraard ook VITO zelf voor de financiële ondersteuning van het onderzoek.

Verder wens ik ook Wim Goedheer te bedanken voor de hulp die ik heb ontvangen tijdens mijn doctoraat. Telkens ik van Nieuwegein terugkwam had ik een hele reeks nieuwe ideeën om uit te proberen. Gert-Jan Nienhuis, die me in den beginne goed heeft geholpen met het vloeistof modelleerwerk. Bedankt daarvoor!!

Min Yan wens ik ook uitdrukkelijk te bedanken voor de hulp bij de aanvang van het doctoraat, onder meer voor het aanpassen van het Monte Carlo model en de koppeling van het vloeistof met het Monte Carlo model.

Voorts wil ik mijn collega's op den bureau bedanken. Neyda, Myriam, Kathleen. Bedankt voor de aangename werksfeer!! Uiteraard heb ik ook plezierige momenten beleefd met de overige collega's van de plasma groep: Ivan, Andy, Erik, Chen, Violeta. Ook nog eventjes Luc Van 't dack bedanken voor de hulp bij bestellingen van allerhande zaken.

Verder de dames van het secretariaat: Nelly, Tania en Ingrid: bedankt voor de hulp tijdens de voorbije jaren.

De voorbije jaren heb ik het genoeg gehad om assistent te zijn aan het departement. Ik heb er leuke momenten beleefd met de collega-assistenten, de studenten en de proffen. Hierbij wens ik ook de mensen te bedanken verantwoordelijk voor de practicum ondersteuning, met name Vera en Fabiana (UIA), Jan, Andre en Dina op het RUCA.

De computer specialist Koen De Cauwsemaecker wens ik te bedanken voor de vele momenten waarop hij mij uit de nood heeft geholpen, als mijn windows bak weer eens niet werkte... En natuurlijk ook voor de momenten 's middags aan tafel ☺, *Sir* Koen.

Voor de aangename momenten buiten de werkuren kon ik vooral rekenen op Bart 19 en Cis 4: de kritische (en doortastende) blik waarmee jullie de alledaagse zaken bekijken heeft mij al veel bijgeleerd. Leve de creatieve cel!

En tenslotte nog alle mensen die ik zo af en toe op regelmatige basis tegenkwam op de UIA (het huizeken,...).

Woudloper!! Woudloper !! Tell me what feeling you get when you are running and some peacocks start calling...

Overview

Chapter 1: Introduction	9
1.1. Deposition methods	9
1.2. A plasma	9
1.3. RF Capacitively Coupled Discharges	10
1.4. Numerical modelling of plasmas	13
1.4.1. Numerical modelling of methane plasmas	15
1.4.2. Numerical modelling of silane plasmas	16
1.5. References	17
Chapter 2: Description of the numerical model	19
2.1. Introduction	19
2.2. The one-dimensional fluid model	19
2.3. Input information for the fluid model	24
2.4. Numerical solution of the fluid model, in combination with EEDF	29
2.5. References	34
Chapter 3: Results of the 1D model for a methane plasma	35
3.1. The fluid model applied to a methane/hydrogen plasma	35
3.2. Electron impact collisions taken into account in the model	36
3.3. Ion reactions included in the model	38
3.4. Neutral-Neutral reactions incorporated in the model	39
3.5. Results and discussion	40
3.5.1. Calculated densities of the plasma species versus distance in the plasma	41
3.5.2. The effect of varying power	43
3.5.3. Effect of varying gas flow mixture	46
3.5.4. Effect of varying total gas flow	47
3.5.5. Effect of varying pressure	48
3.5.6. Information of the fluxes towards the electrodes	50
3.6. References	51

Chapter 4: Comparison between a one-dimensional and a two-dimensional model for a methane plasma	53
4.1. Introduction	53
4.2. Description of the two-dimensional fluid model	53
4.3. Comparison of the results of the 1D and 2D fluid models	55
4.4. Conclusions	65
4.5. Future modelling plans	65
4.6. References	66
Chapter 5: One-dimensional fluid model for an acetylene rf discharge: study of the plasma chemistry	67
5.1. Fluid model developed for an acetylene discharge	67
5.2. Results of the model	73
5.2.1. The acetylene discharge	73
5.2.2. Comparison of the results obtained for an acetylene and a methane plasma	76
5.2.3. The acetylene/helium discharge	79
5.3. Conclusions	82
5.4. References	83
Chapter 6: One-dimensional modelling of a capacitively coupled rf plasma in silane/helium, including small concentrations of O ₂ and N ₂	85
6.1. Introduction	85
6.2. Description of the 1D fluid model	85
6.2.1. The silane plasma	85
6.2.2. The silane/helium plasma	88
6.2.3. The silane/helium plasma containing small concentrations of O ₂ and N ₂	89
6.3. Results of the models	93
6.3.1. The silane discharge	94
6.3.2. The silane/helium discharge	95
6.3.3. The effect of small amounts of air in a SiH ₄ /He plasma.	96
6.4. Conclusions	100
6.5. References	101

Chapter 7: Comparison of a Boltzmann model and a Monte Carlo model for the calculation of the electron reaction rate coefficients	103
7.1. Introduction	103
7.2. Description of the one-dimensional fluid model	104
7.3. The one-dimensional Monte Carlo model	104
7.4. Comparison of the results obtained with a fluid model using input of a Boltzmann and a Monte Carlo model.	107
7.4.1. Condition 1: 0.14 Torr	107
7.4.2. Condition 2: 0.5 Torr	113
7.5 Conclusions	115
7.6. References	116
Samenvatting	117
Summary	123
Gepubliceerde artikels	127

Chapter 1: Introduction

1.1. Deposition methods

The deposition of thin solid films on a number of substrates can be performed using different deposition techniques. In *Thermal Vapour Deposition* [1], a solid amount of the material, which has to be deposited, is placed in a crucible in a vacuum chamber, together with the substrate (i.e., the material on which a coating must be applied). The solid material is heated, evaporates and is deposited on the substrate.

Chemical Vapour Deposition (CVD) and *Plasma-Assisted Chemical Vapour Deposition (PACVD)* are widely used to deposit thin solid films, using gaseous precursors (i.e., the precursor gas is used for the deposition of the thin solid films). In the CVD process, thermal energy is used to supply the activation energy of the chemical reactions [2]. Hence this deposition process is carried out at relatively high temperatures (250 - 1000 °C).

In the Plasma-Assisted CVD process (also called Plasma-Enhanced CVD (PECVD)), a plasma is used for the deposition of thin solid films. The advantage of PACVD as compared to the CVD-process, is that the deposition can be carried out at much lower substrate temperatures (<100 °C), and hence also temperature sensitive substrates can be coated [3]. Plasma-Assisted Chemical Vapour Deposition is nowadays generally used for the production of amorphous silicon (a-Si:H) layers, used in microelectronic industry (i.e., the production of electronic components), and for the production of solar cells [4]. Further, amorphous carbon layers (a-C:H) can also be deposited using PACVD [5]. These carbon layers are mainly deposited as protective layers, on a variety of substrates. The amorphous carbon layers (also called diamond-like carbon (dlc) layers) combine some interesting features: high hardness, very low friction coefficient, chemical inertness and infrared transparency, and are therefore widely used as wear-resistant coatings [5].

1.2. A plasma

The deposition of several kinds of thin solid films can easily be performed using low temperature plasmas, in the low pressure region [6]. These plasmas consist of a number of different species, namely electrons, (positive and negative) ions and neutrals (radicals and molecules). The electron density of such plasmas is normally in

the order of 10^{15} m^{-3} (pressure region: 10 – 100 Pa), with the densities of the negative and positive species in the plasma nearly equal to each other. These plasmas are also characterized by an ionisation degree (electron density/neutral density) in the order of 10^{-5} , classified as weakly-ionized plasmas.

Different techniques are available in which such a plasma can be generated: dc, rf and microwave discharges [3]. In a *DC glow discharge* (dc: direct current), a plasma is created in a low pressure chamber, between two metal plates: one grounded and the other connected to a dc power supply. A plasma generated in a *RF glow discharge* (rf: radio frequent) is generated in a similar way, but here an rf power supply is used. These discharges are further subdivided in *capacitively coupled discharges* (CCD), in which a plasma is generated between two parallel plates, and *inductively coupled discharges* (ICD), where rf-coils outside the discharge maintain the plasma.

Further, plasmas for deposition purposes can also be produced using *microwave discharges* (2.45 GHz). A special variant of this technique is the ECR-microwave discharge (Electron Cyclotron Resonance), which makes use of a magnetic field [3].

1.3. RF Capacitively Coupled Discharges

Rf Capacitively Coupled discharges make use of a radio frequent power supply (typically 13.56 MHz) to generate a plasma between two parallel plates (see figure 1).

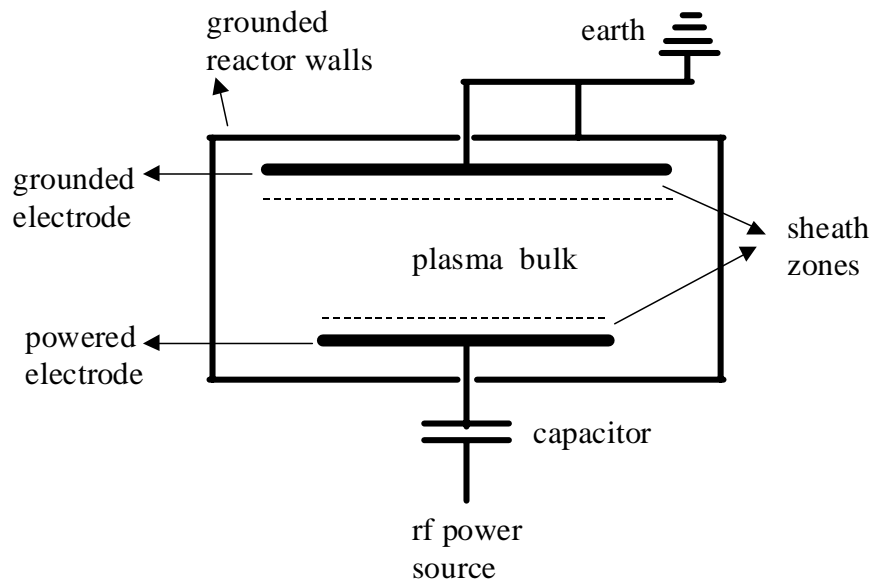


Figure 1: Schematic view of a capacitively coupled rf reactor with parallel plates

Usually, the above electrode is grounded, together with the reactor walls, while the lower electrode is connected to the rf power supply. The distance between these electrodes is normally in the order of a few centimetres, for small reactors. The pressure region in which this plasma operates is about 10 – 100 Pa. The precursor gas is introduced in the reactor chamber by a gas inlet, while the reactor vessel is kept at low pressure by a vacuum system (not shown in figure 1).

The power going into the plasma is normally in the order of 1-100 Watt. The rf power supply, connected to the powered electrode, generates an alternating (sinusoidal) voltage at this electrode, leading to a changing electric field (as a function of time in the rf cycle) between the two plates, from which the electrons (and ions) gain energy. This electron energy is mainly lost in inelastic collisions, producing a number of reactive species (radicals, ions and excited species). The background gas (i.e., a mixture of input precursor gas and neutral species, created in the plasma, and present at relatively high densities) has temperatures in the order of 400 K. The ions, gaining energy from the electric field, have comparable temperatures. This follows from the fact that ions lose easily their energy in collisions with background species (since ions and neutral species have comparable masses). The electrons, however, have temperatures in the order of 10^4 K. They have much lower masses, which makes it far more difficult to equilibrate energy with the background molecules.

As can be seen from figure 1, a capacitor is placed in the circuit, which makes that the net total current over 1 rf cycle must be zero. The region between the two plates of the capacitively coupled discharge is characterized by a large *plasma bulk* region, and a small *plasma sheath* zone in front of both electrodes. When a plasma is generated, more electrons than ions reach the electrodes (because of their higher mobility), and hence both electrodes are initially negatively charged up. This leads to an increase in positive ion density near the electrodes, creating high electric fields in the plasma sheaths. This electric field repels back the electrons in the plasma bulk, and attracts the positive ions towards the electrodes, which finally leads to the situation that, after a few rf-cycles, the time-averaged electron and ion fluxes towards both electrodes become nearly equal.

Normally, the powered electrode is smaller than the grounded electrode. This leads to a dc auto bias voltage at this powered electrode, ensuring that the electronic currents towards both electrodes are equal. The applied voltage at the powered electrode is still sinusoidal, but is superposed on a negative dc-bias (see figure 2).

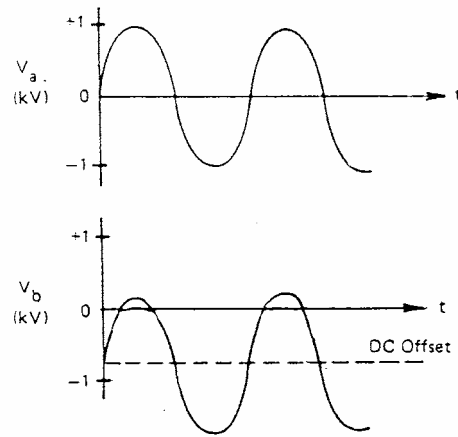


Figure 2: above: applied sinusoidal voltage (2 parallel plates of equal size)

under: applied sinusoidal voltage superimposed on a negative dc bias (powered electrode smaller than grounded electrode).

Because of this bias voltage, higher electric fields are obtained in the plasma sheath in front of the powered electrode. Also the ion fluxes towards the powered electrode will be higher compared to the ion fluxes towards the grounded electrode. In contrast to the plasma sheath, the large plasma bulk zone is characterized by a low electric field, and is quasi-neutral. Hence, the densities of the positive and negative species are nearly equal in this region.

In general, for low rf voltages (under 600 V), the plasma operates in the *alpha-regime* (α -regime). This means that the electrons emitted at the electrode due to ion bombardment (i.e., so called secondary electrons) do not play an important role in maintaining the plasma. When higher rf voltages are applied (gamma-regime (γ -regime)), secondary electrons become of major importance in maintaining the discharge [6, 7].

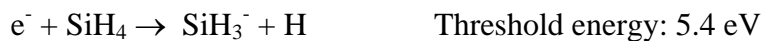
For the deposition of amorphous silicon and carbon layers, generally silane (SiH_4) and methane (CH_4), or acetylene (C_2H_2) gases are used as precursor gases, respectively. A number of different electron-neutral reactions take place in the plasma:

- *vibrational excitation*: an electron collides with a neutral molecule, which is excited from ground level to a vibrationally excited level. Threshold energies (i.e., minimum electron energies required for these reactions) are in the order of 0.1 eV.

- *electronic excitation*: an electron collides with a neutral molecule which is excited from ground level, to a higher electron excited level. For these reactions, threshold energies are in the order of 5 - 8 eV.
- *ionisation*: an electron collides with a neutral species and ionises this species. A positive ion is formed together with an additional electron. Because more energy is required to ionise a molecule, compared to electron excitation, the threshold energies will be higher (i.e., starting from 10 eV)
- *dissociation*: in this reaction, a neutral molecule is divided in two (or more) species, for example the following reaction:



- *electron attachment*: an electron collides with a neutral molecule and creates a negative ion. For example:



These attachment reactions are mainly important in electronegative discharges like in silane, in which negative ions play an important role. In methane plasmas, which are electropositive plasmas, negative ions are of minor importance and hence these reactions can be ignored.

In all these electron reactions, a variety of species (ions, radicals, excited species) are formed, which will also participate in the plasma chemistry, leading to neutral-neutral, ion-neutral and ion-ion reactions. Hence, the combination of all the different electron reactions, together with the plasma-chemistry, leads to a complex plasma, in which species are produced and consumed in a variety of reactions.

1.4. Numerical modelling of plasmas

In order to improve the knowledge for deposition, or sputtering (erosion of a target) by means of plasma technology, plasma modelling can be of great use to predict the composition of the plasma, and to optimize the plasma parameters (pressure, power, gas flow, gas mixture). The most important output obtained from plasma models are, beside the basic plasma characteristics (potential, average electron energy,...), the densities of different plasma species. Hence, in this way, the results of these numerical models (species densities) can be compared with experimental data (species densities), in order to validate these models. Afterwards, these validated plasma models can be used for further model developments, and for optimizing the plasma

parameters, in order to obtain a better deposition process. For example, for plasma deposition, it is important to have a plasma which is as uniform as possible, as a function of reactor radius. A uniform plasma implies uniform species fluxes to the substrate (as a function of reactor radius), and gives hence, uniformly deposited coatings.

In recent years, a number of different numerical models have been published, for the modelling of capacitively coupled rf plasmas, used in a variety of applications. The most commonly used models for plasma modelling nowadays are: fluid models [8 - 18], particle-in-cell/Monte Carlo (PIC/MC) models [19 - 22] and hybrid models [23 - 25].

A *fluid model* is generally based on a number of density balance equations (one for each species in the plasma (i.e., ions, electrons and neutrals)), combined with the electron energy equation. Further, the Poisson equation is also considered, to obtain the electric field self-consistently. These fluid models are widely used for the modelling of different kinds of plasmas. Methane [13 - 18] and silane [10 - 12] plasmas are used for deposition purposes. Argon plasmas [8, 9, 23, 24] are important for analytical purposes (spectroscopic sources), while CF_4 plasmas play a role for sputtering applications [26] in the microelectronics industry. Although these fluid models are good tools for plasma modelling, they require a number of input parameters: species, the number of species, electron-neutral reactions (and corresponding cross sections), neutral-neutral reactions (and corresponding reaction rate coefficients). Hence, the results of these models depend largely on the input information, which makes that the results of different models, using different input values, will vary to some extent. It should also be considered that, when the complexity of the model is increased (i.e., more species and reactions considered in the model), more equations will have to be introduced into the model, which will increase calculation time. However, the computational effort of the fluid model is normally still lower compared to the other numerical techniques (PIC/MC and hybrid models), for plasma modelling. Hence, this makes a fluid model a useful tool for the modelling of capacitively coupled rf plasmas.

Particle-in-cell/Monte Carlo (PIC/MC) models are generally known as the most accurate approach, because they consider the plasma species on their lowest microscopic level. The trajectory of each species is calculated using Newton's laws, while the collisions between the plasma species depend on the cross sections, and are

determined by random numbers. Because a large number of particles have to be followed to obtain statistically valid results, the PIC/MC model is very time consuming. Hence, in order to keep the calculation time reasonable, the number of different kinds of plasma species, taken into account in the plasma model, should be limited. Although a fluid model is not as accurate as a PIC/MC model, its main advantage is that it requires less computational time compared to a PIC/MC model, and also a large number of plasma species can be considered without significantly increasing the calculation time.

Further, plasmas can also be described using fluid models, in combination with a Monte Carlo model for the electronic kinetics, the so-called *hybrid models*. In this kind of model, the main advantage of the fluid model (less computational effort) and the Monte Carlo model (more accurate) are combined.

1.4.1. Numerical modelling of methane plasmas

For the modelling of methane plasmas, a number of different numerical models are presented in literature [13 – 18, 27 - 34]. These models differ in the way the plasma chemistry is treated, and the approximations used. Mostly, fluid models are applied, in one dimension (i.e., the distance between the parallel plates), because it is found that these models already give a satisfactory description of a plasma [9, 12]. Also, these 1D models are less time-consuming than the more extensive 2D models. These findings were already found in past for an argon discharge [35]. From this, it follows that the 1D models are a useful tool to investigate the plasma chemistry (i.e., the importance of several reactions can be investigated, and hence in this way, only the most important species and reactions can be maintained in the final plasma model).

Tachibana [27] developed a straightforward methane plasma model, in which all particle density balances are solved. Further, a PIC/MC model, considering a limited number of plasma species, is presented in [22]. However, most commonly 1D fluid models are used for the modelling of methane plasmas [13 - 18]. These models differ from each other in the way they describe the plasma chemistry (i.e., the number of species, reactions,...). A distinction can also be made in the way they treat the electron dynamics. In some models [28, 29], constant electron reaction rate coefficients were used, whereas the plasma model described in [30] used the reaction rate coefficients as fitting parameters. In other cases, a Maxwellian [34] or a Druyvenstein-like [30 - 31] electron energy distribution function (EEDF) was

assumed, for the calculation of the electron reaction rate coefficients. The most accurate way to describe the electron kinetics, is to use the Boltzmann equation, which specifies the number of electrons at a certain time, with corresponding energy and position. However, this Boltzmann equation is rather complex to solve. Hence, in some cases, a simplified Boltzmann model is used for the calculation of the EEDF [13, 14]. With this model, the electron reaction rate coefficients are obtained for every electron reaction, as a function of average electron energy.

Further, also some 2D models for methane plasmas have been presented [15 – 18]. When assuming a cylindrical reactor geometry, the plasma characteristics are obtained in axial (the distance between the electrodes) and radial position (as a function of electrode radius). However, the disadvantage of these 2D models is that they are more time consuming.

1.4.2. Numerical modelling of silane plasmas

One and two-dimensional fluid models were developed by Nienhuis et al. for capacitively coupled rf silane plasmas [10 - 12]. This fluid model is coupled with a simplified Boltzmann model, to obtain the rate coefficients for the different electron-neutral reactions. A similar silane fluid model was also developed by Kushner [36], albeit for a somewhat different plasma application (i.e., a remote PACVD process, in which the substrate is placed outside the plasma region). A hybrid fluid/Monte Carlo model for SiH_4/H_2 mixtures is presented in [25]. A two-dimensional fluid model was also used by Leroy for the study of silane plasmas [37]. A particle-in-cell/Monte Carlo model (also 1D and 2D) was developed by Yan et al. for rf silane plasmas [20 - 21]. Further, the plasma chemistry of SiH_4/He mixtures, combined with O_2 and N_2O has been investigated [38].

1.5. References

- [1] S. R. Bunshah, *Physics of Amorphous Materials*, Longman Scientific and Technical, New York, 1990
- [2] K. J. Kuijlaars, Ph. D. Thesis, TU Delft (1996)
- [3] H. Schlüter, A. Shivarova, *Advanced Technologies on Wave and Beam Generated Plasmas*, Nato Science Series, Kluwer Academic Publishers (1998)
- [4] J. Perin, O. Leroy, M.C. Bordage, *Contrib. Plasma Phys.*, **36**, 3 (1996)
- [5] E. Dekempeneer, J. Smeets, J. Meneve, L. Eersels, R. Jacobs, *Thin Solid Films*, **241**, 269 (1994)
- [6] B. Chapman, *Glow Discharge Processes*, John Wiley & Son, New York, 1980
- [7] A. Bogaerts, R. Gijbels, W.J. Goedheer, *Jpn. J. Appl. Phys.*, **38**, 4404 (1999)
- [8] W. J. Goedheer, P. M. Meijer, J. Bezemer, J. Diederick, P. Passchier, W. G. J. H. M. van Sark, *IEEE Transactions on Plasma Science*, **23**, 644 (1995)
- [9] D. Passchier, Ph. D. Thesis, Utrecht, 1994
- [10] G. J. Nienhuis, W. J. Goedheer, E. A. G. Hamers, W. G. J. H. M. van Sark, J. Bezemer, *J. of Appl. Phys.*, **82**, 2060 (1997)
- [11] G. J. Nienhuis, W. J. Goedheer, *Plasma Sources Sci. Techn.*, **8**, 295, 1999
- [12] G.J. Nienhuis, Ph. D. Thesis, Utrecht (1998)
- [13] E. Gogolides, C. Buteau, A. Rhallabi, G. Turban, *J. Phys. D: Appl. Phys.*, **27**, 818 (1994)
- [14] E. Gogolides, D. Mary, A. Rhallabi, G. Turban, *Jap. J. of Appl. Phys.*, **34**, 261 (1995)
- [15] K. Bera, B. Farouk, Y.H. Lee, *J. of Electrochem. Soc.*, **146**, 3264 (1999)
- [16] K. Bera, J. W. Yi, B. Farouk, Y. H. Lee, *IEEE Transactions on Plasma Science*, **27**, 5 (1997)
- [17] K. Bera, B. Farouk, Y. H. Lee, *Plasma Sources Sci. Techn.*, **10**, 211, 2001
- [18] K. Bera, B. Farouk, Y. H. Lee, *Plasma Sources Sci. Techn.*, **8**, 412, 1999
- [19] D. Vender, W. Boswell, *IEEE Transactions on Plasma Science*, **18**, 725, 1990
- [20] M. Yan, W. J. Goedheer, *IEEE Transactions on Plasma Science*, **27**, 1399 (1999)
- [21] M. Yan, W. J. Goedheer, *Plasma Sources Sci. Techn.*, **8**, 349 (1999)
- [22] K. Nagayama, B. Farouk, Y. H. Lee, *IEEE Transactions on Plasma Science*, **26**, 125 (1998)
- [23] A. Bogaerts, R. Gijbels, W.J. Goedheer, *J. Appl. Phys.*, **78**, 2233 (1995)
- [24] A. Bogaerts, R. Gijbels, W. Goedheer, *Anal. Chem.*, **68**, 2296 (1996)

- [25] H. Sato, H. Tagashiro, , IEEE Transactions on Plasma Science, **19**, 108 (1991)
- [26] David B. Graves, AIChE Journal, **35**, 1, 1989
- [27] K. Tachibana, M. Nishida, H. Harima, Y. Urano, J. Phys. D: Appl. Phys, **17**, 1727 (1984)
- [28] N. Mutsukura, S. Inoue, Y. Machi, J. Appl. Phys, **72**, 43 (1992)
- [29] L. E. Kline, W. D. Partlow, W. E. Bies, J. Appl. Phys, **65**, 70 (1998)
- [30] A. Rhallabi, Y. Catherine, IEEE Transactions on Plasma Science, **19**, 270 (1991)
- [31] C. Cavalotti, M. Masi, S. Carrà, J. of Electrochem. Soc, **145**, 4332 (1998)
- [32] D. J. Dagel, C. M. Mallouris, J. R. Doyle, J. Appl. Phys, **79**, 8735 (1996)
- [33] M. Masi, C. Cavalotti, S. Carrà, Chemical Engineering science, **53**, 3875 (1998)
- [34] A. Von Keudell, W. Möller, J. Appl. Phys, **75**, 7718 (1994)
- [35] A. Bogaerts, R. Gijbels, Fresenius'Z, Anal. Chem., **359**, 331 (1997)
- [36] M. J. Kushner, J, Appl. Phys, **63**, 2532 (1998)
- [37] O. Leroy, G. Gousset, L. L. Alves, J. Perin, J. Joly, Plasma Sources Sci. Techn., **7**, 348 (1998)
- [38] M. J. Kushner, J. Appl. Phys, **71**, 6358 (1993)

Chapter 2: Description of the numerical model

2.1. Introduction

In this chapter, a brief description will be given of the 1D fluid model, which is used in our work for the modelling of silane, methane and acetylene plasmas. The fluid model itself was originally developed in the research group of W. Goedheer (Institute of Plasma Physics “Rijnhuizen” (NL)) for the modelling of rf discharges using atomic noble gases [1 - 3]. In a later stage, this fluid model was extended (and combined) with a numerical part for the modelling of plasma chemistry [4 - 6], and a separate numerical model for the description of the electron kinetics. Hence, in this way, the model could be used for the modelling of molecular (silane) plasmas, in which the plasma chemistry (neutral-neutral, ion-neutral and ion-ion reactions) also plays an important role.

For the description of the electron kinetics, a simplified Boltzmann model was used, developed originally by Meijer et al. [7]. This model calculates the electron reaction rate coefficients of all the electron-neutral reactions, as a function of average electron energy, which can afterwards be used as input in the fluid model. Further, the fluid model also requires input information related to the used precursor gas (species, reactions, transport coefficients,...). Because some of the necessary input data were not available in the literature, approximations had to be made here.

Afterwards, the one-dimensional fluid model was also extended in geometry (i.e., a two-dimensional fluid model), which allowed the modelling of cylindrical reactor geometries.

2.2. The one-dimensional fluid model

A fluid model is based on a set of balance equations, namely one for every species. Further the electron energy and Poisson equation are considered (see below). In this way, information is obtained – among other things - about the densities of the charged species in the plasma, as a function of space (distance between the plates), and as a function of time (evolution in rf-cycle). The main limitation to use the fluid model is that the mean free path of the particles should be much less than the characteristic dimensions of the reactor (i.e., in one-dimension, the distance between the plates).

From this, it follows that fluid models are generally not suitable for pressures lower than 10 Pa.

A schematic view of the reactor vessel used for plasma deposition is shown in figure 1. In the fluid model, only one dimension is considered, namely the distance between the electrodes (z -direction). Hence, in this way, only information of the plasma characteristics (species densities) can be obtained as a function of the z -direction.

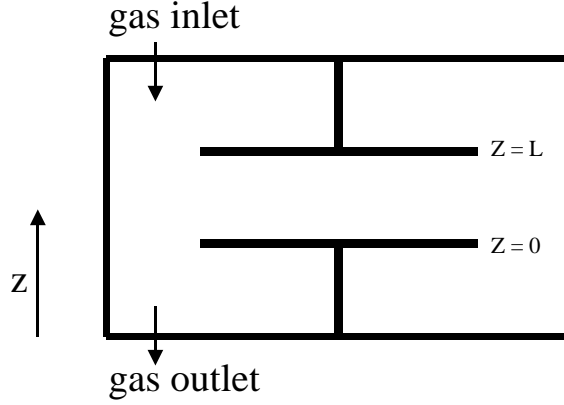


Figure 1: schematic view of the reactor geometry

The plasma is generated between the parallel plates (discharge region), while the region outside the parallel plates is normally discharge-free (only neutral molecules are found here). All simulations presented in this work are for small deposition reactors, in which the distance between the electrodes is in the order of a few centimetres. Note that the regions above and below the electrodes (gas input and output flow area) are not considered in detail in the model. From this, it follows that the input and output of gas are introduced by extra source terms in the neutral particle balances.

The number of species present in the discharge, at a certain pressure, is given by the ideal gas law:

$$P_{tot} = k_B T_{gas} \sum n \quad (2.1)$$

in which k_B equals $1.38 \cdot 10^{-23}$ J/K (Boltzmann constant). The term T_{gas} represents the gas temperature (400 K). The last term represents the summation of the densities of all the different species.

For the density balances, a distinction is made between neutral background gases (i.e., the precursor gas and the neutral molecules present in the discharge at high densities), and the reactive species present in the plasma (discharge volume). The density of the neutral background species j in the discharge is given by:

$$n_j = \frac{\tau}{V_f} \left(Q_j^{\text{in}} + \int_{\text{discharge}} S_{\text{reac},j} dV \right) \quad (2.2)$$

The term Q_j^{in} represents the number of precursor species introduced in the reactor vessel (i.e., the gas flow). To maintain the discharge at a certain pressure, given in as an input parameter in the numerical code, a number of background species have to be pumped out of the reactor vessel. In order to obtain the required pressure, the average residence time τ is iteratively adapted in the code, until the pressure reaches the correct input pressure value. Note that the average residence time depends on the reactor vessel volume V_f . Finally, the last term in the above equation represents the molecules consumed in the chemical reactions (electron-neutral, ion-neutral and neutral-neutral reactions). Note that no time-derivative term is considered in equation 2.2 because a steady-state solution is assumed.

For the other species (electrons, ions and radicals) present in the discharge, the density balance can be written as:

$$\frac{\partial n_j}{\partial t} + \frac{\partial \Gamma_j}{\partial z} = S_{\text{reac},j} \quad (2.3)$$

The first term describes the time-variation (as a function of rf-cycle), while Γ_j represents the flux of the species in the z -direction. The term on the right-hand side (i.e., the total source term) gives the number of species consumed and created in the plasma-chemistry. The production source term for a species, obtained from an electron reaction, is given by the product $kN_e N_{\text{gas}}$. The term k equals the reaction rate coefficient, N_e represents the electron density, and N_{gas} is gas density of the gas which is involved in the reaction. The source term for a species formed in a neutral-neutral reaction (or ion-ion, or ion-neutral reaction) is obtained in a similar way (i.e., $kN_{\text{gas}1}N_{\text{gas}2}$, where k is the reaction rate coefficient and $N_{\text{gas}1}$ and $N_{\text{gas}2}$ the densities of the species involved in the reaction). The loss term for a species in a reaction is calculated in a similar way, but is represented with a negative sign. Hence, the total

source term for the density balance equation of a species is obtained by summation of the production and loss terms of all the reactions included.

The flux term Γ_j can further be written as:

$$\Gamma_j = \mu_j n_j E - D_j \frac{\partial n_j}{\partial z} \quad (2.4)$$

The first term represents the migration of the charged species, under influence of an electric field, with μ_j equal to the mobility coefficient. Negative ions and electrons are characterized with a negative mobility coefficient, while the positive ions have a positive coefficient. The second term gives the diffusion in the z-direction, in which D_j represents the diffusion coefficient.

The potential V can be obtained from the Poisson equation, which is given by:

$$\frac{\partial^2 V}{\partial z^2} = -\frac{e}{\epsilon_0} (n_{\text{pos}} - n_{\text{neg}} - n_e) \quad (2.5)$$

In this equation, ϵ_0 gives the permittivity of free space, while n_{pos} and n_{neg} represent the densities of the positive and negative ions (Note that in equation 2.5. is assumed that all ions have one charge). Further, the electron density is given by n_e .

The electric field is then obtained by taking the gradient of the potential:

$$E = -\frac{\partial V}{\partial x} \quad (2.6)$$

The boundary conditions for the Poisson equation are as follows: the potential at the grounded electrode is set to zero, while the potential at the powered electrode is function of rf-cycle, according to:

$$V(t) = V_{\text{rf}} \sin(2\pi\nu_{\text{rf}} t) \quad (2.7)$$

V_{rf} is the amplitude of the potential applied to the powered electrode, while ν_{rf} represents the rf-frequency (13.56 MHz). From the sinusoidal boundary condition applied to the powered electrode, it follows that the potential, and hence also the electric field, will vary as a function of rf-cycle.

Beside the pressure and distance between the electrode, the power introduced into the plasma is also an input parameter (normally in the order 1-100 Watt). This power is introduced in the plasma by means of an alternating potential applied at the powered electrode, leading to an alternating electric field. It is from this electric field that the charged species will gain energy (“Ohmic heating”), and hence maintain the plasma.

In order to generate a plasma with a certain power, the amplitude V_{rf} in equation 2.7 is adapted gradually, until the power introduced in the plasma (equation 2.8) reaches the required power value.

$$P = \frac{\pi R^2}{\tau} \sum_{\substack{j=\text{charged} \\ \text{species}}} \int_0^\tau \int_0^z E(z,t) \Gamma_j(z,t) q_j dz dt \quad (2.8)$$

were τ equals the rf-period. The symbol E gives the electric field, while Γ represents the flux of the corresponding species. Further the charge of the species is given by q_j (positive for positive ions, and negative for negative ions and electrons).

As mentioned above, the electrons and ions gain energy from the electric field, which varies as a function of the rf-cycle. At 13.56 MHz (i.e., the frequency used for our simulation conditions), only the electrons can follow the alternating electric field immediately. The ions, characterized by a large mass, can not instantaneously follow the electric field and hence, an effective electric field E_{eff} is introduced for them:

$$\frac{\partial E_{\text{eff},i}}{\partial t} = \nu_{m,i} (E - E_{\text{eff},i}) \quad (2.9)$$

In equation 2.9, $\nu_{m,i}$ equals the momentum transfer frequency, given by $e/\mu_i m_i$ (with e and m_i respectively the charge and mass of the ion).

Finally, the electron energy density (w_e) balance is also considered in the fluid model:

$$\frac{\partial w_e}{\partial t} + \frac{\partial \Gamma_w}{\partial z} = -e \Gamma_e E + S_w \quad (2.10)$$

with the electron energy density flux equation equal to:

$$\Gamma_w = \frac{5}{3} \mu_e w_e E - \frac{5}{3} D_e \frac{\partial w_e}{\partial z} \quad (2.11)$$

From the calculated electron density n_e and electron energy density w_e , the average electron energy ε (w_e/n_e) is obtained, as a function of time (rf-cycle) and position (distance between the plates).

In order to solve equations 2.3, 2.4, 2.10 and 2.11, some extra boundary conditions have to be specified. The electron density n_e is set to zero at both electrodes, together with the negative ion densities (i.e., the negative ions are mainly present in the plasma bulk region, and not in the plasma sheath zones). A zero electron density at the

electrodes leads also to an electron energy equal to zero. Further, it is assumed that the ion flux at the walls is only due to migration.

2.3. Input information for the fluid model

As mentioned in the introduction, the fluid model needs some input information. First of all, the plasma parameters (such as: the distance between the electrodes, pressure, rf-frequency and power) have to be defined. The gas introduced in the plasma is involved in a number of reactions, creating a variety of species. Normally, a number of neutral molecules are formed, in combination with some radicals, ions (positive and negative) and electrons. For methane, the neutral molecules CH_4 , H_2 , C_2H_2 , C_2H_6 , C_2H_4 and C_3H_8 are considered, together with the ions CH_4^+ , CH_3^+ , CH_5^+ and C_2H_5^+ (only the most important ones are given, see further). Further a number of radicals are also considered: C_2H_5 , CH_3 and H (a more complete overview of the methane plasma model is given in chapter 3). Beside the number of species which have to be specified, also the *chemical reactions* taking place in the plasma have to be specified. A distinction is made between the electron-neutral reactions and the plasma-chemistry itself, which contains the neutral-neutral, ion-neutral and ion-ion reactions. A detailed overview of the reactions considered in the methane, acetylene and silane model will be given in chapters 3, 5 and 6 respectively.

For the electron-neutral reactions, the reaction rate coefficients for every reaction are calculated as a function of average electron energy (0 – 20 eV), using a simplified Boltzmann model. The Boltzmann equation itself is given by

$$\frac{\partial f}{\partial t} + \vec{\nabla}_r \cdot (\vec{v}f) - \vec{\nabla}_v \cdot \left(\frac{e}{m_e} \vec{E}(\vec{r}, t) f \right) = \left(\frac{\partial f}{\partial t} \right)_{col} \quad (2.12)$$

with e and m_e respectively the electron charge and mass. The solution of the Boltzmann equation gives us the electron energy distribution function f (EEDF). This function gives information about the number of electrons at a certain time t , with a velocity \mathbf{v} and position \mathbf{r} . However, the Boltzmann equation is too complicated to solve easily, hence some approximations are made: in velocity space the distribution function is taken as a series of Legendre Polynomials, of which the first two are

considered (Lorentz approximation). Further, in this Boltzmann model, a temporally constant electric field is assumed.

Because the electron reaction rate coefficients depend strongly on the electron energy distribution function (EEDF), the EEDF is obtained for a large number of electric field values from the simplified Boltzmann equation, for a given background gas density and composition. The distribution functions obtained in this way are used to construct a “look-up” table (i.e., for every value of the electric field, both the average electron energy and the various reaction rate coefficients are calculated from the EEDF, and this leads to a look-up table (reaction rate coefficients as a function of average electron energy) for every electron reaction) which can be used as input for the fluid model. It should also be mentioned that, for the calculation of the rate coefficients, the corresponding cross sections also have to be known.

The reaction rate coefficient for a certain electron-neutral reaction is calculated as follows, using an EEDF obtained from a constant electric field:

$$k = \left(\frac{2e}{m_e} \right)^{1/2} \frac{\int_0^{\infty} u \sigma_j f_0(u) du}{\int_0^{\infty} f_0(u) du} \quad (2.13)$$

in which u represents the kinetic energy ($m_e v^2/2$). σ_j denotes the cross section of the electron reaction considered, while f_0 represents the isotropic part of the EEDF, which associates with the first Legendre Polynomial in the series expansion.

The average electron energy (eq. 2.14) and electron mobility coefficients are calculated in a similar way [4]:

$$\varepsilon = \frac{\int_0^{\infty} u f_0(u) \sqrt{u} du}{\int_0^{\infty} f_0(u) \sqrt{u} du} \quad (2.14)$$

Since in the fluid model (see section 2.2), the average electron energy is calculated as a function of time and space, the corresponding electron reaction rates can be obtained using the look-up tables, in order to calculate the source terms (i.e., production and loss terms in the different reactions) of the different species.

The reaction rate coefficients of the neutral-neutral, ion-neutral and ion-ion reactions, also required for the calculation of the source terms in the density balance equations,

are assumed to be constant and are taken from the literature (see further). Also here, some approximations had to be made when data were lacking.

Further, the transport coefficients (mobility and diffusion coefficients) have to be defined in the model for every species. The electron transport coefficients are obtained from the simplified Boltzmann model. For all the other species described in the model, the diffusion coefficients and the mobility coefficients (only for the ions) are calculated in the way described below. The calculation procedure will be explained for the species in a methane plasma. The calculation of the transport coefficients of the species present in a silane or acetylene plasma is similar.

For the **neutral species** (radicals and background neutrals), the diffusion coefficients D_{ij} (m²/s) of the neutral species j in each of the background gases i (i.e., a species present in the discharge at high density, namely CH₄, H₂, C₂H₆, C₃H₈, C₂H₄, C₂H₂) are obtained using the following expression [8]:

$$D_{ij} = \frac{3k_b T_{gas} \sqrt{4\pi k_b T_{gas} / 2\mu_{ij}}}{16 p_{tot} \pi \sigma_{ij}^2 \Omega_D(\Psi)} \quad (2.15)$$

where k_b is the Boltzmann constant. T_{gas} stands for the gas temperature of the neutrals which is assumed here to be 400 K. The total pressure is given by p_{tot} (Pa). The reduced mass μ_{ij} is given by $m_i m_j / (m_i + m_j)$. σ_{ij} is the binary collision diameter and Ψ is the dimensionless temperature. The calculation of σ_{ij} and Ψ requires the Lennard Jones parameters σ (Å) and ε (K) for every species, given in table 1.

Species	σ_j (Å)	ϵ_j (K)	α (Å ³)
CH ₄	3.758 ^a	148.6 ^a	2.6
CH ₃	3.620	121.6	
CH ₂	3.491	95.2	
H	2.708 ^a	37.0 ^a	
C ₂ H ₆	4.443 ^a	215.7 ^a	4.47
C ₂ H ₅	4.443	215.7	
C ₃ H ₈	5.118 ^a	237.1 ^a	6.33
CH	3.370 ^a	68.6 ^a	
H ₂	2.827 ^a	59.7 ^a	0.819
C ₂ H ₄	4.163 ^a	224.7 ^a	4.22
C ₂ H ₂	4.033 ^a	231.8 ^a	3.49

Table 1: Lennard-Jones parameters and polarisabilities of some species present in a methane plasma. The values marked with an *a* are taken from reference [9], while the others are calculated by interpolation.

As can be seen from table 1, the Lennard-Jones parameters were found for most of the neutrals (CH₄, C₂H₆, C₃H₈, H₂, C₂H₄, C₂H₂) and for some radicals (H, CH) [9]. For the other species, these parameters were calculated by linear interpolation. For example, the Lennard-Jones parameters for the radicals CH₂ and CH₃ were obtained by linear interpolation (from the data for CH and CH₄) using the following formulas [10]:

$$\sigma_{\text{CH}_x} = \sigma_{\text{CH}} + \frac{x-1}{3}(\sigma_{\text{CH}_4} - \sigma_{\text{CH}}) \quad (2.16)$$

$$\epsilon_{\text{CH}_x} = \epsilon_{\text{CH}} + \frac{x-1}{3}(\epsilon_{\text{CH}_4} - \epsilon_{\text{CH}}) \quad (2.17)$$

where *x* has the value of 2 and 3 for CH₂ and CH₃ respectively. For C₂H₅, the Lennard-Jones parameters could not be obtained by linear interpolation (due to the difference in molecule configuration between C₂H₆ (sp³) and C₂H₄ (sp²)); therefore we used the values of C₂H₆.

The binary collision diameter σ_{ij} , also necessary in equation 2.15, is given by $(\sigma_i + \sigma_j)/2$, and the dimensionless temperature Ψ equals $T_{\text{gas}}/\epsilon_{ij}$ (with $\epsilon_{ij} = (\epsilon_i \epsilon_j)^{0.5}$). The

dimensionless temperature is necessary for the calculation of the dimensionless diffusion collision integral Ω_D , which is given by [8]:

$$\Omega_D(\Psi) = \frac{A}{\Psi^B} + \frac{C}{e^{D\Psi}} + \frac{E}{e^{F\Psi}} + \frac{G}{e^{H\Psi}} \quad (2.18)$$

where A, B, C, D, E, F, G and H are parameters obtained from [8] (A= 1.06, B = 0.16, C = 0.19, D = 0.48, E = 1.04, F = 1.53, G = 1.76 and H = 3.89).

Finally, the diffusion coefficient D_j of the species j *in the entire gas mixture* (the sum of all the background gases i) is obtained from the different D_{ij} -values (obtained from 2.15) using [11]:

$$\frac{p_{tot}}{D_j} = \sum_{i=\text{background}} \frac{p_i}{D_{ij}} \quad (2.19)$$

with p_{tot} the total pressure and p_i the partial pressure of the background gas i .

The ion mobility coefficients μ_j (m^2/Vs) of the **ions** in the gas mixture can be calculated in a similar way as the diffusion coefficients for the neutral species. First the ion mobility coefficient $\mu_{i,j}$ of an ion j in each of the background gases i is calculated using [11]:

$$\mu_{i,j} = 0.514 \frac{T_{gas}}{p_{tot} \sqrt{\mu_{ij} \alpha_i}} \quad (2.20)$$

The reduced mass μ_{ij} is here given in amu, while α_i (\AA^3) is the polarisability of the background gas i . The polarisabilities are taken from [12] and are also presented in table 1. All other parameters used in equation 2.20 have been defined before. Afterwards, the mobility coefficient of the ion j in the total gas mixture can be calculated in a similar way as the diffusion coefficient for the neutrals, described above.

Finally, the ion diffusion coefficient D_j of an ion j in the total gas mixture can directly be obtained using the Einstein relation:

$$D_j = \frac{k_b T_{ion}}{e} \mu_j \quad (2.21)$$

with T_{ion} the ion temperature (which is assumed to be equal to the gas temperature) and μ_j the mobility coefficient of the ion in the gas mixture.

Finally, the boundary conditions also have to be specified for the plasma-wall interactions (i.e. deposition process) in the density balances. These boundary conditions for the different species are incorporated in the fluid model by means of a “sticking model” [6]. In this way, also some preliminary information can be obtained about the growth of the layer. The sticking model considers that the radicals and the ions react at the surface, while the non-radical neutral molecules (CH_4 , H_2 and others) do not influence the growth of the layer. For the ions, it is assumed that they have a sticking coefficient of 1 [13].

The radical-wall interactions are described by means of a surface reaction coefficient β_j , which describes the fraction of species reacting at the wall (for example: β_j equal to 0.15 means that for 100 species impinging the wall, 15 will react at the wall, while the other 85 will be immediately reintroduced in the plasma). This surface reaction coefficient β_j can further be written as:

$$\beta_j = s_j + \gamma_j \quad (2.22)$$

The term s_j specifies the number of reacting species, really contributing to the growth of the layer (i.e., by sticking to the substrate), while the term γ_j gives the number of species which were attached – in a first stage - to the substrate, but are afterwards introduced back in the plasma, after having been involved in a plasma-wall interaction. Note that some information about these sticking coefficients is available from literature, but the values are subject to uncertainties.

2.4. Numerical solution of the fluid model, in combination with EEDF

For the differential equations presented in section 2.2., **analytical solutions**, which give information of the variables throughout the whole domain, are very difficult to obtain. Hence, in order to solve the differential equations, these equations are discretized (in space and time). Discretization implies that the partial derivatives are written as algebraic difference quotients, yielding a system of algebraic equations,

which can be solved more easily. In this way, **numerical solutions** are obtained for the differential equations, only in the discrete points in the domain, called grid points. For this, the distance between the two electrodes (normally 3 cm for the 1D model) is divided in 64 cells, using a Sharfetter-Gummel exponential scheme [1 – 3]. A fully implicit method is used to solve the time evolution [14, 15]. The term “fully implicit” refers to the fact that, when a differential equation is written as a set of algebraic equations, this set of algebraic equations has to be solved simultaneously. The time step in the rf cycle (13.56 MHz) is set to $9.2 \cdot 10^{-10}$ s (i.e., 80 time steps in one rf-cycle).

The calculation procedure for the charged species starts normally at the *beginning of the rf-cycle* ($t = 0$). First of all, the electron density balance is solved in combination with the Poisson equation, in order to avoid numerical instabilities. Afterwards, the ion density balance equations (one for every ion) and the electron energy density equation are also solved. Hence in this way, the electron density, potential, ion densities and average electron energy are obtained at this particularly time-step (as a function of space). For the calculation of these variables, a Newton-Raphson method is used (also called Newton’s iteration). This method enables us to find the – as good as possible – solution, which approaches the analytical solution. The principle of a Newton-Raphson method is given in figure 2.

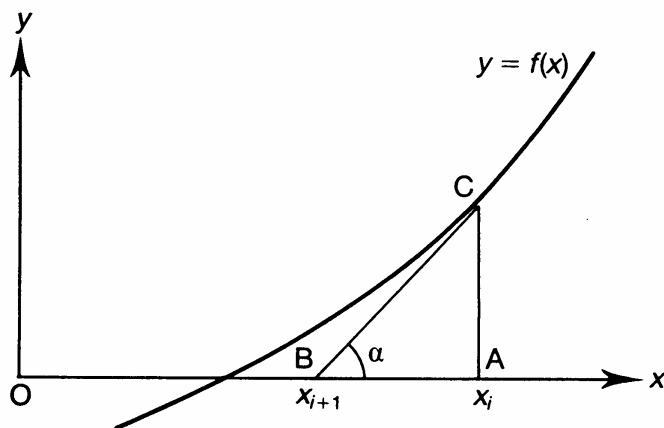


Figure 2: principle of a Newton-Raphson method [16]

To solve a non-linear function $y = f(x_i)$, the derivative of the function $f'(x_i)$ can be used in order to obtain a better, closer result (x_{i+1}) of the real root of the function:

$$x_{i+1} = x_i + \frac{f(x_i)}{f'(x_i)} \quad (2.23)$$

Starting with a logical guess x_i , x_{i+1} can be found using equation 2.23, when $f(x_i)$ and $f'(x_i)$ are known (i.e., respectively the function and the derivative of the function (also equal to $\tan(\alpha)$). It can be seen that, when the Newton-Raphson method is repeated from point x_{i+1} , again a better approximation will be obtained for the root. Hence, when this procedure is repeated a number of times, a very good estimation of the root is obtained in this way.

Afterwards, the procedure for the solution of differential equations is started again, but for the *next time step* (with a new boundary condition for the potential at the powered electrode). Note that the equations are solved in such a way that the results of the next time-step ($t_{k+\Delta t}$) depend also on the previous time-step (t_k), due to the fact that the time derivative term is also discretized. The time derivative term for a variable n can be written as:

$$\left(\frac{\partial n}{\partial t} \right) = \frac{n^{k+1} - n^k}{\Delta t} \quad (2.24)$$

with Δt equal to the time step, and n^k the value known from the previous time-step. The unknown value n^{k+1} (value at the present time $t + \Delta t$) is the value which has to be calculated. Note that in the model, a Backward Euler method is used, considering values of three time steps. In order to obtain exact results at this time-step, the Newton convergence method is also applied for this time-step.

Afterwards, this procedure is repeated for the whole rf-cycle (i.e., 80 time-steps). Further, a large number of rf-cycles have to be calculated, in order to obtain convergence.

The convergence criterion of the fluid model is defined as the error between the discharge parameters (densities of the various species, potential, electron energy, electron density) at the beginning of two subsequent rf periods, and is typically set to $10^{-6} - 10^{-7}$. Further, also the plasma-chemistry (neutral-neutral, ion-neutral and ion-ion reactions) has to be calculated. For this procedure, normally a time step of 10^{-6} s is used.

As discussed above, the fluid model needs the electron reaction rate coefficients (as a function of average electron energy) obtained from the Boltzmann equation as input, and on the other hand the latter requires the densities of the background gases calculated from the fluid code in order to construct the look-up tables. Hence both parts (fluid part and EEDF part) are run iteratively until the changes in the density of the background gases are less than 10^{-4} . A general overview of the total numerical code can be found in figure 3.

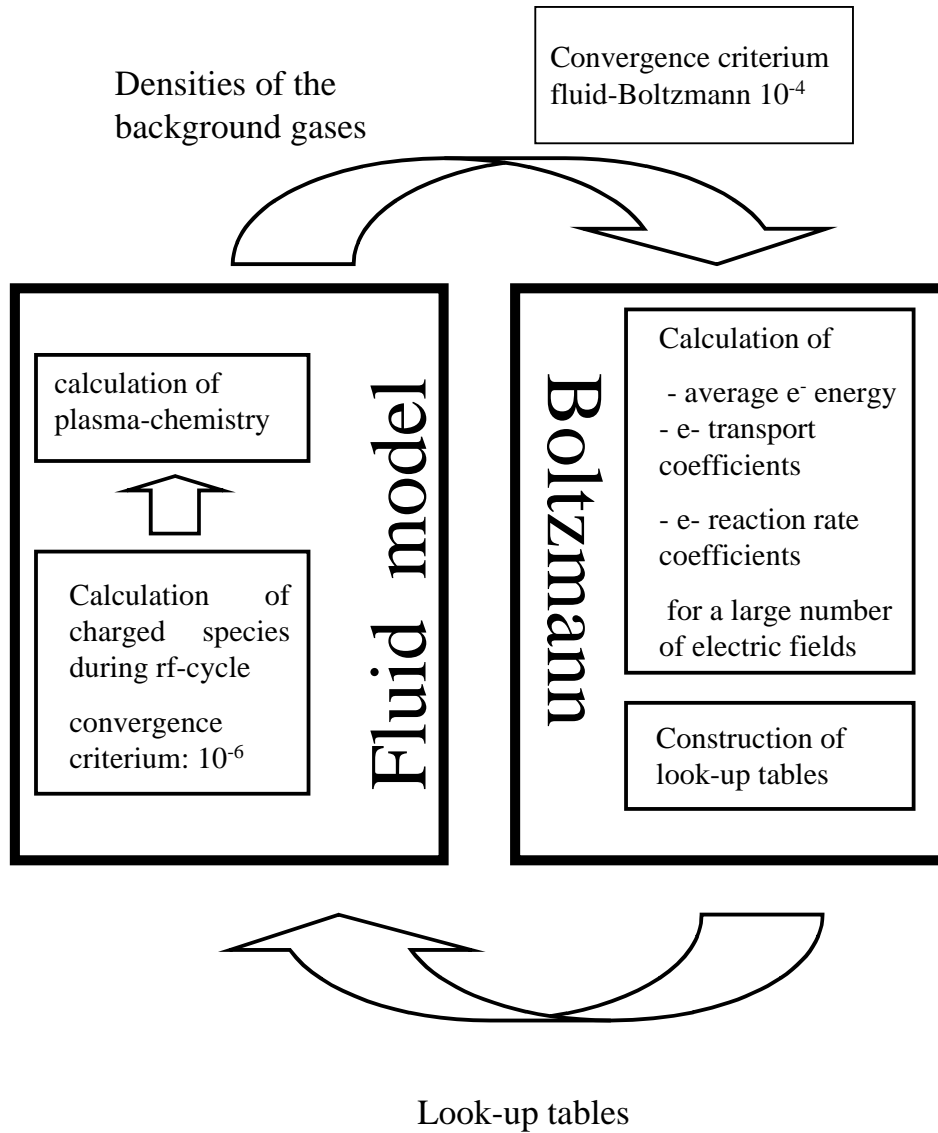


Figure 3: schematic overview of the numerical code

2.5. References

- [1] J. D. P. Passchier, W. J. Goedheer, *J. Appl. Phys.*, **74**, 3744 (1993)
- [2] W. J. Goedheer, P. M. Meijer, J. Bezemer, J. Diederick, P. Passchier, W. G. J. H. M. van Sark, *IEEE Transactions on Plasma Science*, **23**, 644 (1995)
- [3] D. Passchier, Ph. D. thesis, Utrecht, 1994
- [4] G. J. Nienhuis, W. J. Goedheer, E. A. G. Hamers, W. G. J. H. M. van Sark, J. Bezemer, *J. of Appl. Phys.*, **82**, 2060 (1997)
- [5] G. J. Nienhuis, W. J. Goedheer, *Plasma Sources Sci. Techn.*, **8**, 295, 1999
- [6] G.J. Nienhuis, Ph. D. thesis, Utrecht (1998)
- [7] P. M. Meijer, Ph. D. thesis, Utrecht (1991)
- [8] J. Perin, O. Leroy, M.C. Bordage, *Contrib. Plasma Phys.*, **36**, 3 (1996)
- [9] R.H. Svela, NASA Report, NASA-TR-132 (1962)
- [10] M.E. Coltrin, R.J. Kee, J.A. Miller, *J. Electrochemical Society*, **133**, 1206 (1986)
- [11] E.W. Mc Daniel, E.A. Mason, *The Mobility and Diffusion of ions in Gases*, John Wiley & Sons Inc., 1973
- [12] C.J.F. Böttcher, P. Bordewijk, *Theory of Electric Polarisation*, volume 2, Elsevier Scientific Publishing company, Amsterdam, 178
- [13] A. Von Keudell, W. Möller, *J. Appl. Phys.*, **75**, 7718 (1994)
- [14] A. D. Anderson, J. C. Tannehill, R. H. Pletcher, *Computational Fluid Mechanics and Heat Transfer*, New York, McGraw-Hill, 1984
- [15] S. V. Patankar, *Numerical Heat Transfer and Fluid Flow*, Memisphere Publishing Corporation, 1980
- [16] T. M. R. Ellis, *Fortran 77 Programming, second edition*, Adison-Wesley Publishing Company, Wokingham (UK), 1993

Chapter 3: Results of the 1D model for a methane plasma

3.1. The fluid model applied to a methane/hydrogen plasma

In this chapter, a 1D fluid model is applied to the modelling of methane plasmas. Results are presented for a variety of plasma conditions (pressure, power, gas inlet flow). In order to validate the methane plasma model, the calculated species densities are compared with experimental results (species densities) from literature.

After a sensitivity analysis, it was found that the methane/hydrogen plasma could be modelled in a realistic way using 20 species. An overview of the species (electrons, ions, radicals and background neutrals) taken into account in the model is given in table 1.

Neutrals		Ions			Radicals	
CH ₄	H ₂	CH ₄ ⁺	CH ₃ ⁺	H ₂ ⁺	C ₂ H ₅	CH ₃
C ₂ H ₆	C ₃ H ₈	CH ₅ ⁺	C ₂ H ₅ ⁺	H ₃ ⁺	CH ₂	CH
C ₂ H ₄	C ₂ H ₂	C ₂ H ₄ ⁺	C ₂ H ₂ ⁺		H	

Table 1: Different species taken into account in the methane plasma model, beside electrons

First of all, the inlet gas (CH₄ or a mixture of CH₄/H₂) plays an important role in the plasma, and it is present in the plasma at high density. It is found in the literature [1, 2] that also higher order neutral molecules (C₂H₆, C₃H₈, C₂H₄, C₂H₂) are formed in the plasma at high densities; hence these species are also included in our model. Although we have included for every non-radical neutral molecule two or more vibrational excitation reactions, these vibrationally excited species are not taken into account separately in order to limit the number of species in the model. Furthermore, 8 ionic and 5 radical species are included in the model (see Table 1). It is experimentally found that some other radical and ionic species (e.g., C₂H₃, C₃H₄, C₂H₃⁺, ...) are present in a methane plasma, but because they have lower densities [3], they are not considered in our model. Negative ions (mainly CH₂⁻ and H⁻) are not incorporated either, because it is found [4] that the negative ion density in a methane plasma is about one order of magnitude lower than the electron and positive ion densities. Hence, a CH₄ plasma has a strong electropositive character. This is in

contrast to a SiH₄ plasma, where negative ions play a much more important role in the plasma (electronegative discharge) [5].

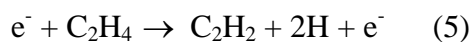
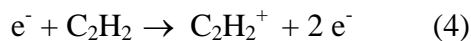
3.2. Electron impact collisions taken into account in the model

An overview of the electron impact reactions (i.e., ionisation, dissociation and vibrational excitation) considered in the model is given in Table 2.

Reaction	Chemical reaction	Ref.
CH₄		
vibr. exc.	$e^- + \text{CH}_4 \rightarrow \text{CH}_4^* + e^-$ (2)	6
ionisation	$e^- + \text{CH}_4 \rightarrow \text{CH}_4^+ + 2 e^-$	6
ionisation	$e^- + \text{CH}_4 \rightarrow \text{CH}_3^+ + \text{H} + 2 e^-$	6
dissociation	$e^- + \text{CH}_4 \rightarrow \text{CH}_3 + \text{H} + e^-$	7
dissociation	$e^- + \text{CH}_4 \rightarrow \text{CH}_2 + 2 \text{H} + e^-$	7
H₂		
vibr. exc.	$e^- + \text{H}_2 \rightarrow \text{H}_2^* + e^-$ (3)	8
dissociation	$e^- + \text{H}_2 \rightarrow 2 \text{H} + e^-$	9
ionisation	$e^- + \text{H}_2 \rightarrow \text{H}_2^+ + 2 e^-$	10
C₂H₆		
vibr. exc.	$e^- + \text{C}_2\text{H}_6 \rightarrow \text{C}_2\text{H}_6^* + e^-$ (3)	11
ionisation	$e^- + \text{C}_2\text{H}_6 \rightarrow \text{C}_2\text{H}_4^+ + \text{H}_2 + 2 e^-$	12
dissociation	$e^- + \text{C}_2\text{H}_6 \rightarrow \text{C}_2\text{H}_5 + \text{H} + e^-$	13
C₃H₈		
vibr. exc.	$e^- + \text{C}_3\text{H}_8 \rightarrow \text{C}_3\text{H}_8^* + e^-$ (2)	11
dissociation	$e^- + \text{C}_3\text{H}_8 \rightarrow \text{C}_2\text{H}_4 + \text{CH}_4 + e^-$	13
C₂H₄		
vibr. exc.	$e^- + \text{C}_2\text{H}_4 \rightarrow \text{C}_2\text{H}_4^* + e^-$ (2)	11
ionisation	$e^- + \text{C}_2\text{H}_4 \rightarrow \text{C}_2\text{H}_4^+ + 2 e^-$	11
dissociation	$e^- + \text{C}_2\text{H}_4 \rightarrow \text{C}_2\text{H}_2 + 2\text{H} + e^-$	11
C₂H₂		
vibr. exc.	$e^- + \text{C}_2\text{H}_2 \rightarrow \text{C}_2\text{H}_2^* + e^-$ (3)	11
ionisation	$e^- + \text{C}_2\text{H}_2 \rightarrow \text{C}_2\text{H}_2^+ + 2 e^-$	11

Table 2 : Electron reactions with molecules, taken into account in our model.

The number of different vibrational excitation reactions is given between brackets in Table 2. Electronic excitation reactions were not included in the model because it is found in the literature that for methane all excited states of these molecules lead to dissociation [14]. The same is true for silane and disilane [15], Hence we have also assumed that the electron reactions causing electronically excited states for the higher order neutrals (C_2H_6 , C_3H_8 , C_2H_4 , C_2H_2) lead to dissociation. Information about the cross sections of rotational excitation of the various non-radical neutral molecules is very difficult to find, but since rotational excitation takes clearly less energy away from the electrons than vibrational excitation, it is justified not to include rotational excitation in the model. The references of cross sections used in the model for the various reactions are also indicated in Table 2. For a methane plasma, detailed information about the cross sections is known from the literature [6 - 11]. In order to obtain a detailed description of the different species in the plasma, “partial” cross sections were used in the model instead of the total cross sections. However, for the following electron reactions, no information about the corresponding cross sections could be obtained:



Therefore, the following approximations are made. For reactions 1 and 2, the total dissociation cross section of C_2H_6 [13] is used, hence no other dissociation channel is considered. For reactions 3 and 4, the total ionisation cross sections of C_2H_4 and C_2H_2 were taken (hence assuming that $C_2H_4^+$ and $C_2H_2^+$ are the only ionisation products). It is mentioned in the literature [16, 17] that reaction 5 is also very important, but no information about this cross section was found. Therefore, we used a cross section based on the combination of two excitation cross sections [11]. This is assumed to be a good approximation because it is stated [14, 15] that all excited states of the smaller molecules (CH_4 , SiH_4 and Si_2H_6) lead to dissociation. Moreover it will be demonstrated further that this approximation gives results comparable with data found in the literature. Finally, the cross sections of the momentum transfer reactions of the

background neutrals, necessary for the solution of the Boltzmann equation (see chapter 2), are taken from [8] for H_2 , and from [6] for the hydrocarbon molecules (CH_4 , C_2H_2 , C_2H_4 , C_2H_6 , C_3H_8). These cross sections are not mentioned explicitly in table 2.

3.3. Ion reactions included in the model

Seven ion-neutral reactions have been included in the model. An overview of these reactions, as well as the reaction rate coefficients can be found in Table 3.

Ion-neutral reactions	Reaction rate coefficient (m^3/s)	Ref.
$CH_4^+ + CH_4 \rightarrow CH_5^+ + CH_3$	1.5×10^{-15}	18
$CH_3^+ + CH_4 \rightarrow C_2H_5^+ + H_2$	1.2×10^{-15}	18
$CH_5^+ + C_2H_6 \rightarrow C_2H_5^+ + CH_4 + H_2$	5.0×10^{-16}	18
$H_2 + H_2^+ \rightarrow H_3^+ + H$	2.5×10^{-15}	19
$H_3^+ + CH_4 \rightarrow CH_5^+ + H_2$	1.6×10^{-15}	19
$H_3^+ + C_2H_6 \rightarrow C_2H_5^+ + 2 H_2$	2.0×10^{-15}	19
$H_3^+ + C_2H_4 \rightarrow C_2H_5^+ + H_2$	1.9×10^{-15}	19

Table 3: Ion-neutral reactions taken into account in the model

The first three reactions are taken from [18], whereas the reactions involving H_3^+ ions are adopted from [19]. Although some more ion-neutral reactions have been taken into account in the methane model described in [18], it is found from our calculations (see further) that the present plasma model with 7 ion-neutral reactions gives results comparable with (experimental and calculated) data found in the literature for a wide range of process parameters (pressure, gas inlet flow, power).

3.4. Neutral-neutral reactions incorporated in the model

In Table 4, an overview is given of the neutral-neutral reactions included in the plasma model.

Neutral-neutral reactions	Reaction rate coefficient (m ³ /s)	Ref.
$\text{CH}_3 + \text{CH}_3 \rightarrow \text{C}_2\text{H}_6$	3.7×10^{-17}	18
$\text{CH}_3 + \text{H} \rightarrow \text{CH}_4$	7.0×10^{-18}	18
$\text{C}_2\text{H}_5 + \text{H} \rightarrow \text{CH}_3 + \text{CH}_3$	6.0×10^{-17}	18
$\text{C}_2\text{H}_5 + \text{CH}_3 \rightarrow \text{C}_3\text{H}_8$	4.2×10^{-18}	18
$\text{CH}_2 + \text{H} \rightarrow \text{CH} + \text{H}_2$	2.7×10^{-16}	18
$\text{CH} + \text{CH}_4 \rightarrow \text{C}_2\text{H}_5$	1.0×10^{-16}	18
$\text{CH}_2 + \text{CH}_4 \rightarrow \text{CH}_3 + \text{CH}_3$	^a 1.7×10^{-17}	1
$\text{CH}_2 + \text{CH}_4 \rightarrow \text{C}_2\text{H}_4 + \text{H}_2$	^a 1.7×10^{-17}	1
$\text{CH}_4 + \text{CH} \rightarrow \text{C}_2\text{H}_4 + \text{H}$	^a 1.0×10^{-16}	1
$\text{CH}_3 + \text{CH}_2 \rightarrow \text{C}_2\text{H}_4 + \text{H}$	3.3×10^{-17}	1
$\text{C}_2\text{H}_5 + \text{H} \rightarrow \text{C}_2\text{H}_4 + \text{H}_2$	3.0×10^{-18}	1
$\text{CH}_2 + \text{CH}_2 \rightarrow \text{C}_2\text{H}_2 + \text{H}_2$	1.1×10^{-17}	4

Table 4: Neutral-neutral reactions incorporated in the model

Tachibana et al. [1] described a plasma model with 23 neutral-neutral reactions. We considered only the 12 most important neutral-neutral reactions in order to keep the computational effort low. It can be found from [1] that a CH_4 molecule reacts with a CH_2 radical to form the excited molecule C_2H_6^* , which dissociates rapidly into two CH_3 radicals. Since the dissociation occurs on a short timescale, no excited intermediate state molecules are taken into account in our model. The same applies for some other neutral-neutral reactions, marked with an ‘a’ in Table 4.

3.5. Results and discussion

Typical results of the fluid model are the densities of the various species, the electric field and the electron density as a function of distance between the electrodes and as a function of time in the rf cycle. Moreover, information is obtained about the fluxes of the different species towards the electrodes, and about the plasma characteristics (rf voltage, plasma potential, ohmic heating of the electrons and various ions). In this work, we will concentrate on the calculated density profiles of the various plasma species between the electrodes. The effect of power, gas mixture (CH_4/H_2), gas inlet flow and pressure will be investigated. The parameter ranges for which the calculations are performed are given in table 5.

Discharge parameters	Value
RF-frequency	13.56 MHz
Electrode spacing	0.03 m
Electrode radius	0.1 m
Gas temperature	400 K
Power	15-100 W
CH_4 gas flow	5-25 sccm
H_2 gas flow	0-10 sccm
Pressure	0.14-0.5 Torr

Table 5: Discharge parameters for which the calculations are performed. The power, CH_4 and H_2 gas flow and the pressure are varied in the range indicated, in order to investigate their effect on the calculated results.

3.5.1. Calculated densities of the plasma species versus distance in the plasma

Figure 1 illustrates the calculated densities of the non-radical neutral molecules, the radicals and the ions considered in the model at 0.14 Torr, 25 W, 13.56 MHz and 20 sccm CH₄ inlet.

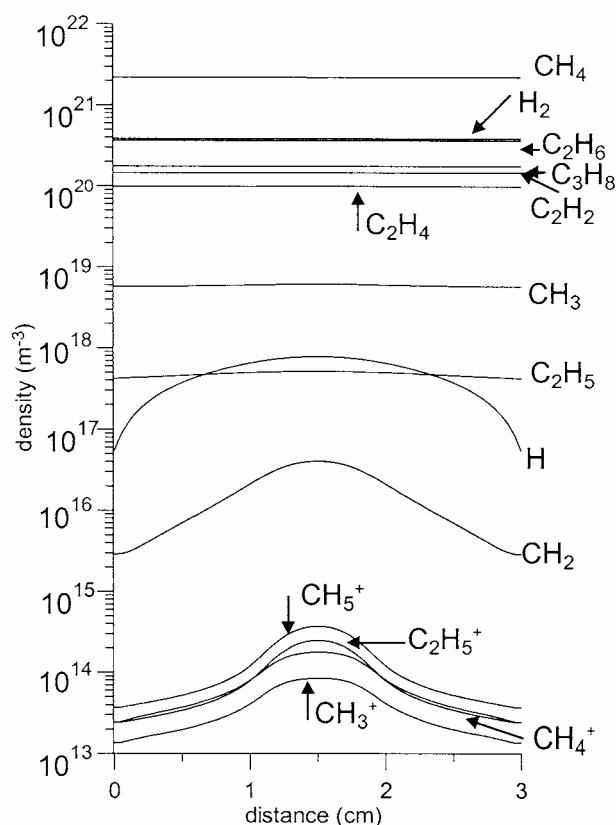


Figure 1: Calculated densities of the non-radical neutrals, radicals and ions as a function of distance from the electrode at 0.14 Torr, 25 W, 13.56 MHz and 20 sccm inlet methane (no H₂ inlet).

The densities of the background neutrals (CH₄, H₂, C₂H₆, C₂H₄, C₂H₂, C₃H₈) are homogeneously distributed between the electrodes. It can be seen that the higher order hydrocarbon molecules (C₂H₆, C₂H₄, C₂H₂, C₃H₈), which are formed by the neutral-neutral reactions mentioned in table 4, are not negligible compared to CH₄ (i.e., only one order of magnitude lower density). The presence of these higher order hydrocarbon molecules at high densities in a methane plasma differs from a silane plasma, where only SiH₄, H₂ and Si₂H₆ are present at such high densities [5]. By means of mass spectrometry, Dagel et al. [2] measured the partial pressures of these background neutrals in an rf methane plasma. These experiments have been carried out under somewhat different experimental conditions (0.03 Torr, methane gas flow

varying between 2.4-10.4 sccm) than the parameters used in our theoretical calculations. However, the same tendency (i.e. the presence of the higher order hydrocarbon molecules in the plasma) was found. It should be mentioned that the influence of the gas inlet and the background pressure on the relative abundancies of the species densities is rather small (see figures 6 and 7 further in this chapter), so that the comparison of the experimental data with our calculated result is justified.

Further, it follows from figure 1 that the most important radical in the plasma is found to be CH_3 with a density of about $5 \times 10^{18} \text{ m}^{-3}$ (more or less constant throughout the plasma). This is in agreement with the experimental density of CH_3 (about 10^{18} m^{-3} at 0.123 Torr and 10 W) obtained by Sugai et al. [20], and the density calculated by Bera et al [21] (about 10^{18} m^{-3} at 0.123 Torr). The calculated CH_2 radical density (in the order of 10^{16} m^{-3}) also agrees with the results measured by Sugai et al. [20] (i.e., also in the order of 10^{16} m^{-3} (at 0.123 Torr and 10 W)).

The calculated density of the C_2H_2 molecules (about 10^{20} m^{-3}) is also in good agreement with the C_2H_2 density (10^{20} m^{-3} at 0.2 Torr and 500 W) measured by Wormhoudt [22]. Although the power used in the experiment (500 W) is much higher than the power assumed in the calculation (25 W), the density values are the same. This is however logical because our calculations predict that the densities of the non-radical molecules do not vary significantly with power (see figure 3 below). In general, the densities calculated with our model also correspond with the results obtained by Tachibana [1], who calculated the densities of a variety of species in a wide range of power ($10^{-1} - 10^3 \text{ W}$) at 0.22 Torr.

Finally, figure 1 presents also the densities of the ions in the plasma. Only the densities of the most important ions (CH_5^+ , C_2H_5^+ , CH_4^+ and CH_3^+) are shown; the densities of the other ions considered in the model (C_2H_4^+ , C_2H_2^+ , H_2^+ and H_3^+) are not given. Note that the C_2H_4^+ and C_2H_2^+ densities actually represent the group of ions (i.e., for C_2H_4 : C_2H_4^+ , C_2H_3^+ , C_2H_2^+ , CH_3^+ , CH_2^+) formed in the ionisation reactions with C_2H_4 and C_2H_2 respectively. The reason is that we used the total ionisation cross sections for these two reactions. It should be noted that for the ion density the time averaged value is given, because the ion density changes slightly with time in the sheath zone. The densities of the radicals and neutrals, on the other hand, do not change as a function of time.

The electron density is found to be in the order of $10^{15} \text{ electrons/m}^3$. In figure 2, the electron density is shown at 4 phases ($\pi/2$, π , $3\pi/2$, 2π) of the rf cycle. It can be seen

that the electron density changes strongly as a function of time in the sheath zone, whereas the density in the bulk plasma stays nearly constant.

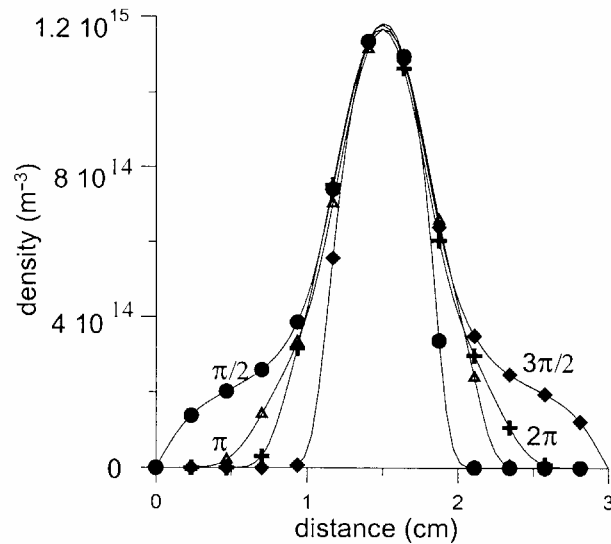


Figure 2: Calculated electron density at 4 phases of the rf cycle ($\pi/2$ (●), π (▲), $3\pi/2$ (◆) and 2π (+)) at 0.14 Torr, 25 W, 13.56 MHz and 20 sccm inlet methane (no H_2 inlet).

3.5.2. The effect of varying power

We have carried out 6 simulations in the power range between 15 W and 100 W, while all other plasma parameters were kept constant (see 3.1.). The densities (in the middle of the plasma) of the most important non-radical neutral background molecules, the electrons, the ions and the radicals are plotted in figure 3 as a function of power.

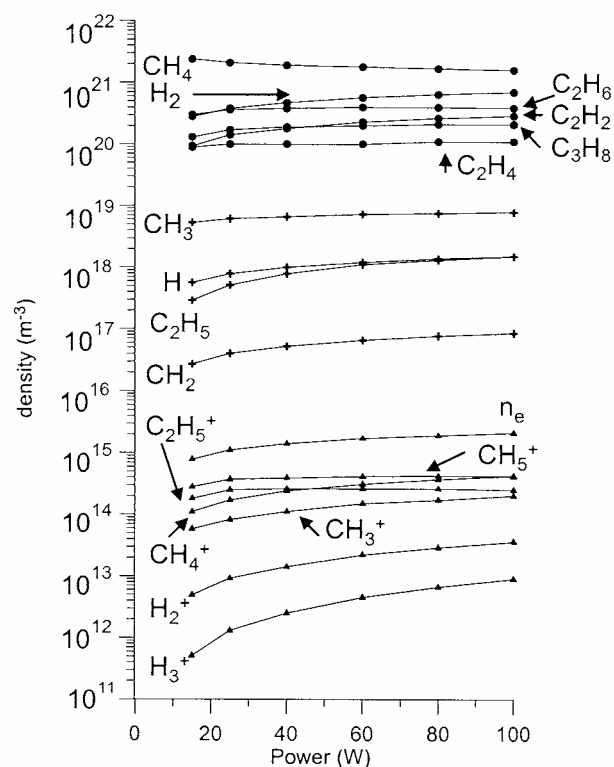


Figure 3: Calculated densities of the non-radical neutrals (●), radicals (+), ions and electrons (▲) as a function of power going into the plasma at 0.14 Torr, 25 W, 13.56 MHz and 20 sccm inlet methane (no H₂ inlet).

From this figure, it can be seen that the CH₄ density decreases somewhat (more consumed in the reactions) with increasing power, whereas all the other plasma species densities (non-radical neutrals, radicals, ions and electrons) are slightly increasing. The tendencies in our results are in agreement with the results found by Tachibana [1], who performed simulations in a much wider range of power ($10^{-1} - 10^3$ W) for a similar discharge pressure (0.22 Torr). Good agreement was also reached between our results and the calculated densities of the radicals and the neutrals found by Rhallabi [23] at 0.08 Torr and by Gogolides [4] at 0.14 Torr.

The most important ion at low power (15 W) is clearly found to be CH₅⁺, while at the highest power (100 W) CH₄⁺ becomes equally important. The electron density increases from about $8 \times 10^{14} \text{ m}^{-3}$ at 15 W to about $2 \times 10^{15} \text{ m}^{-3}$ at 100 W.

Dekempeneer et al. [24] have measured, by use of mass spectrometry, the so-called conversion factor of CH₄ under varying power conditions (0-120 W), at different pressures. The conversion factor cf was defined by [24]:

$$cf = 1 - \frac{I}{I_0}$$

where I and I_0 are the CH_4 densities in the plasma when the discharge was on and off respectively. It is worthwhile mentioning that although this factor was called “dissociation degree” in [24], we prefer to call it *conversion factor*, because the term gives information about how many methane molecules have reacted, not only due to dissociation but also to ionisation and neutral-neutral reactions. A comparison between the experimental and calculated values for the conversion factor as a function of power, at the same plasma conditions as in the experiment (20 Pa, 8 sccm CH_4 and 4 sccm H_2), is given in figure 4.

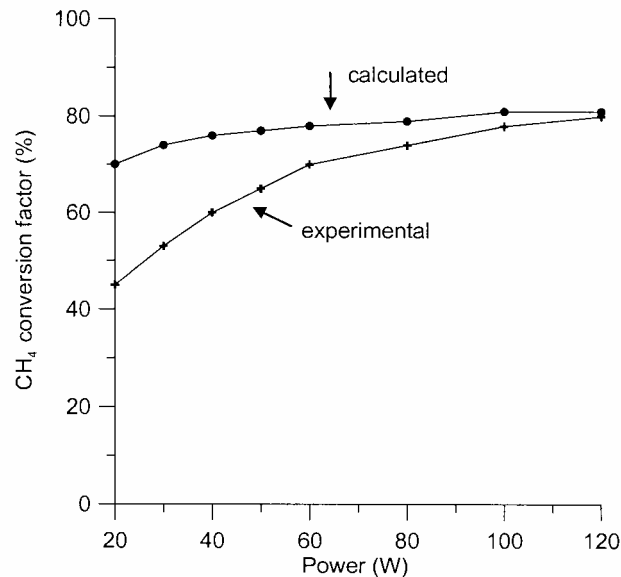


Figure 4: Comparison between the experimental and calculated methane conversion factor as a function of power.

It can be seen that in both cases the conversion factor increases with rising power. At higher power, a good agreement was reached, whereas at low power the agreement is less satisfactory. It should be noted that the power values used in the model (and in the figures) correspond to the powers that are effectively put into the plasma. It is generally known that not all the power from the rf generator effectively goes into the plasma, but the exact percentage is not known. We assumed that the *power going into the plasma is 50 %* of the generator power, in analogy to [5]. Hence, it is very difficult

to compare the calculated and experimental results in absolute terms, but the general trends appear to be already in satisfactory agreement.

3.5.3. Effect of varying gas flow mixture

To investigate the effect of the gas flow mixture, the latter was changed from 20 sccm pure CH₄ to a mixture of 10 sccm CH₄ and 10 sccm H₂ (with intervals of 2 sccm). All the simulations were carried out with a total gas flow of 20 sccm while all other plasma parameters were kept constant (see 3.5.1.). The results of these simulations can be found in figure 5 for the densities of the neutral molecules, the radicals, the ions, and the electrons.

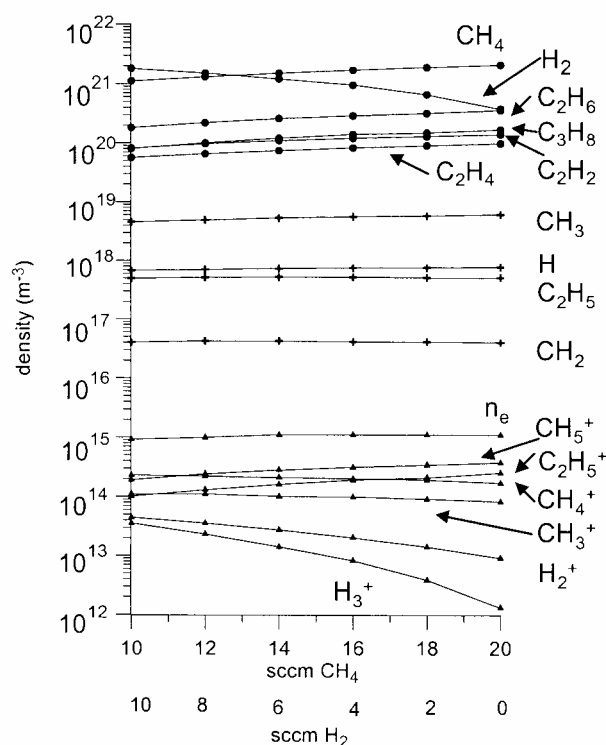


Figure 5: Calculated densities of the non-radical neutrals (●), radicals (+), ions and electrons (▲) as a function of CH₄ and H₂ gas flow mixture. The total gas flow is kept constant at 20 sccm; the CH₄ gas flow varies between 10 and 20 sccm, whereas the H₂ gas flow varies between 0 and 10 sccm at 0.14 Torr, 25 W, 13.56 MHz

On this semi-log plot, the densities of the non-radical neutrals increase in the same linear way with rising CH₄ sccm gas flow, except for the H₂ density, which is logical because the H₂ gas flow decreases. The densities of the radicals appear not to be

significantly influenced by the change of CH₄/H₂ gas flow mixture, except for the density of CH₃, which increases slightly with increasing CH₄ gas flow. As far as the ions are concerned, the H₂⁺ and H₃⁺ ion densities decrease more drastically with rising CH₄ gas flow (as is expected, because of the decreasing H₂ gas flow) than the CH₄⁺ and CH₃⁺ densities, which also decrease to a certain extent. The densities of the CH₅⁺ and C₂H₅⁺ ions, on the other hand, appear to increase with rising CH₄ gas mixture. This can be explained by the ion-neutral reactions which create mainly CH₅⁺ and C₂H₅⁺ at rising CH₄ gas flow.

3.5.4. Effect of varying total gas flow

The calculated densities of the non-radical neutral molecules, the radicals, the ions and the electrons as a function of increasing total gas flow (i.e., 5 - 25 sccm CH₄, no H₂) are shown in figure 6. All other plasma parameters were kept constant (see 3.5.1.).

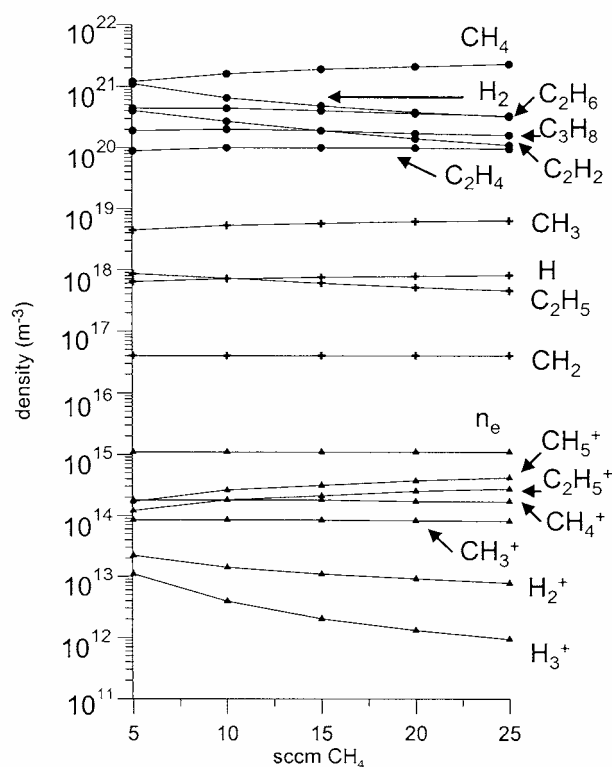


Figure 6: Calculated densities of the non-radical neutrals (●), radicals (+), ions and electrons (▲) as a function of CH₄ sccm (no H₂ inlet) at 0.14 Torr, 25 W, 13.56 MHz.

As can be seen from figure 6, the CH_4 density increases with rising CH_4 gas inlet flow, which is logical. The densities of the other species remain more or less constant, or decrease slightly. As a consequence of the constant pressure, the residence time of the different species decreases when the inlet flow of CH_4 rises. When the residence time of the species decreases, the molecules are pumped out of the reactor more rapidly. This implies that less reactions (neutral-neutral and ion-neutral reactions) can occur between these molecules, so less H_2 is formed. Indeed, H_2 is the major reaction product in most of the reactions (see tables 3 and 4). This explains why the H_2 density decreases when more CH_4 is introduced in the reactor at constant pressure. The densities of the radicals and the hydrocarbon ions (CH_5^+ , C_2H_5^+ , CH_4^+ , CH_3^+) are not heavily influenced by changing the CH_4 gas flow. The H_2^+ and the H_3^+ ion densities drop more clearly with rising CH_4 gas flow, because less H_2 is present in the plasma (see above) and because H_2^+ reacts further to H_3^+ , which afterwards reacts to CH_5^+ or C_2H_5^+ by ion-neutral reactions.

3.5.5. Effect of varying pressure

In order to study the effect of gas pressure, 5 simulations were carried out in the range varying from 0.14 Torr to 0.5 Torr. The densities of the non-radical neutrals, the radicals, the ions and the electrons are plotted as a function of pressure in figure 7.

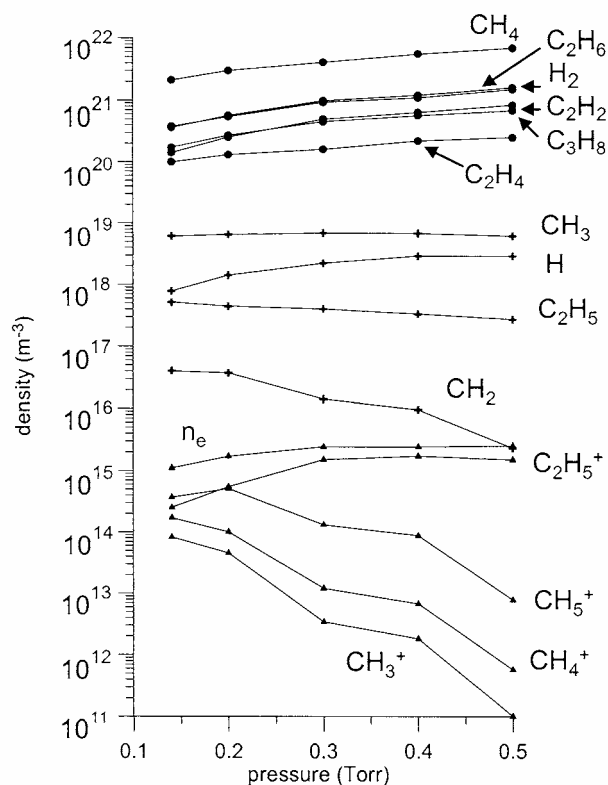


Figure 7: Calculated densities of the non-radical neutrals (●), radicals (+), ions and electrons (▲) as a function of gas pressure at 0.14 Torr, 25 W, 13.56 MHz

The densities of the non-radical neutrals increase slightly for all species as a function of pressure. The densities of the radicals do not vary significantly with pressure. Only CH₂ decreases significantly at rising pressures, because it is consumed in the neutral-neutral reactions, which are more important at higher pressures. The C₂H₅⁺ ion density increases to the same extent with rising pressure as the non-radical neutrals, while all the other ion densities (CH₅⁺, CH₄⁺, CH₃⁺) drop drastically. This can be explained by the fact that at higher pressures ion-neutral reactions become more important. As can be seen from table 3, in most of the ion-neutral reactions, CH₅⁺ and C₂H₅⁺ are formed. CH₅⁺ can also react further to C₂H₅⁺, hence this explains why C₂H₅⁺ becomes the major ion at higher pressures.

3.5.6. Information of the fluxes towards the electrodes.

As mentioned in 2.2.5., the growth of the layer depends on the fluxes of the radical and ionic species towards the electrodes. In figure 8, the fluxes ($\text{m}^{-2}\text{s}^{-1}$) of the radicals (CH_3 , CH_2 , C_2H_5 , H) and ions (CH_4^+ , CH_3^+ , CH_5^+ , C_2H_5^+) are presented as a function of power. The other plasma parameters were kept constant (see 3.5.1.). It can be seen from figure 8 that all the fluxes increase slightly as a function of power. Because no bias voltage can be applied in the 1D model, the fluxes towards both electrodes (powered and grounded electrode) are the same.

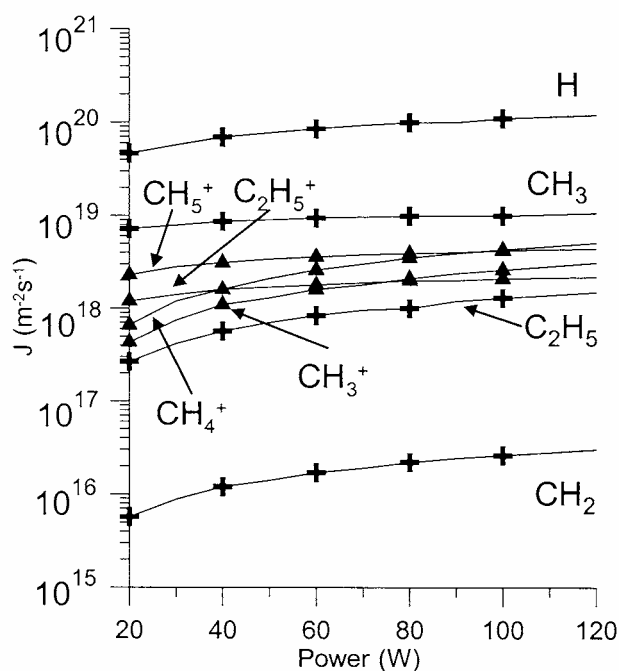


Figure 8: Calculated radical (CH_3 , CH_2 , C_2H_5 , H) and ion (CH_4^+ , CH_3^+ , CH_5^+ , C_2H_5^+) fluxes towards the electrodes as a function of power at 0.14 Torr, 25 W, 13.56 MHz.

3.6. References

- [1] K. Tachibana, M. Nishida, H. Harima, Y. Urano, *J. Phys. D., Appl. Phys.*, **17**, 1727 (1984)
- [2] D.J. Dagel, C.M. Mallouris, J.R. Doyle, *J. Appl. Phys.*, **79**, 8735 (1996)
- [3] G. Smolinski, M.J. Vasile, *International Journal of Mass Spectrometry and Ion Physics*, **16**, 137 (1975)
- [4] E. Gogolides, D. Mary , A. Rhaballi, G. Turban, *Jpn. J. Appl. Phys.*, **34**, 261 (1995)
- [5] G.J. Nienhuis, W.J. Goedheer, E.A.G. Hamers, W.G.J.H.M Van Sark., J. Bezemer, *J. Appl. Phys.*, **82** , 2060 (1997)
- [6] H. Tawara, Y. Itikawa, H. Nishimura, H. Tanaka, Y. Nakamura, *Research Report NIFS-DATA6*, ISSN 0915-6364, Nagano (JAPAN), 1990
- [7] T. Nakanu, H. Toyoda, H. Sugai, *Japn. J. Apply. Phys.*, **30**, 2912 (1991)
- [8] L. Ehrhardt, L. Langhans, F. Linder, H.S. Taylor, *Phys. Rev.*, **173**, 222 (1968)
- [9] A.G. Engelhardt, A.V. Phelps, *Phys. Rev.*, **131**, 2115 (1963)
- [10] H. Tawara, T. Kato, *At. Data and Nucl. Data Tables*, **36**, 167 (1987)
- [11] H. Tawara, *Electron Collision Processes involving Hydrocarbons (Chapter 16)*, *Atomic And Molecular Processes in Fusion Edge Plasmas*, R. K. Janev, Plenum Press, New York, 1995
- [12] H. Chatman, D. Hils, R. Robertson, A. Gallagher, *J. Chem. Phys.*, **81**, 1770 (1984)
- [13] F. Winters, *Chemical Physics*, **36**, 353 (1979)
- [14] W.L. Morgan, *Plasma Chemistry and Plasma Processing*, **12**, 477 (1992)
- [15] J. Perin, O. Leroy, M.C. Bordage, *Contrib. Plasma Phys.*, **36**, 3 (1996)
- [16] M. Masi, C. Cavalotti, S. Carrà, *Chemical Engineering Science*, **53**, 3875 (1998)
- [17] R. Gordon, P. Ausloos, *J. of Chem. Phys.*, **47**, 1977 (1967)
- [18] L.E. Kline, W.D. Partlow, W.E. Bies, *J. Appl. Phys.*, **65**, 70 (1988)
- [19] J.A. Burt, J.L. Dunn, M.J. McEwan, M.M. Sutton, A.E. Roche, H.I. Schiff, *Journal of Chem. Phys.*, **52**, 6062 (1970)
- [20] H. Sugai, H. Koijma, A. Ishida, H. Toyoda, *Appl. Phys. Lett.*, **56**, 2616 (1990)
- [21] K. Bera, B. Farouk, Y.H. Lee, *J. of Electrochem. Soc.*, **146**, 3264 (1999)
- [22] J. Wormhoudt, *J. Vac. Sci. Technol. A.*, **8**, 1722 (1990)
- [23] A. Rhallabi, Y. Catherine, *IEEE Transactions on Plasma Science*, **19**, 270 (1991)

[24] E. Dekempeneer, J. Smeets, J. Meneve, L. Eersels, R. Jacobs, *Thin Solid Films*, **241**, 269 (1994)

Chapter 4: Comparison between a one-dimensional and a two-dimensional fluid model for a methane plasma

4.1. Introduction

In this chapter, the one-dimensional fluid model for a rf methane plasma, described in chapter 3, is extended to two dimensions, and a comparison is made between the one-dimensional (1D) and two-dimensional (2D) fluid model. Both fluid models consider the same species (i.e., 20 in total; neutrals, radicals, ions and electrons) and the same electron-neutral, ion-neutral and neutral-neutral reactions (described in chapter 3). Whereas the 1D fluid model considers only the distance between the electrodes (axial direction), the 2D fluid model takes into account the axial as well as the radial direction (i.e., distance between the electrodes and the radius of the plasma reactor, respectively). Hence, the 2D fluid model can give additional information on the plasma species and fluxes towards the electrodes, as a function of electrode radius.

4.2. Description of the 2D fluid model

As mentioned above, the two-dimensional fluid model considers the same species and reactions as in the one-dimensional model (see chapter 3). A scheme of the reactor (cylindrically symmetrical) geometry is given in figure 1.

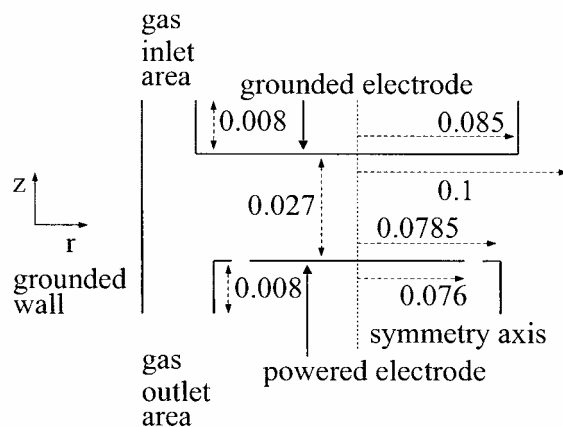


Figure 1: Schematic diagram of the cylindrically symmetric plasma reactor (with H-geometry) used for the 2D calculations. The various dimensions are indicated in m.

This kind of reactor is often used for the deposition of thin layers on materials [1, 2]. The distance between the electrodes is 2.7 cm, whereas the total radius of the plasma

reactor is 10 cm. The geometry is a so-called (cylindrically symmetrical) H-geometry. On the upper side, the grounded electrode (with a radius of 8.5 cm) is located next to the inlet region. On the lower side, the rf powered electrode (with a radius of 7.6 cm) is situated next to the outlet region. Except for the rf electrode, all other surfaces are grounded. The gas inlet and outlet are situated near the grounded and powered electrode respectively.

In order to avoid numerical instabilities in the numerical method, the grid should contain enough grid points in z and r-position. The distance between the electrodes (2.7 cm) is divided in 96 grid points, while the r-position (10 cm) contains 72 grid points. The z-directions of the inlet and outlet region are further divided in 32 grid points.

The transport of the neutrals is assumed to be governed only by diffusion. Hence, no convective flow is taken into account. This seems justified when the distance between the electrodes is small enough (i.e. only a few centimetres) [2, 3], and when the gas inlet flow is rather small (i.e. 20 sccm in our case).

In the model, the applied voltage is prescribed as:

$$V_t = V_{rf} \sin(2\pi\nu_{rf}t) + V_{dc}$$

where V_{rf} is adapted to meet the preset power, in a similar way as in the 1-D model (see chapter 3).

Averaged over one rf cycle, the total electron and ion flux towards both electrodes must be equal to each other. In order to reach this condition at the powered electrode, a V_{dc} bias voltage arises. In the code, the value of V_{dc} is gradually adapted until the fluxes of the electrons and ions to the rf electrode, averaged over 1 rf-cycle, are equal to each other.

The disadvantage of the 2D fluid model is however, that these simulations are very computer intensive (i.e., the 2D fluid model can be regarded as a large number of 1D fluid models which have to be solved, in order to take into account the radial and axial direction). While the 1D simulation takes approximately half a day computer time on a professional workstation (alpha processor: EV67), the 2D fluid model requires nearly one week computer time.

4.3. Comparison of the results of the 1D and 2D fluid models.

Simulations have been carried out with both fluid models at four different power values: 5, 10, 15 and 20 W, whereas the other plasma parameters are kept constant. The rf-frequency is set to 13.56 MHz. The pressure is set to 0.225 Torr. The inlet gas flow is set to 20 sccm CH₄, while no H₂ is pumped in. For the 2 fluid models, the distance between the electrodes is set to 2.7 cm.

For the 1D fluid model for methane (chapter 3), an extensive comparison was already made between the calculated and experimental species densities available in the literature. In the 1D model, the densities of the charged species and the radicals reach a maximum in the middle of the plasma between the 2 electrodes. With the 2D fluid model, information is also obtained on the species densities as a function of radial direction. Figure 2 shows the electron density at four phases ($\pi/2$, π , $3\pi/2$, 2π) in the rf-cycle, calculated with the 2D fluid model, at a power of 5 Watt.

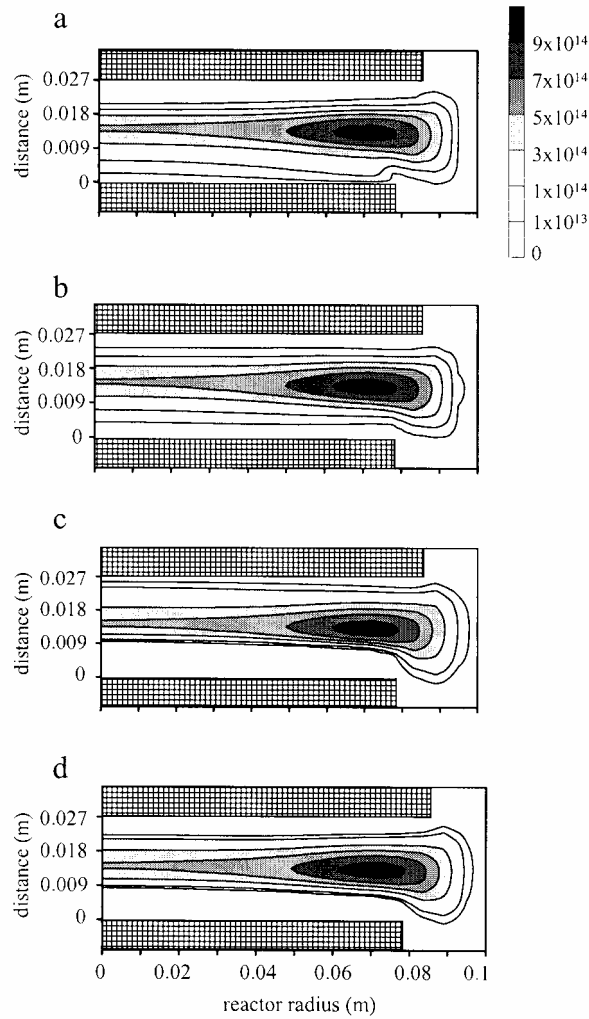


Figure 2: Calculated 2D electron density profiles (m^{-3}) at the four different phases in the rf-cycle, at a power of 5 W. (a: phase $\pi/2$, b: phase π , c: phase $3\pi/2$, d: phase 2π). The grounded and powered electrodes are situated respectively above and under in the reactor geometry. Note that only one side of the reactor is given.

As appears from this figure, the electron density (at the four phases in the rf-cycle) is at maximum (nearly 10^{15} m^{-3}) at a radial distance of about 7 cm, which corresponds more or less to the maximum radius of the powered electrode. Note that, while the electron density remains – more or less – the same in the plasma bulk zone, the electron density shows some large changes in both sheath zones, as a function of time. In figure 3, the potential distribution is given at four phases of the rf-cycle. From the potential, the electric field can be calculated ($E = -\nabla V$).

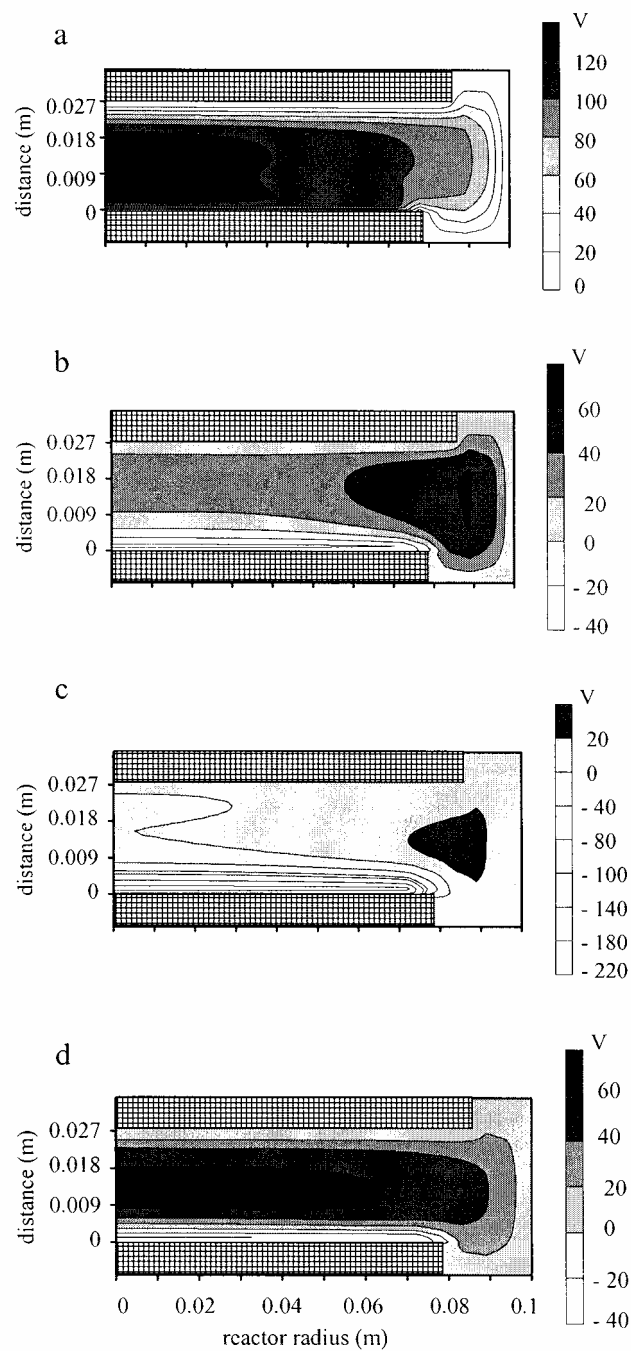


Figure 3: Calculated 2D potential profiles at the four different phases in the rf-cycle, at a power of 5 W. (a: phase $\pi/2$, b: phase π , c: phase $3\pi/2$, d: phase 2π).

Due to the larger potential differences at the end of the powered electrode (compared to the region near the cylinder axis), the electric field is larger in this region. Hence in this region, electrons will obtain more energy. This leads to more electron-neutral reactions (i.e., also ionisation reactions from which electrons are created) in this

region, resulting in a higher electron density (about 10^{15} m^{-3}), compared to the region near the axis (nearly $5 \times 10^{14} \text{ m}^{-3}$, see figure 2). Similar 2D electron density profiles are also found in [4, 5] for conditions comparable with our input parameters (power, frequency, pressure). Figure 4 shows the calculated time-averaged 2D ion density profile of the main ion species, i.e., CH_5^+ , at a power of 5 Watt. It is worth mentioning that for the ions, the changes of the ion densities in the sheath zones are relatively small. It is clear that the ion density is also at its maximum ($5 \times 10^{14} \text{ m}^{-3}$) at the edge of the electrode (i.e. radius of 7 cm).

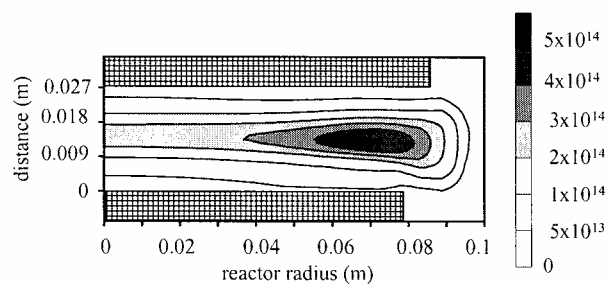


Figure 4: Calculated 2D time-averaged ion density profile of CH_5^+ (m^{-3}), at a power of 5 Watt.

This high ion density near the end of the powered electrode, can also be explained from the more frequent electron reactions in this region (which create these ions). The CH_5^+ density in the middle of the reactor, between the two electrodes, is of the order of $2 \times 10^{14} \text{ m}^{-3}$. It is interesting to note that all other ionic species are characterized by a similar profile, albeit at somewhat lower densities.

A density profile of CH_3 (the main radical) is given in figure 5.

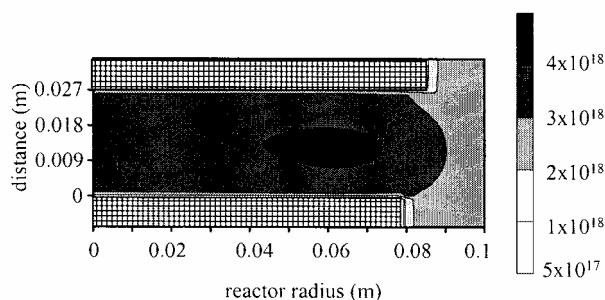


Figure 5: Calculated CH_3 density profile (m^{-3}), at a power of 5 W.

As can be seen from this figure, the highest CH_3 density (about $4 \times 10^{18} \text{ m}^{-3}$) is again obtained in the radial direction near the side end of the powered electrode, and halfway between the two electrodes in the axial direction. In this region, CH_3 is formed by electron-neutral reactions and neutral-neutral reactions. Outside the region between the two electrodes, the CH_3 radicals are also present at a relatively high density. This can be explained from the neutral-neutral reactions forming a considerable number of CH_3 radicals. It should be mentioned that analogous density profiles were also obtained for the other radicals present in the model (C_2H_5 , H, CH_2 and CH). However, for the CH_2 and CH radicals, the density is only high in the plasma region (i.e., the region between the 2 electrodes), and very low outside this region. These species are, indeed, not only formed, but predominantly consumed in the neutral-neutral reactions. The densities of the neutral molecules (CH_4 and others) are nearly uniformly distributed as a function of axial and radial directions. The calculated densities of the neutrals, radicals and ions are in agreement with the results obtained from other 2D models [4, 7], although somewhat different reactions and species are considered in the models.

In general, the species densities calculated for the conditions investigated with the 1D and 2D fluid models are in relatively good agreement. In Figure 6, the calculated densities (maximum value) as a function of power are given for the most important plasma species (CH_4 , H_2 , CH_5^+ , CH_4^+ , CH_3 and electron density).

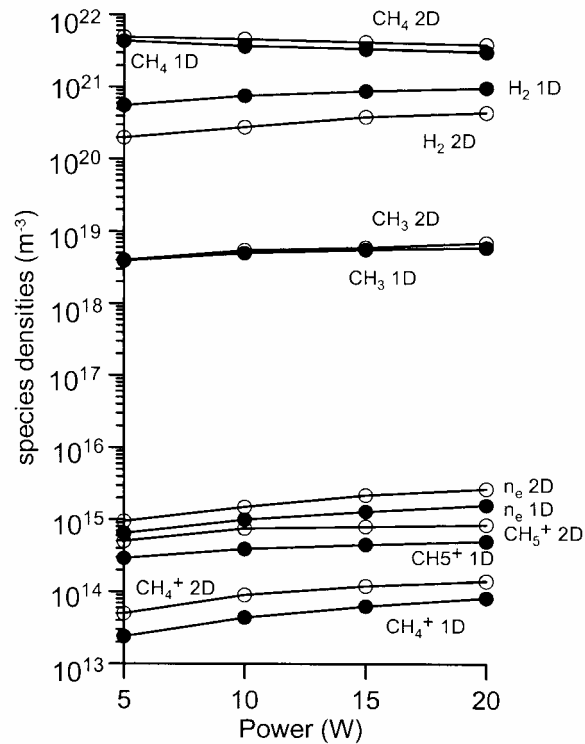


Figure 6: Calculated densities of the most important plasma species, obtained with the 1D (black circles) and 2D (open circles) model, as a function of power

In the 2D model, the CH_4 density is somewhat higher than in the 1D model, while the other - background - molecules (H_2 , C_2H_6 and others) have somewhat lower densities in the 2D model. In general, the agreement between the one-dimensional and two-dimensional model results is reasonable. Since the 1D model results were validated with experimental data (see chapter 3), the 2D results can also be considered to be reliable.

With the 2D model, additional information can be obtained about the species fluxes as a function of radial direction. For the simulation at 5W, the fluxes of the ions, electrons and radicals are discussed. Figure 7 presents the calculated time-averaged electron flux towards both electrodes (i.e., powered electrode at the lower side with 7.6 cm radius and grounded electrode at the upper side with a radius of 8.5 cm).

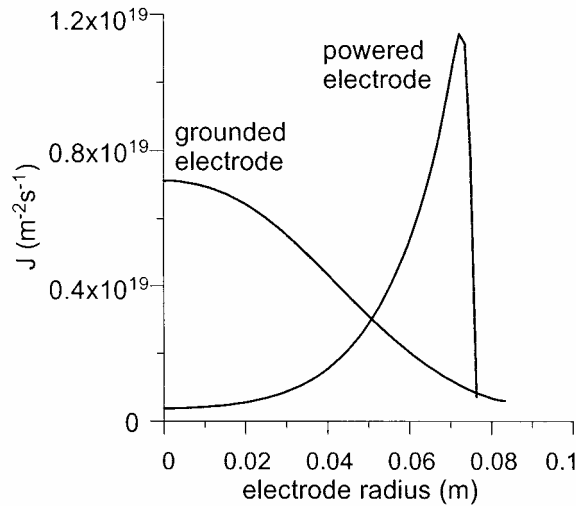


Figure 7: Calculated time-averaged electron flux towards the powered and grounded electrode, as a function of radial direction, at a power of 5W.

It appears that the time-averaged electron flux towards the powered electrode increases from the middle of the electrode (about $10^{18} \text{ m}^{-2}\text{s}^{-1}$) to the side end of the electrode (about $1.2 \times 10^{19} \text{ m}^{-2}\text{s}^{-1}$). This is logical because the electron density is the highest near the side end of the powered electrode. Due to the larger changes in electric field at the end of the electrode, as a function of time in the rf-cycle, more electrons are pushed towards the side end of the powered electrode. The calculated time-averaged electron flux towards the grounded electrode shows an opposite profile. In the middle of the grounded electrode, the time-averaged electron flux has its maximum ($7 \times 10^{18} \text{ m}^{-2}\text{s}^{-1}$), and decreases gradually towards the outer end of the grounded electrode ($10^{18} \text{ m}^{-2}\text{s}^{-1}$). This electron flux profile can again be explained from the electric field (as a function of rf-cycle). However, the difference as a function of radial direction for the time-averaged electron flux towards the grounded electrode is lower than towards the powered electrode. Finally, it is worth to mention that the electron fluxes towards both electrodes are calculated to be about $3 \times 10^{18} \text{ m}^{-2} \text{ s}^{-1}$ in the 1D model, which is of the same order of magnitude as the fluxes obtained with the 2D model (see figure 7).

However, it should be realized that in the 1D model the fluxes towards both electrodes are equal, because no dc self bias voltage is calculated at the powered electrode.

The time-averaged ion flux of CH_5^+ (i.e., the main ion in the plasma) towards both electrodes is given in figure 8.

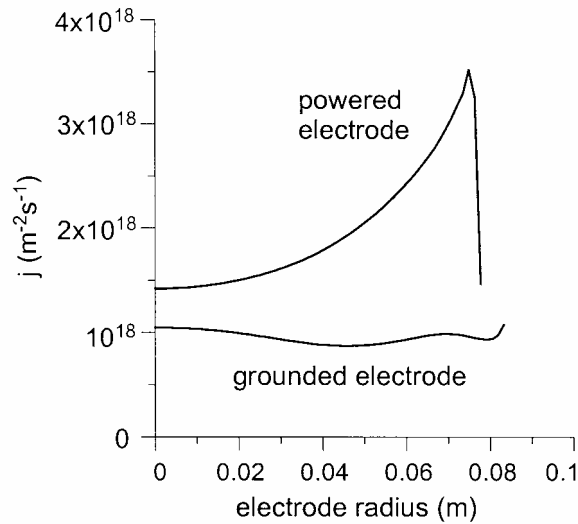


Figure 8: Calculated time-averaged CH_5^+ ion flux towards the powered and grounded electrode, as a function of radial direction, at a power of 5W.

The time-averaged ion flux towards the powered electrode shows a similar profile as the time-averaged electron flux, and is related to the maximum ion density near the side end of the powered electrode. The CH_5^+ ion flux towards the grounded electrode shows a quite uniform behaviour as a function of electrode radius (i.e., about $10^{18} \text{ m}^{-2} \text{ s}^{-1}$). This value of $10^{18} \text{ m}^{-2} \text{ s}^{-1}$ is also calculated with the 1D model for the CH_5^+ ion flux towards both electrodes, hence, the 1D and 2D models yield similar results. Finally, these characteristic ion flux profiles towards both electrodes are also calculated in 2D for all other ionic species.

The calculated fluxes of the main radical, i.e. CH_3 , towards both electrodes are given in figure 9.

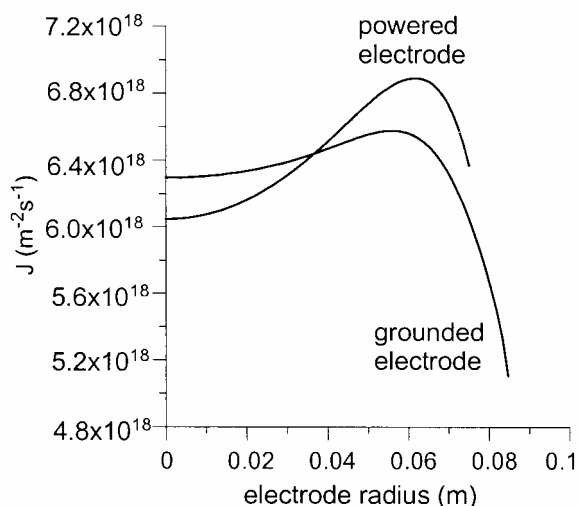


Figure 9: Calculated CH_3 flux towards the powered and grounded electrode, as a function of radial direction, at a power of 5W.

The CH_3 flux towards the grounded electrode is in the order of $6 \times 10^{18} \text{ m}^{-2}\text{s}^{-1}$, and increases slightly as a function of radial direction. However, it decreases at the side end of the grounded electrode. The calculated CH_3 flux towards the powered electrode shows a similar profile, but here, the difference in flux as a function of radial direction is somewhat larger. The maxima in CH_3 fluxes, at the side end of both electrodes, can again be explained from the fact that the CH_3 density is at its maximum in that region between the electrodes. The CH_3 flux calculated with the 1D model is in the same order (i.e., about $6 \times 10^{18} \text{ m}^{-2}\text{s}^{-1}$) as the values obtained with the 2D model. For the other radicals, similar flux profiles towards both electrodes have been calculated.

Finally, as mentioned above, the power is one of the inputs in the model. From this power, the voltage at the rf-powered electrode (also called rf-voltage), is calculated in both models. Further, the dc bias voltage is also calculated in the 2D model. It should be noted that no dc self-bias can be obtained in the 1D model.

The comparison of the amplitude of the rf voltage values, as calculated with the 1D and 2D fluid models, is shown in figure 10, as a function of power.

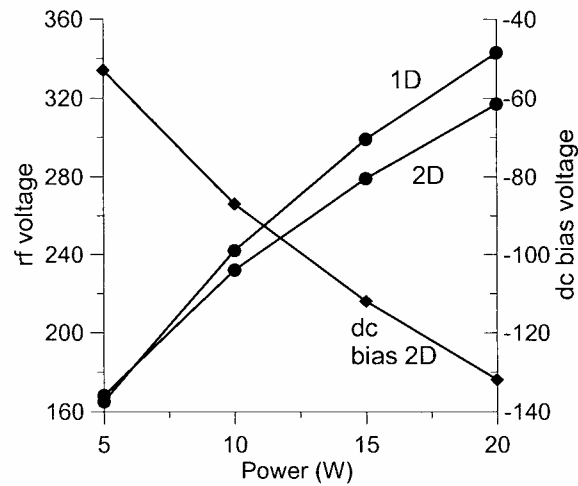


Figure 10: Comparison of the rf voltage values, as a function of power, as calculated with the 1D and 2D fluid model. The dc self bias voltage obtained with the 2D fluid model is also given.

It is clear from figure 10 that the rf voltage values obtained with both models are in relatively good agreement for the four power values. However, the 2D model gives additional information on the dc bias voltage. The rf-voltage values, obtained with both models, show an increase as a function of power. The increase in rf-voltage, as a function of power, is also accompanied with a decrease of dc bias voltage in the 2D model.

4.4. Conclusions

A comparison is made between the results of the 1D and 2D fluid model for a methane plasma. The species densities calculated with both models are in relatively good agreement. The 2D model results reveal that the electrons, ions and radicals have their maximum density near the side end of the electrodes (in the radial direction), and in the middle between the electrodes (in axial direction). The time-averaged fluxes of the ions and electrons towards the powered electrode show a similar profile. Indeed, these fluxes are characterized by a peak at the end of the electrode. The time averaged electron flux towards the grounded electrode reaches its maximum at the central region of the electrode, whereas the time-averaged ion fluxes to the grounded electrode show a more or less uniform profile, in radial direction. Finally, the fluxes of the radical species were found to be quite similar towards both electrodes, i.e., increasing slightly as a function of radial direction, and with a drop at the side end of the electrode. The density and flux profiles of the different plasma species can be explained from the changes of the electric field in the radial and axial direction, as a function of rf-cycle.

4.5. Future modelling plans

The information concerning the species fluxes towards the electrodes as a function of radial direction is of interest for the uniformity of the deposited layer in PACVD. It is important as input in a Molecular Dynamics model that will be developed for the simulation of the growth of the layer. Moreover, the 2D model will also be used to investigate the influence of convective flow for the neutrals on the plasma characteristics, which is also carried out in our research group.

4.6. References

- [1] G.J. Nienhuis, W. J. Goedheer, E.A.G. Hamers, W.G.J.H.M. van Sark, J. Bezemer, *J. Appl. Phys*, **82**, 2060 (1997)
- [2] G.J. Nienhuis, W. Goedheer, *Plasma Sources Sci. Technology*, **8**, 295 (1999)
- [3] G.J. Nienhuis, Ph.D. thesis, Utrecht University 1998
- [4] K. Bera, J. W. Yi, B. Farouk, Y. H. Lee, *IEEE Trans. Plasma Science*, **27**, 5, (1999)
- [5] K. Bera, B. Farouk, Y. H. Lee, *Plasma Sources Sci. Technol.*, **10**, 211 (2001)
- [6] K. Bera, B. Farouk, Y. H. Lee, *Plasma Sources Sci. Technol.*, **8**, 412 (1999)
- [7] K. Nagayama, B. Farouk, Y. H. Lee, *IEEE Trans. Plasma Science*, **26**, 125 (1998)

Chapter 5: A one-dimensional fluid model for an acetylene rf discharge: study of the plasma chemistry

5.1. Fluid model developed for an acetylene discharge

The one-dimensional fluid model, described in chapter 2, is also applied for the modelling of the plasma chemistry in an acetylene (C_2H_2) plasma. These plasmas can also be used for the deposition of diamond-like carbon layers (using acetylene as input gas). As in the methane case, a capacitively coupled rf plasma is considered, used for plasma assisted chemical vapour deposition (PACVD) [1, 2]. However, it is worth mentioning that also different plasma types are reported in literature for this deposition purposes, namely microwave discharges [3, 4] or expanding arc plasmas [5 - 8].

The electron kinetics are, similar to the methane case, obtained from a simplified Boltzmann model, while the fluid model describes the transport and the reactions of species in the plasma. However, in comparison to the methane plasmas, experimental data of acetylene plasmas is very scarce in literature. Hence, validation is in this case not so evident. For this, we compared the calculated species densities with the few experimental data in literature, where possible. Further, a unique reaction pathway in the plasma chemistry is the “polymerisation” reaction of acetylene, which forms higher order radical carbon species C_xH_y (with $x > y$, see further). These reactions are also considered in the chemistry model and it appears that our calculated results considering these reactions are in analogy (at least the trend) with the experimental data, describing this phenomenon (see further).

In total, 24 species (neutrals, radicals, electrons and ions) are considered, given in Table I. The only neutral species that play a role are C_2H_2 and H_2 . Thirteen radical species are included, of which the carbon rich species C_xH_y (with $x > y$) are present in large amounts [1, 2]. Further, 8 ionic species are considered.

Neutrals	Radicals				Ions	
C ₂ H ₂	C ₄ H ₂	C ₆ H ₂	H	C ₈ H	C ₂ H ₂ ⁺	C ₂ H ⁺
H ₂	CH	CH ₂	C ₂ H		C ₂ ⁺	CH ⁺
	C ₂ H ₃	C ₄ H ₃	C ₆ H ₃		C ⁺	H ₂ ⁺
	C ₄ H	C ₆ H	C ₈ H ₂		C ₄ H ₂ ⁺	C ₆ H ₂ ⁺

Table I: Different species taken into account in the C₂H₂ plasma model, beside electrons

As an approximation, the ionic species C₂H₂⁺ and C₂H₃⁺ are considered as one species, namely C₂H₂⁺. In the same way, C₄H₂⁺ and C₆H₂⁺ represent respectively the ions C₄H₂⁺, C₄H₃⁺ and, C₆H₂⁺ and C₆H₃⁺.

In Table II, the 19 electron-neutral reactions taken into account in the model are presented.

Reaction	Chemical reaction	Ref.
	C ₂ H ₂	
vibr. exc.	$e^- + C_2H_2 \rightarrow C_2H_2^* + e^-$ (3)	9
ionisation	$e^- + C_2H_2 \rightarrow C_2H_2^+ + 2 e^-$	9
ionisation	$e^- + C_2H_2 \rightarrow C_2H^+ + H + 2 e^-$	9
ionisation	$e^- + C_2H_2 \rightarrow C_2^+ + H_2 + 2 e^-$	9
ionisation	$e^- + C_2H_2 \rightarrow CH^+ + CH + 2 e^-$	9
ionisation	$e^- + C_2H_2 \rightarrow C^+ + CH_2 + 2 e^-$	9
dissociation	$e^- + C_2H_2 \rightarrow C_2H + H + e^-$	10
	H ₂	
vibr. exc.	$e^- + H_2 \rightarrow H_2^* + e^-$ (3)	11
dissociation	$e^- + H_2 \rightarrow 2 H + e^-$	12
ionisation	$e^- + H_2 \rightarrow H_2^+ + 2 e^-$	13
	C ₄ H ₂	
dissociation	$e^- + C_4H_2 \rightarrow C_4H + H + e^-$	*
ionisation	$e^- + C_4H_2 \rightarrow C_4H_2^+ + 2 e^-$	*

	C_6H_2		
dissociation	$e^- + C_6H_2 \rightarrow C_6H + H + e^-$		*
ionisation	$e^- + C_6H_2 \rightarrow C_6H_2^+ + 2 e^-$		*
	C_8H_2		
dissociation	$e^- + C_8H_2 \rightarrow C_8H + H + e^-$		*

Table II: Electron-neutral reactions taken into account in the model, as well as the references where the cross sections are taken from. The number of different vibrational excitation (vibr. exc.) reactions is given between brackets. The asterix (*) refers to the electron-radical reactions for which no cross sections data were found in literature, and hence estimations had to be made.

The electron-neutral reactions can be divided in three categories: vibrational excitation, dissociation and ionisation reactions. Electron-neutral reactions have been considered with the neutral species C_2H_2 , H_2 and the radical species C_4H_2 , C_6H_2 and C_8H_2 . The electron-radical reactions are also considered because it is found that these radical species are abundant at high densities in the discharge (see below). For the ionisation reactions of acetylene, the partial cross sections are only known at higher electron energy (region 100 – 1000 eV) [9]. Hence, the partial ionisation cross sections in the lower electron energy region are obtained by fitting (interpolation), based on the total ionisation cross section (which is known in the whole electron energy region), and starting from the threshold energies for the given ions [9]. For the dissociation reaction of acetylene (into C_2H and H), no cross section was found in literature. As an approximation, an electron excitation cross section was used here. The approach of using electron excitation cross sections for unknown dissociation cross sections has also been applied for the modelling of CH_4 plasmas with reasonable results (i.e., a good agreement was obtained between the calculated and experimental species densities, see chapter 3), and it gives also reasonable results for the present simulations (see further). For the carbon rich radicals (C_4H_2 , C_6H_2 and C_8H_2), no information concerning cross sections can be found and hence, approximations have been used in this case as well (i.e., the ionisation and dissociation cross sections of C_2H_2 were also used for the electron-radical reactions).

In total, 1 ion-neutral (Table III) and 17 neutral-neutral reactions (Table IV) are included in the model. The ion-neutral reaction between $C_2H_2^+$ and C_2H_2 is described in detail in reference [2].

Ion-neutral reaction	Reaction rate coefficient (m^3/s)	Ref.
$C_2H_2 + C_2H_2^+ \rightarrow C_4H_2^+ + H_2$	1.0×10^{-15}	2 *

Table III: Ion-neutral reaction taken into account in the model

* : reaction rate coefficient is not known from literature, hence this value is assumed based on data for similar ion-neutral reactions.

In this ion-neutral reaction, an intermediate ion ($C_4H_4^{+*}$) is assumed, leading to the formation of the ions $C_4H_4^+$, $C_4H_3^+$, $C_4H_2^+$ and $C_2H_3^+$. As an assumption, only the formation of the ion $C_4H_2^+$ is considered in the model (hence also neglecting the intermediate ion state). Note that only this ion is considered in the above reaction because it is found that this is the main ion in the acetylene plasma [2]. Because no reaction rate coefficient for this reaction is found in literature, a value of $10^{-15} m^3/s$ is assumed. This value is similar to the data for other ion-neutral reactions used in the plasma model for methane. It will be shown further that this value yields good agreement between the calculated species densities from the model and the experimental data available in literature.

The neutral-neutral reactions are obtained from different sources, and are presented in Table IV.

Neutral-neutral reactions	Reaction rate coefficient (m^3/s)	Ref.
$C_2H + C_2H_2 \rightarrow C_4H_2 + H$	4.0×10^{-17}	1
$C_2H + C_4H_2 \rightarrow C_6H_2 + H$	5.0×10^{-18}	1 *
$CH + H_2 \rightarrow CH_2 + H$	6.8×10^{-19}	14
$C_2H + H_2 \rightarrow C_2H_2 + H$	1.3×10^{-19}	14
$C_2H + H \rightarrow C_2H_2$	3.0×10^{-16}	15
$CH_2 + H \rightarrow CH + H_2$	2.7×10^{-17}	16
$CH_2 + CH_2 \rightarrow C_2H_2 + H_2$	5.3×10^{-17}	17
$H + C_2H_2 \rightarrow C_2H_3$	1.0×10^{-21}	1
$H + C_4H_2 \rightarrow C_4H_3$	2.6×10^{-18}	1

$\text{H} + \text{C}_6\text{H}_2 \rightarrow \text{C}_6\text{H}_3$	2.6×10^{-18}	1 *
$\text{H} + \text{C}_2\text{H}_3 \rightarrow \text{C}_2\text{H}_2 + \text{H}_2$	2.0×10^{-17}	14
$\text{C}_2\text{H} + \text{C}_2\text{H}_3 \rightarrow \text{C}_2\text{H}_2 + \text{C}_2\text{H}_2$	1.6×10^{-18}	15
$\text{H} + \text{C}_4\text{H}_3 \rightarrow \text{H}_2 + \text{C}_4\text{H}_2$	2.0×10^{-17}	1
$\text{H} + \text{C}_6\text{H}_3 \rightarrow \text{H}_2 + \text{C}_6\text{H}_2$	2.0×10^{-17}	1 *
$\text{C}_4\text{H} + \text{C}_2\text{H}_2 \rightarrow \text{C}_6\text{H}_2 + \text{H}$	5.0×10^{-18}	1 *
$\text{C}_2\text{H} + \text{C}_6\text{H}_2 \rightarrow \text{C}_8\text{H}_2 + \text{H}$	5.0×10^{-19}	1 *
$\text{C}_6\text{H} + \text{C}_2\text{H}_2 \rightarrow \text{C}_8\text{H}_2 + \text{H}$	5.0×10^{-19}	1 *

Table IV: Neutral-neutral reactions incorporated in the model

* : reaction rate coefficients are estimated.

Note that for some reactions, the reaction rate coefficients are not available. Hence they are given values comparable with the reaction rate coefficients from similar reactions. The use of fitting parameters is a common approach in modelling when exact data are lacking [1, 18] Finally, it should also be noticed that nearly no information is available on electron-neutral or neutral-neutral reactions, in which the higher carbon molecules (like C_4H_2 , C_6H_2 and C_8H_2) dissociate in 2 (or more) carbon rich species, by breaking a carbon-carbon bond. A possible reason is that the carbon-carbon bonds in these molecules have a strong double or triple bond character, which makes it quite difficult to break them. Hence, it is more likely that if such a reaction occurs, a carbon-hydrogen bond will be broken (for example: $e^- + \text{C}_4\text{H}_2 \rightarrow \text{C}_4\text{H} + \text{H} + e^-$). Only for C_2H_2 , 3 dissociative (ionisation) electron- C_2H_2 reactions are described in literature in which the carbon-carbon bond is broken (see table II). However, the cross sections of these electron-neutral reactions are rather low, and they are all characterized by a rather high threshold energy (i.e., about 20 eV).

In order to predict the layer growth, a simple deposition model is included by means of “sticking coefficients”. For the radicals C_2H_3 , C_4H_3 and C_6H_3 , a sticking coefficient of 0.3 is used [19], whereas a value of 0.25 is assumed for the species CH and CH_2 [22]. It is known from literature [19] that the C_2H species have a large sticking coefficient (i.e., in the order of 0.8). However, it should be mentioned that a somewhat lower value is obtained from other studies [17, 20]. Because this sticking coefficient is subject to a large uncertainty, we have slightly adapted this value, in order to match the theoretical deposition rate with the experimental values obtained

by Doyle [21] (in the power region of 0 - 20 Watt, giving deposition rates in the order of 0.05 to 0.4 nm/s). As an approximation, the radicals C_4H_2 , C_6H_2 and C_8H_2 , present in the discharge at high densities, are not considered in the deposition model (i.e., the sticking coefficients of these species are set to zero). Note that, for similar plasma conditions, the experimental deposition rates obtained using an acetylene plasma [1], are higher compared to a methane plasma [23].

5.2. Results of the model

In this section, the results of several simulations will be discussed and compared with other (experimental and theoretical) data available from literature. The reactor radius of the plasma reactor is set to 10 cm, while the distance between the two electrodes is 3 cm. In section 5.2.1, the results of the acetylene plasma will be discussed, whereas in section 5.2.2., a comparison is made between the results of an acetylene and a methane plasma. Finally, the influence of helium, used as a dilution gas, on the plasma chemistry, is investigated in section 5.2.3.

5.2.1. The C_2H_2 discharge

For the simulations of the acetylene plasma, an input gas flow of 20 sccm acetylene is used. The power going into the plasma is 10 Watt, while the pressure is set to 0.14 Torr.

In figure 1, the densities of the most important species (neutrals, radicals, ions and electrons) are given, as a function of distance between the electrodes (3 cm).

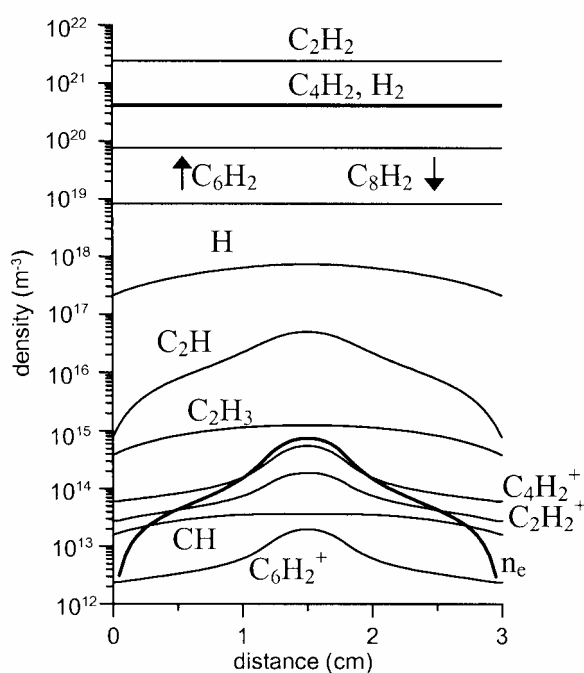


Figure 1: Calculated densities (m^{-3}) of the non-radical neutrals, radicals, ions and electrons as a function of distance from the electrode at 0.14 Torr, 10 W, 13.56 MHz and 20 sccm acetylene inlet.

As can be seen from this figure, the most important non-reactive neutrals are C_2H_2 and H_2 . Despite of the fact that no H_2 molecules are introduced in the plasma, the hydrogen density is very high. This can be explained from the ion-neutral (Table III) and neutral-neutral reactions (Table IV), in which a lot of H_2 molecules are formed. Similar results were also obtained for the modelling of methane [see chapter 3] and silane [see next chapter] plasmas. Further, the radicals C_4H_2 , C_6H_2 and C_8H_2 are also present at high densities. These species are mainly formed in the neutral-neutral reactions with C_xH (with x equal to 2, 4 and 6). The presence of these radical species and neutral species (C_2H_2 and H_2) at high densities in an acetylene plasma is also found by others [1, 2].

Other radicals present in the discharge at relative high densities are H , C_2H and C_xH_3 (with $x = 2, 4$ and 6). In figure 1, only the density of C_2H_3 is presented. The densities of C_4H_3 and C_6H_3 (not shown in figure 1) are in the order of 10^{16} m^{-3} . Further, it was also found that the species C_xH (with $x = 2, 4, 6$ and 8) are present in the discharge at rather high densities. Because all C_xH species have comparable densities, only the density of C_2H is presented in figure 1. Unfortunately, no experimental data on the densities of these species are available in literature, and hence no comparison with the calculated data we obtained, was possible. Finally, the densities of CH_2 and CH are in the order of 10^{13} m^{-3} (only the density of CH is shown in figure 1).

The most important ionic species are found to be $C_4H_2^+$, $C_2H_2^+$ and $C_6H_2^+$ respectively. These results are in agreement with experiments [2, 24]. Finally, the electron density is also given in figure 1. Because the electron density shows considerable variations in the sheath zones, as a function of time in the rf cycle, the time-averaged electron density is given. Although the ion densities do hardly vary during the rf cycle, also the time-averaged ion density profiles are given in figure 1. Results of a mass spectrometry study of the acetylene plasma by Deschenaux et al. [24] show the presence of the species with mass 2 (H_2), 13 (CH), 25 (C_2H), 27 (C_2H_3), 49 (C_4H), 50 (C_4H_2) and 51 (C_4H_3), which are also considered in our model.

In figure 2, the densities of various plasma species are plotted as a function of generator power.

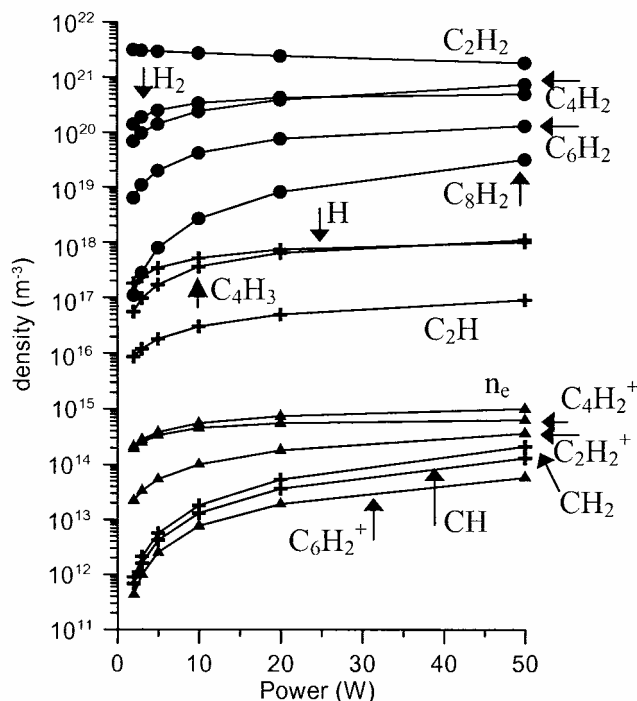


Figure 2: Calculated densities (m^{-3}) of the non-radical neutrals, radicals, ions and electrons as a function of power. The other parameters are kept the same as in figure 1.

As can be seen from this figure, the density of C_2H_2 decreases as a function of power, which is logical because, the higher the power, the more C_2H_2 is “consumed” in the different reactions. All other densities increase as a function of power, because they are formed in the chemical reactions.

In figure 3, the fluxes ($\text{m}^{-2}\text{s}^{-1}$) of the different species towards the electrodes are given, as a function of power.

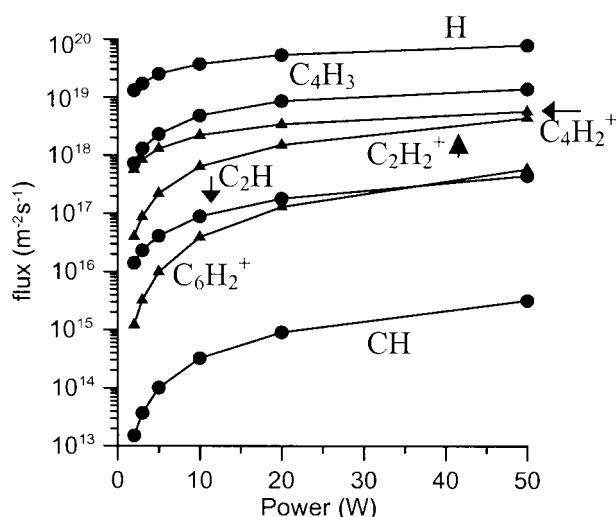


Figure 3: Calculated radical and ion fluxes ($\text{m}^{-2}\text{s}^{-1}$) towards the electrodes as a function of generator power (acetylene plasma). The other parameters are kept the same as in figure 1.

As can be seen from this figure, all species fluxes increase significantly at low power, and more slightly at high power. The fluxes of the radical species C_xH are all of the same order, hence only the C_2H flux is given. The same is true for the fluxes of the species C_xH_3 , for which only C_4H_3 is given. Note that, due to the limitations of the 1D model, the fluxes towards both electrodes (i.e., powered and grounded electrode) are equal.

5.2.2. Comparison of the results obtained for an acetylene and a methane plasma.

In order to compare the results of a methane plasma with an acetylene plasma, a number of simulations (13.56 MHz, 0.14 Torr) were obtained for a methane plasma (described in detail in chapter 3), with varying generator power (figure 4).

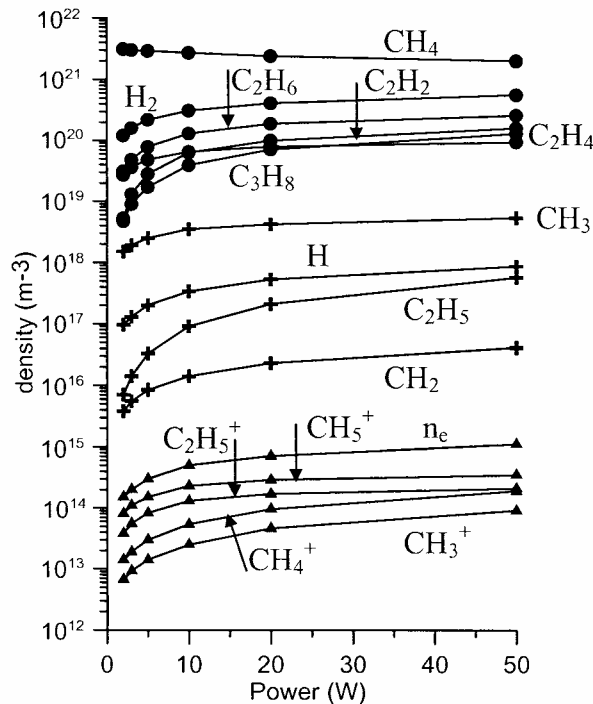


Figure 4: Calculated densities (m^{-3}) of the non-radical neutrals, radicals, ions and electrons as a function of power. The other parameters are kept the same as in figure 1.

It can be seen that, when comparing figures 4 (methane plasma) and 2 (acetylene plasma), both plasmas are characterized by a number of neutral background gases, present at high densities in the discharge, and formed in the neutral-neutral chemistry. Typical for an acetylene discharge is the presence of the radical species C_4H_2 , C_6H_2 , and C_8H_2 at high densities [2]. These species are formed in the neutral-neutral reactions with C_2H (see Table IV). In a methane plasma, the neutral species C_2H_2 , C_2H_4 , C_2H_6 and C_3H_8 are abundant at relatively high densities, while the most important radicals are found to be CH_3 , H and C_2H_5 . Beside the radical species C_xH_y ($x > y$) mentioned above, the radicals H , C_2H and C_xH_2 (with x equal to 2, 4 and 6) are also present in the acetylene discharge. The fact that other radical species (C_2H , $\text{C}_x\text{H}_2, \dots$) are present in an acetylene discharge, compared to a methane plasma, can be explained from the neutral-neutral chemistry, which is totally different in both plasmas. Indeed, the neutral-neutral chemistry in an acetylene discharge depends strongly on the reactions of C_2H with other species (see Table IV), while the neutral-neutral chemistry in a methane plasma is characterized by reactions between all kinds

of species (CH_4 , CH_3 , CH_2 , H , C_2H_5 ,...). It is also worth mentioning that, whereas in the methane plasma model 7 ion-neutral reactions were considered, only 1 ion-neutral reaction is considered in the acetylene plasma (Table III) [2]. The most important ions in a methane plasma are CH_5^+ , C_2H_5^+ (formed in the ion-neutral chemistry), and CH_4^+ and CH_3^+ , created in the electron-methane ionisation reactions. In an acetylene plasma on the other hand, the species C_4H_2^+ , C_2H_2^+ and C_6H_2^+ are found to be the most prevalent ionic species.

When comparing the species fluxes to the electrodes in an acetylene (figure 3) and a methane plasma (figure 5), it can be seen that the H radical flux is comparable in both cases.

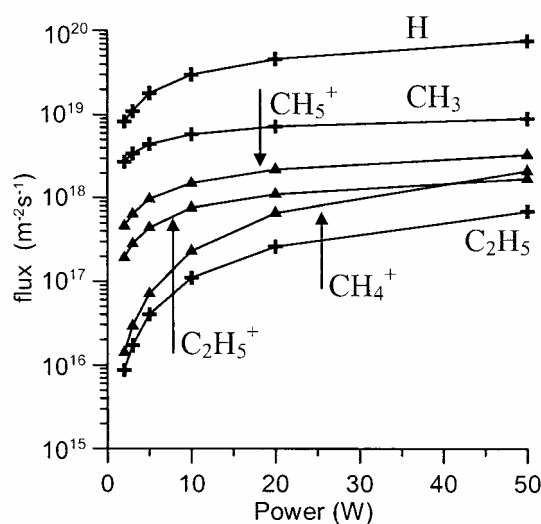


Figure 5: Calculated radical and ion fluxes ($\text{m}^{-2}\text{s}^{-1}$) towards the electrodes as a function of generator power (methane plasma). The other parameters are kept the same as in figure 1.

Further, the fluxes of the species C_xH_3 , C_xH and C_xH_2^+ (with x equal to 2, 4 and 6) are important in an acetylene plasma, whereas in the methane plasma the most important species fluxes towards the electrodes are CH_3 , C_2H_5 , CH_5^+ and C_2H_5^+ . Hence, it can be concluded that both plasmas are characterized by other species fluxes towards the substrates, influencing the growth of the amorphous carbon layer. It is found that, when using an acetylene plasma, higher deposition rates are obtained [1], compared to a methane plasma [23]. However, a detailed investigation of these plasma-wall interactions (i.e., a study of the growth of the layer) is beyond the scope of this work.

5.2.3. The acetylene/helium discharge

Because in practical set-ups, the acetylene gas is often diluted with helium for safety reasons, we investigate here the influence of helium addition to the acetylene discharge. For this purpose, three more species have to be included in the model: the neutral atoms helium (He), the ion He^+ , and He^* representing the excited helium atoms summed over all levels. As a crude approximation, no difference is made between the metastable levels and the other excited levels. Further, one electron-ionisation reaction, which forms the ion He^+ , and one electron-excitation reaction is considered, using the total excitation cross section [25] (see Table 5).

Reaction	Chemical reaction	Ref.
total excitation	$e^- + \text{He} \rightarrow \text{He}^* + e^-$	25
ionisation	$e^- + \text{He} \rightarrow \text{He}^+ + 2 e^-$	25

Table V: Electron/helium reactions considered in the acetylene/helium discharge.

In figure 6, the densities of the most important species are given as a function of acetylene gas inlet flow. In total, 5 simulations have been carried out with a total gas inlet of 20 sccm, but with a different acetylene/helium flow ratio (generator power: 10 Watt, pressure: 0.4 Torr).

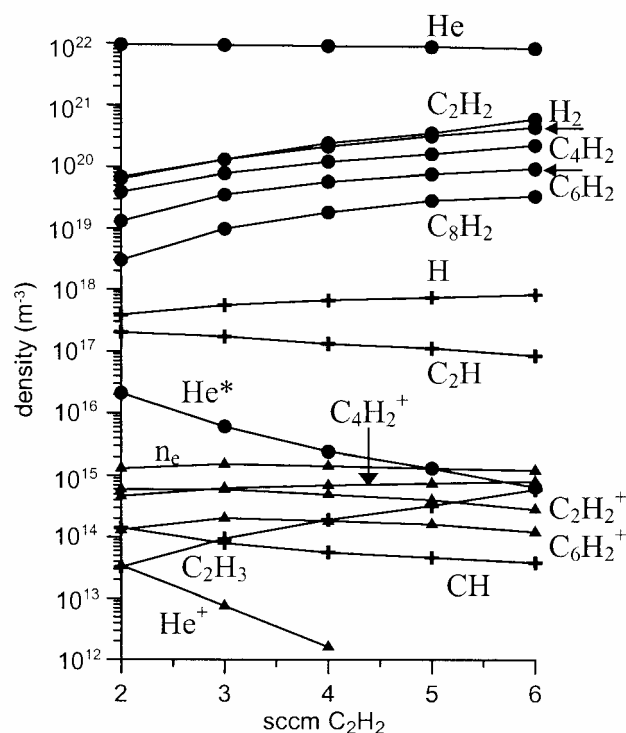
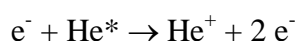


Figure 6: Calculated densities (m^{-3}) of the non-radical neutrals, radicals, ions and electrons as a function of acetylene gas inlet, at 10 Watt and a pressure of 0.4 Torr. Note that in total 20 sccm is introduced (i.e., a mixture of acetylene/helium).

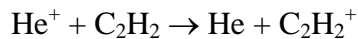
The helium neutrals appear to be the most important species in the plasma. Indeed, the helium flow is higher than the acetylene flow for all conditions investigated, and moreover, the acetylene species react further in the plasma in the different electron and radical reactions. As can be seen from figure 6, also the higher carbon molecules, created from the neutral-neutral reactions, are present in the discharge at relatively high densities, comparable to a pure acetylene plasma.

Because the threshold energies of the electron-helium reactions (excitation: 19.8 eV, ionisation: 24.6 eV) are rather high, the densities of He^* and He^+ species will generally not be very high. However, for the simulation with only a minor gas input of acetylene (i.e., 2 sccm C_2H_2), it can be seen from figure 6 that also a considerable amount of He^* excited species are formed (and consequently, that a large amount of electron energy will be lost in these excitation reactions). Because of this, the He^+ ions created from the He^* excited state are also considered:



For simplicity, only the ionisation cross section [26 - 28] of the excited helium state 2s is considered. A far more complete review of all the different excited helium levels can be found in [29]. Finally, it should however also be considered that no loss processes of He* are taken into account in our model.

In literature, information can be found about a charge exchange reaction for argon and acetylene [30, 17], but not for helium. A sensitivity study, assuming a similar reaction rate coefficient ($10^{-16} \text{ m}^3/\text{s}$) for the reaction



as for argon showed us that, if this reaction occurs in the plasma, its influence is of minor importance, and can be neglected in our plasma model.

Beside the fact that, in the region of our simulations, a certain amount of electron energy goes to the formation of the He* and He⁺ species, it can be seen that the helium gas does not really affect the acetylene discharge/chemistry. Hence, the helium gas can be regarded as a – more or less – dilution gas [31]. The most important ion in the C₂H₂/He discharge is found to be C₄H₂⁺, while the He⁺ density remains low over the whole region of simulations.

5.3. Conclusions

In an acetylene plasma, it is found that the neutral species C_2H_2 and H_2 are present in the discharge at high density, together with a number of hydrocarbon molecules (C_4H_2 , C_6H_2 and C_8H_2). The other radical species are also present in the discharge at relatively high densities, because they are formed in the neutral-neutral reactions. The main ions in the model are $C_2H_2^+$, $C_4H_2^+$ and $C_6H_2^+$. A number of $C_2H_2^+$ ions react further (in an ion-neutral reaction with C_2H_2) to form $C_4H_2^+$ and $C_6H_2^+$. Further, a comparison is made between a methane and an acetylene plasma, both used for the deposition of amorphous carbon layers. It is found that both discharge gases yield a completely different chemistry. Finally, a simple deposition model is – as a first approximation - included. However, it is worth mentioning that, in our research group, a far more detailed deposition model is under development by means of a Molecular Dynamics model, in order to get a better description of the growth of the layer. Finally, the influence of helium, used as a carrier gas, on the acetylene discharge is investigated, and it is shown that due to the incorporation of helium, the plasma-chemistry is not drastically changed.

5.4. References

- [1] R. Doyle, J. Appl. Phys, **82**, 4763 – 4771, 1997.
- [2] M.J. Vasile, G. Smolinsky, Int. J. of Mass. Spec. and Ion. Phys., **24**, 11 – 23, 1977.
- [3] I. Platzner, P. Marcus, Int. J. of Mass Spec. and Ion Phys., **41**, 241 – 250, 1982.
- [4] K. H. Lai, C. Y. Chan, M. K. Fung, I. Bello, C.S. Lee, S.T. Lee, Diamond and Rel. Materials, **10**, 1862 – 1867, 2001.
- [5] A. De Graaf, M.F.A.M. Van Hest, M.C.M. van de Sanden, K.G.Y. Letourneur, D.C. Schram, Appl. Phys. Letters, **74**, 2927 – 2927, 1999.
- [6] A. De Graaf, G. Dinescu, J.L. Longueville, M.C.M. van de Sanden, D.C. Schram, E.H.A. Dekempeneer, L.J. van Ijzendoorn, Thin Solid Films, **333**, 29 – 34, 1998.
- [7] J.W.A.M. Gielen, W.M.M. Kessels, M.C.M. van de Sanden, D.C. Schram, J. Appl. Phys, **82**, 2643 – 2654, 1997.
- [8] J.W.A.M. Gielen, M.C.M. van de Sanden, D.C. Schram, Appl. Phys. Letters, **69**, 152 – 154, 1996.
- [9] H. Tawara, Y. Itikawa, H. Nishimura, H. Tanaka, H. Nakamura, "Collision data involving Hydro-carbon molecules", NIFS-DATA-6, 1990, Nagano Japan, ISSN 0915-6364.
- [10] H. Tawara, "Electron collision processes involving hydrocarbons", Atomic and Molecular processes in Fusion Edge plasmas, 461 – 495, edited by R.K. Janev (Plenum, New York, 1995), New York.
- [11] L. Ehrhardt, L. Langhans, F. Linder, H.S. Taylor, Phys. Rev, **173**, 222 – 230, 1968.
- [12] A. G. Engelhardt, A.V. Phelps, Phys. Rev, **131**, 2115 – 2128, 1963.
- [13] H. Tawara, T. Kato, At. Data Nucl. Data Tables, **36**, p. 167, 1987.
- [14] D. L. Baulch et al., Phys. Chem. Ref. Data, **21**, 411 – 734, 1992.
- [15] W. Tsang, R.F. Hampson, J. Phys. Chem. Ref. Data, **15**, 1087 – 1279, 1986.
- [16] L.E. Kline, W.D. Partlow, W.E. Bies, J. Appl. Phys, **65**, 70 – 78, 1988.
- [17] Ariel De Graaf, Deposition of CNH materials: Plasma and film characterization, Ph.D. thesis, (University of Eindhoven), 2000.
- [18] A. Rhallabi, Y. Catherine, IEEE transactions on plasma science, **19**, 270 – 277, 1991.
- [19] A. Von Keudell, C. Hopf, T. Schwarz-Selinger, W. Jacob, Nuclear Fusion, **39**, 1451 – 1462, 1999.

- [20] M.D. Perry, L.M. Raff, J. Phys. Chem., **98**, 8128 – 8135, 1994
- [21] R. Doyle, private communication
- [22] D. Herrebout, A. Bogaerts, M. Yan, R. Gijbels, W. Goedheer, E. Dekempeneer, J. Appl. Phys., **90**, p. 570 - 579, 2001.
- [23] E. Dekempeneer, J. Smeets, J. Meneve, L. Eersels, R. Jacobs, Thin Solid Films, **241**, p. 269 – 273, 1994.
- [24] Ch. Deschenaux, A. Affolter, D. Magni, Ch Hollenstein P. Fayet, J. Phys. D., Appl. Phys., **32**, 1876 - 1886, 1999
- [25] A. V. Phelps: ftp://jila.colorado.edu/collision_data
- [26] H. Tawara, T. Kato, Atomic Data and Nucluar Data Tables, **36**, 167 (1987)
- [27] Dixon A. J., Harrison M. F. H., Smith A. C. H., J. Phys. B, **9**, 2617 (1976)
- [28] Long D. R., Geballe R., Phys. Rev A, **1**, 260 (1970)
- [29] Alves L.L., Ferreira C. M., J. Phys D: Appl. Phys, **24**, 581 (1991)
- [30] W. B. Maier, J. Chem. Phys., **42**, 1790 (1965)
- [31] S. F. Durrant, N. Marçal, S. G. Castro, R. C. G. Vinhas, M. A. Bica de Moraes, J. H. Nicola, Thin solid films, **259**, 139 (1995)

Chapter 6: One-dimensional modelling of a capacitively coupled rf plasma in silane/helium, including small concentrations of O₂ and N₂

6.1. Introduction

Functional coating deposition using silane plasmas is broadly used in the industrial production process of solar cells and other electronic devices. The active gas (silane) is often diluted in a gas that helps stabilizing the discharge like helium or argon. In addition, the discharge can be contaminated by an uncontrolled external gas source like air, or oxygen from water adsorbed at reactor walls. In this chapter, we study the influence of small concentrations of air (containing about 82 % N₂ and 18 % O₂) on the plasma chemistry in a silane/helium plasma.

For this research, we started from the silane fluid model developed by Nienhuis and Goedheer. [1 - 3]. Firstly, this silane model was extended, i.e. some extra species and reactions were incorporated. Afterwards, the role of helium (used as a carrier gas), and the addition of small amounts of air (containing 18 % O₂ and 82 % N₂) to the silane/helium plasma was investigated.

6.2. Description of the 1D fluid model

The fluid model is the same as described in chapter 2, and is also combined with the Boltzmann model to obtain information of the reaction rate coefficients of the different electron-neutral reactions.

6.2.1. The silane plasma

In table I, the different species (electrons, ions, neutrals, radicals and excited species) considered in the silane/helium model are given.

Neutral molecules		Radicals & excited species			Ions
SiH ₄	Si ₂ H ₆	SiH ₃	SiH ₂	Si ₂ H ₅	SiH₂⁺
Si ₃ H ₈	Si ₄ H ₁₀	Si ₃ H ₇	Si ₄ H ₉	Si ₅ H ₁₁	SiH₃⁺
Si ₅ H ₁₂	Si ₆ H ₁₄	Si ₆ H ₁₃	Si ₇ H ₁₅	Si ₈ H ₁₇	Si ₂ H ₄ ⁺
Si ₇ H ₁₆	Si ₈ H ₁₈				SiH ₃ ⁻
H ₂		H			H ₂ ⁺
He		He*			He ⁺

Table I: Different species taken into account in the silane/helium plasma model, beside electrons. Excited species are marked with an asterisk (*)

The electron-neutral, ion-neutral and neutral-neutral reactions considered in the model are given in tables II, III and IV respectively. The extra species and reactions added to the original silane model of Nienhuis are marked in bold.

Reaction type	Reaction equation	Ref.
SiH₄		
vibr. exc.	$e^- + \text{SiH}_4 \rightarrow \text{SiH}_4^* + e^-$ (2)	4
ionisation	$e^- + \text{SiH}_4 \rightarrow \text{SiH}_2^+ + 2 \text{H} + 2 e^-$	5
ionisation	$e^- + \text{SiH}_4 \rightarrow \text{SiH}_3^+ + \text{H} + 2 e^-$	5
dissociation	$e^- + \text{SiH}_4 \rightarrow \text{SiH}_3 + \text{H} + e^-$	6
dissociation	$e^- + \text{SiH}_4 \rightarrow \text{SiH}_2 + 2 \text{H} + e^-$	6
attachment	$e^- + \text{SiH}_4 \rightarrow \text{SiH}_3^- + \text{H}$	7
H₂		
vibr. exc.	$e^- + \text{H}_2 \rightarrow \text{H}_2^* + e^-$ (3)	8
dissociation	$e^- + \text{H}_2 \rightarrow 2 \text{H} + e^-$	9
ionisation	$e^- + \text{H}_2 \rightarrow \text{H}_2^+ + 2 e^-$	10
Si₂H₆		
dissociation	$e^- + \text{Si}_2\text{H}_6 \rightarrow \text{SiH}_3 + \text{SiH}_2 + \text{H} + e^-$	6
ionisation	$e^- + \text{Si}_2\text{H}_6 \rightarrow \text{Si}_2\text{H}_4^+ + 2 \text{H} + 2e^-$	11

He		
total excitation	$e^- + \text{He} \rightarrow \text{He}^* + e^-$	12
ionisation	$e^- + \text{He} \rightarrow \text{He}^+ + 2e^-$	12

Table II: Electron-neutral reactions taken into account in the model, as well as the references where the cross sections are taken from. Vibr. exc. stands for vibrational excitation, the number of different vibrational excitation reactions is given between brackets.

Ion reactions	Reaction rate coefficient (m^3/s)	Ref.
$\text{SiH}_3^- + \text{SiH}_2^+ \rightarrow \text{SiH}_3 + \text{SiH}_2$	2.5×10^{-13}	13, 14
$\text{SiH}_3^- + \text{SiH}_3^+ \rightarrow \text{SiH}_3 + \text{SiH}_3$	5.0×10^{-13}	13, 14
$\text{SiH}_3^- + \text{Si}_2\text{H}_4^+ \rightarrow \text{SiH}_3 + 2 \text{SiH}_2$	1.0×10^{-13}	13, 14
$\text{SiH}_3^- + \text{H}_2^+ \rightarrow \text{SiH}_3 + \text{H}_2$	1.0×10^{-13}	13, 14
$\text{SiH}_2^+ + \text{SiH}_4 \rightarrow \text{SiH}_3^+ + \text{SiH}_3$	1.0×10^{-15}	15
$\text{SiH}_2^+ + \text{SiH}_4 \rightarrow \text{Si}_2\text{H}_4^+ + \text{H}_2$	2.5×10^{-16}	16
$\text{SiH}_2^+ + \text{H}_2 \rightarrow \text{SiH}_3^+ + \text{H}$	1.0×10^{-16}	17
$\text{SiH}_4 + \text{H}_2^+ \rightarrow \text{SiH}_2^+ + 2 \text{H}_2$	6.6×10^{-17}	17
$\text{SiH}_4 + \text{H}_2^+ \rightarrow \text{SiH}_3^+ + \text{H}_2 + \text{H}$	6.2×10^{-16}	17

Table III: Ion-ion and ion-neutral reactions considered in the model and corresponding reaction rate coefficients, as well as the references where the reaction rate coefficients are taken from.

Neutral-neutral reaction	Reaction rate coefficient (m^3/s)	Ref.
$\text{SiH}_4 + \text{H} \rightarrow \text{H}_2 + \text{SiH}_3$	1.2×10^{-18}	17, 18
$\text{SiH}_3 + \text{SiH}_3 \rightarrow \text{SiH}_2 + \text{SiH}_4$	1.5×10^{-16}	18, 19
$\text{SiH}_2 + \text{H}_2 \rightarrow \text{SiH}_4$	1.4×10^{-20}	18
$\text{SiH}_2 + \text{SiH}_4 \rightarrow \text{Si}_2\text{H}_6$	1.2×10^{-17}	18
$\text{SiH}_2 + \text{Si}_2\text{H}_6 \rightarrow \text{Si}_3\text{H}_8$	2.6×10^{-17}	18
$\text{SiH}_2 + \text{Si}_n\text{H}_{2n+2} \rightarrow \text{Si}_{n+1}\text{H}_{2n+4} \quad (2 < n < 9)$	2.6×10^{-17}	18
$\text{Si}_2\text{H}_6 + \text{H} \rightarrow \text{Si}_2\text{H}_5 + \text{H}_2$	7.0×10^{-18}	17, 18
$\text{Si}_2\text{H}_6 + \text{H} \rightarrow \text{SiH}_3 + \text{SiH}_4$	3.5×10^{-18}	17, 18

$\text{Si}_n\text{H}_{2n+2} + \text{H} \rightarrow \text{Si}_n\text{H}_{2n+1} + \text{H}_2$ ($2 < n < 9$)	1.1×10^{-17}	18
$\text{Si}_2\text{H}_5 + \text{Si}_2\text{H}_5 \rightarrow \text{Si}_4\text{H}_{10}$	1.5×10^{-16}	18
$\text{He}^* + \text{SiH}_4 \rightarrow \text{SiH}_2^+ + 2 \text{H} + \text{He} + \text{e}^-$	7.9×10^{-18}	20
$\text{He}^* + \text{SiH}_4 \rightarrow \text{SiH}_3^+ + \text{H} + \text{He} + \text{e}^-$	7.9×10^{-18}	20

Table IV: Neutral-neutral reactions incorporated in the model and corresponding reaction rate coefficients, as well as the references where the reaction rate coefficients are taken from.

In comparison with the silane model developed by Nienhuis [1 – 3], some modifications were made here. Whereas in the model of Nienhuis it is assumed that only the ion SiH_2^+ is formed from the electron- SiH_4 ionisation reaction, we have also incorporated the electron- SiH_4 ionisation reaction, which produces the ion SiH_3^+ . Hence, for both the electron-ionisation reactions, the partial ionisation cross sections were used [5]. Both ions are considered separately in the model, because a number of ion-neutral reactions were added to the model concerning these ions. Further, several ion-neutral reactions (i.e., the ion reactions with the neutral molecules SiH_4 and H_2) were also added to the original code. For the ion-ion reactions, different reaction rate coefficients are reported in literature (although these values are in the same order of magnitude) [13, 14]. We used in our model the reaction rate coefficients from Kushner [13]. Finally, the neutral-neutral reactions were maintained from the model of Nienhuis. By taking into account these extra reactions and species (i.e., SiH_3^+ and SiH_2^+ instead of only SiH_2^+) the species densities are found to be slightly different in both models (see below).

6.2.2. The silane/helium plasma

Silane plasmas are often diluted with helium for safety reasons, and hence a number of experimental studies concerning silane/helium plasmas can be found in literature [21 - 23]. It is worth to mention, however, that also silane/argon mixtures are sometimes used for the deposition of amorphous silicon layers [24, 25]. For modelling a silane/helium plasma, we extended the silane model described in section 6.2.1. with some helium species (also given in Table I): the neutral atoms helium (He), the ion He^+ , and He^* representing the excited helium atoms summed over all levels (i.e., the

metastable and all other excited levels). It should be noted that this is only an approximation because helium atoms in the metastable levels behave differently from the other excited levels. However, our simulations do not focus on the behavior of the helium excited levels. The species He^* is only considered because it yields a few reactions with SiH_4 (see Table IV, section 6.2.1.), O_2 and N_2 (see below), and because electron impact excitation of helium atoms means an energy loss mechanism for the electrons. For this purpose, the total excitation cross section was used.

To model the plasma chemistry in a silane/helium plasma, two more neutral-neutral reactions are found to be important (i.e., reactions between silane (SiH_4) and the excited atoms He^* , table IV). The four reactions between a He^+ ion and SiH_4 , described in detail in reference [13], were not maintained in the model, because their influence on the plasma chemistry (i.e., the species densities) was found to be negligible. Hence, only a few species and reactions had to be added to model silane/helium discharges.

6.2.3. The silane/helium plasma containing small amounts of O_2 and N_2

To study the influence of small amounts of air (containing O_2 and N_2) in a SiH_4/He plasma, a number of particles containing oxygen and nitrogen have to be considered. The species taken into account in the model are given in Table V.

Neutral molecules	Radicals & excited species				Ions	
O_2	$\text{O}_2(^1\Sigma)$	$\text{O}_2(^1\Delta)$	O	$\text{O}(^1\text{D})$	O_2^+	O^-
	H_2O	OH	SiH_3O	SiH_2O	O^+	
	SiHO	SiO	SiO_2			
N_2	N	$\text{N}(^4\text{D})$	$\text{N}_2(\text{A})$		N_2^+	

Table V: Different species containing oxygen or nitrogen atoms, taken into account in the $\text{SiH}_4/\text{He}/\text{air}$ model. The state of excited species is marked between brackets.

As can be seen from this Table, some silane molecules containing oxygen atoms are also considered (SiHO , SiH_3O , SiO_2 and others). Further, the negative ion O^- is also taken into account. In total, 6 electron-oxygen and 3 electron-nitrogen reactions are

considered, which are presented in Table VI. The cross sections of these electron reactions are obtained from references [26, 27].

Reaction type	Reaction equation	Ref.
O₂		
ionisation	$e^- + O_2 \rightarrow O_2^+ + 2e^-$	26
excitation	$e^- + O_2 \rightarrow O_2 (^1\Delta) + e^-$	26
excitation	$e^- + O_2 \rightarrow O_2 (^1\Sigma) + e^-$	26
diss. exc.	$e^- + O_2 \rightarrow O (^1D) + O + e^-$	26
dissociation	$e^- + O_2 \rightarrow O + O + e^-$	26
attachment	$e^- + O_2 \rightarrow O^- + O$	26
N₂		
ionisation	$e^- + N_2 \rightarrow N_2^+ + 2e^-$	27
excitation	$e^- + N_2 \rightarrow N_2 (A) + e^-$	27
dissociation	$e^- + N_2 \rightarrow N + N + e^-$	27

Table VI: Electron-neutral reactions for O₂ and N₂, as well as the references where the cross sections are taken from. Diss. exc. stands for dissociative excitation.

Further, the ion-neutral and neutral-neutral reactions (considered in the model) in which oxygen or nitrogen species are involved, are given in Tables VII and VIII, respectively.

Ion reactions	Reaction rate coefficient (m ³ /s)	Ref.
$He^* + O_2 \rightarrow O_2^+ + He + e^-$	2.5×10^{-16}	28
$He^+ + O_2 \rightarrow O^+ + O + He$	1.1×10^{-15}	29
$He^+ + O_2 \rightarrow O_2^+ + He$	3.3×10^{-17}	29
$O^+ + SiH_4 \rightarrow SiH_2^+ + H_2 + O$	2.0×10^{-16}	30
$O_2^+ + SiH_4 \rightarrow SiH_2^+ + H_2 + O_2$	2.0×10^{-16}	30
$O_2^+ + O^- \rightarrow O_2 + O$	1.0×10^{-13}	31
$O + O^- \rightarrow O_2 + e^-$	3.0×10^{-16}	32
$O^+ + O^- \rightarrow O + O$	2.7×10^{-13}	31

$\text{He}^* + \text{N}_2 \rightarrow \text{N}_2^+ + \text{He} + \text{e}^-$	7.5×10^{-17}	33
$\text{He}^+ + \text{N}_2 \rightarrow \text{N}_2^+ + \text{He}$	6.4×10^{-16}	29
$\text{N}_2^+ + \text{SiH}_4 \rightarrow \text{N}_2 + \text{SiH}_3^+ + \text{H}$	1.0×10^{-16}	30

Table VII: Ion-ion and ion-neutral reactions with nitrogen or oxygen-containing species, and the corresponding reaction rate coefficients.

Neutral-neutral reactions	Reaction rate coefficient (m^3/s)	Ref.
$\text{O} + \text{O}_2 (^1\Sigma) \rightarrow \text{O} + \text{O}_2 (^1\Delta)$	3.0×10^{-18}	34
$\text{O} (^1\text{D}) + \text{O}_2 \rightarrow \text{O} + \text{O}_2 (^1\Delta)$	4.4×10^{-18}	34
$\text{O} (^1\text{D}) + \text{H}_2\text{O} \rightarrow 2 \text{OH}$	2.2×10^{-16}	35
$\text{O} + \text{OH} \rightarrow \text{H} + \text{O}_2$	3.5×10^{-17}	36
$2 \text{OH} \rightarrow \text{H}_2\text{O} + \text{O}$	2.5×10^{-18}	36
$\text{OH} + \text{H}_2 \rightarrow \text{H}_2\text{O} + \text{H}$	5.6×10^{-20}	37
$\text{H} + \text{O}_2 \rightarrow \text{OH} + \text{O}$	8.5×10^{-16}	38
$\text{SiH}_4 + \text{O} \rightarrow \text{SiH}_3 + \text{OH}$	9.3×10^{-19}	37
$\text{SiH}_4 + \text{OH} \rightarrow \text{SiH}_3 + \text{H}_2\text{O}$	1.2×10^{-17}	37
$\text{SiH}_3 + \text{O} \rightarrow \text{SiH}_2\text{O} + \text{H}$	1.7×10^{-17}	37
$\text{SiH}_3 + \text{OH} \rightarrow \text{SiH}_2\text{O} + \text{H}_2$	8.3×10^{-18}	37
$\text{SiH}_3 + \text{O}_2 \rightarrow \text{SiH}_2\text{O} + \text{OH}$	6.3×10^{-18}	37, 39
$\text{SiH}_3 + \text{O}_2 \rightarrow \text{SiH}_3\text{O} + \text{O}$	6.3×10^{-18}	37, 39
$\text{SiH}_2 + \text{O}_2 \rightarrow \text{SiH}_2\text{O} + \text{O}$	3.7×10^{-18}	40
$\text{SiH}_2 + \text{O}_2 \rightarrow \text{SiHO} + \text{OH}$	3.7×10^{-18}	40
$\text{SiH}_4 + \text{O} (^1\text{D}) \rightarrow \text{OH} + \text{SiH}_3$	3.0×10^{-16}	41
$\text{SiH}_4 + \text{O}_2 (^1\Delta) \rightarrow \text{SiH}_3\text{O} + \text{OH}$	2.5×10^{-18}	30
$\text{SiH}_4 + \text{O}_2 (^1\Sigma) \rightarrow \text{SiH}_3\text{O} + \text{OH}$	5.0×10^{-18}	30
$\text{SiH}_3\text{O} + \text{O} \rightarrow \text{SiH}_2\text{O} + \text{OH}$	1.0×10^{-18}	30
$\text{SiH}_3\text{O} + \text{OH} \rightarrow \text{SiH}_2\text{O} + \text{H}_2\text{O}$	1.0×10^{-17}	42
$\text{SiH}_2\text{O} + \text{O} \rightarrow \text{SiHO} + \text{OH}$	6.2×10^{-19}	43
$\text{SiH}_2\text{O} + \text{OH} \rightarrow \text{SiHO} + \text{H}_2\text{O}$	1.0×10^{-17}	37
$\text{SiHO} + \text{H} \rightarrow \text{SiO} + \text{H}_2$	3.3×10^{-16}	37
$\text{SiHO} + \text{O} \rightarrow \text{SiO} + \text{OH}$	1.6×10^{-16}	37
$\text{SiHO} + \text{OH} \rightarrow \text{SiO} + \text{H}_2\text{O}$	1.6×10^{-16}	37

$\text{SiO} + \text{O}_2 \rightarrow \text{SiO}_2 + \text{O}$	6.7×10^{-20}	37
$\text{N}_2 + \text{O} (^1\text{D}) \rightarrow \text{N}_2 + \text{O}$	3.0×10^{-17}	44
$\text{N} (^4\text{D}) + \text{N} \rightarrow \text{N} + \text{N}$	1.0×10^{-17}	45
$\text{N} (^4\text{D}) + \text{N}_2 \rightarrow \text{N} + \text{N}_2$	2.0×10^{-22}	46
$2 \text{N}_2 (\text{A}) \rightarrow \text{N}_2 (\text{A}) + \text{N}_2$	1.4×10^{-15}	46
$\text{N}_2 (\text{A}) + \text{N}_2 \rightarrow \text{N}_2 + \text{N}_2$	1.9×10^{-19}	46
$\text{N}_2 (\text{A}) + \text{N} \rightarrow \text{N}_2 + \text{N} (^4\text{D})$	5.0×10^{-17}	45
$\text{N}_2 (\text{A}) + \text{O}_2 \rightarrow \text{N}_2 + \text{O} + \text{O}$	2.4×10^{-18}	37
$\text{N}_2 (\text{A}) + \text{SiH}_4 \rightarrow \text{SiH}_3 + \text{H} + \text{N}_2$	5.0×10^{-18}	36
$\text{N}_2 (\text{A}) + \text{SiH}_4 \rightarrow \text{SiH}_2 + \text{H}_2 + \text{N}_2$	5.0×10^{-18}	36

Table VIII: Neutral-neutral reactions with nitrogen or oxygen-containing species, and the corresponding reaction rate coefficients as well as the references where the reaction rate coefficients are taken from.

Most of the reactions given in Tables VII and VIII taken into account are adopted from the detailed work of Kushner [30], although in the tables the original references are also given. In the work of Kushner, many more species and reactions were considered. These species and reactions were also initially included in our model, but a sensitivity study for our conditions (i.e., a capacitively coupled rf discharge) indicated which species and reactions could be neglected. Indeed, when a reaction was included, the effect on the plasma chemistry (i.e., species densities) was checked. Reactions having no large influence (i.e., the difference between a calculation with an extra reaction does not change from the previous calculation) were not further considered in the model. As can be seen from Table VIII, a number of neutral-neutral reactions are considered in which silane and oxygen species are involved. Further, the reactions between two oxygen containing species are also important. Only two reactions between nitrogen and silane species are considered.

Finally, the boundary conditions for the species are defined by means of “sticking coefficients”. The sticking coefficients of the silane species (SiH_3 , SiH_2 , Si_2H_5) are taken from the original code [2, 3], while the sticking coefficients of the radical oxygen and nitrogen species are taken from [13, 30] (i.e., given a value of 0.1). Note that in this way, a large fraction of silane (SiH_2 , SiH_3 , Si_2H_5 and higher order silane

radicals) and oxygen species stick to the substrate. It should be noted that these sticking coefficients are not known very well, and depend on a lot of parameters. The helium excited atoms (He^*) are lost by de-excitation at the walls.

6.3. Results of the models

In this section, the results of the calculations of a silane discharge, a silane/helium discharge and a silane/helium discharge containing a small amount of air will be discussed. For all calculations, the distance between the 2 parallel plates was set to 3 cm, while the electrode radius was assumed to be 10 cm. Further, a power input of 25 Watt is used. The rf frequency is set to 13.56 MHz.

It is generally known that for these conditions, the formation of dust starts playing an important role in a silane plasma [47 – 49]. A small step towards the modelling of dust is included in the present model by allowing the formation of the higher order silane species (Si_7H_{16} , Si_8H_{18} and others, see Table I). A far more complete study of the formation (and the role) of dust in silane plasmas is currently carried out in our research group, but is beyond the scope of our present work.

6.3.1. The silane discharge

In order to compare the results of the silane fluid model developed by Nienhuis [1 – 3] with the extended fluid model described above, a simulation was carried out with each set of reactions, at 0.2 Torr and with a gas flow of 20 sccm silane.

A comparison of the calculated densities (obtained in the middle of the plasma) of the most important species, calculated with both models is given in Table IX.

Species	Original silane model	Extended silane model
SiH ₄	1.2 x 10 ²¹	1.2 x 10 ²¹
H ₂	3.3 x 10 ²¹	3.3 x 10 ²¹
Si ₂ H ₆	1.3 x 10 ²⁰	1.3 x 10 ²⁰
SiH ₃	2.8 x 10 ¹⁸	2.9 x 10 ¹⁸
SiH ₂	3.7 x 10 ¹⁷	3.4 x 10 ¹⁷
H	1.4 x 10 ¹⁸	1.3 x 10 ¹⁸
SiH ₃ ⁺	-	1.3 x 10 ¹⁶
SiH ₂ ⁺	1.9 x 10 ¹⁶	2.2 x 10 ¹⁴
Si ₂ H ₄ ⁺	7.2 x 10 ¹⁵	5.7 x 10 ¹⁵
H ₂ ⁺	1.1 x 10 ¹⁵	5.2 x 10 ¹³
SiH ₃ ⁻	2.7 x 10 ¹⁶	1.8 x 10 ¹⁶
electrons	7.2 x 10 ¹⁴	9.7 x 10 ¹⁴

Table IX: Calculated densities of the most important species (m⁻³) obtained with the original silane model of Nienhuis [1 - 3] and with the extended silane model at 25 Watt, 13.56 MHz, 0.2 Torr, 20 sccm SiH₄.

From these simulations, it follows that the densities of the neutral molecules (SiH₄, H₂, Si₂H₆ and higher order silane molecules) and radicals (SiH₃, SiH₂ and H) were found to be in relatively good agreement. For the ions and the electrons, some differences were observed. As can be seen from table IX, the largest discrepancy was found for the SiH₃⁺ and SiH₂⁺ ions. Indeed, in the original model of Nienhuis, ionisation of SiH₄ was assumed to yield only SiH₂⁺ ions, based on the total ionisation cross section of SiH₄. In our model, we have incorporated the partial ionisation cross sections, leading to the formation of the ions SiH₃⁺ and SiH₂⁺. Because SiH₂⁺ ions are consumed in the ion-neutral reactions, whereas the SiH₃⁺ ions are mainly formed in

these reactions (see Table III), the SiH_3^+ density is found to be considerably higher than the SiH_2^+ density. This calculated result is in agreement with the experimental results obtained by Hamers [25]. Further, some extra ion-neutral reactions are included in our model. This results in a somewhat lower SiH_3^- density compared to the value calculated with the model of Nienhuis, because SiH_3^- is consumed more in these additional ion-neutral reactions.

6.3.2. The silane/helium discharge

For the study of the silane/helium discharge, a number of simulations were carried out using a different input gas mixture: the silane gas flow was varied from 2 to 6 sccm, with the total gas flow fixed to 20 sccm (at a pressure of 0.45 Torr). In Figure 1, the densities of the most important species are presented, as a function of silane inlet gas flow (2 – 6 sccm).

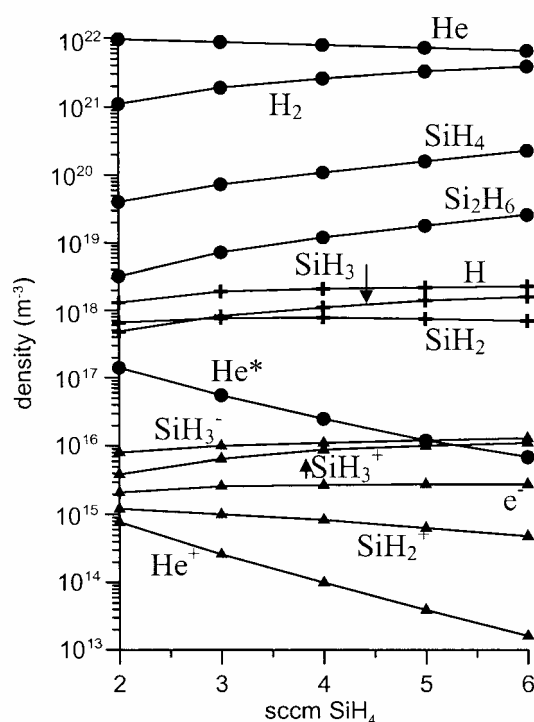


Figure 1: Calculated densities (m^{-3}) of the non-radical neutrals, radicals, ions and electrons, as a function of SiH_4 input gas flow at 25 W, 13.56 MHz, 0.45 Torr.

Note that the densities of the species presented in this figure are taken in the middle of the plasma. While the densities of the neutral background molecules (SiH_4 , He,...) are constant over the distance between the electrode plates, the densities of the electrons,

ions and radicals have their maxima in the middle of the discharge. From figure 1, it can be seen that helium is the major species, which is like expected because of the higher gas input flow. Beside this, the relative importance of the various silane species is comparable to the pure silane plasma described in section 3.1

The most important silane ions are SiH_3^- and SiH_3^+ . The densities of the ions Si_2H_4^+ , SiH_2^+ and H_2^+ are somewhat lower than these of the SiH_3^- and SiH_3^+ ions. In figure 1, only the SiH_3^- , SiH_3^+ and SiH_2^+ densities are shown. Over the whole range of simulations, the electron density appears to be nearly constant (about $2 \times 10^{15} \text{ m}^{-3}$). Further, the He^* and He^+ species become more important when less silane gas (and hence more helium) is introduced into the plasma, which is like expected. In general, the helium gas does not appear to influence (or participate to) the silane plasma to any large extent. This can be explained from the high threshold energies of the electron-He excitation (19.9 eV) and He ionisation (24.6 eV) reactions (which means that the species He^* and He^+ are not created in high abundances), and from the fact that helium is an inert gas (i.e., the chemical reactions between the helium and silane species are of minor importance).

6.3.3. The effect of small amounts of air in a SiH_4/He plasma.

In order to examine the role of small amounts of air (i.e., containing 18 % O_2 and 82 % N_2) added to a silane/helium discharge, a number of simulations have been carried out at 0.45 Torr, using a total gas input of 20 sccm. The air flow is varied within the range of 0.01 – 0.5 sccm. Further, for all simulations, 2 sccm silane is introduced, while the sccm helium added to the plasma is adjusted (17,5 – 17.99 sccm) in order to obtain a total input flow of 20 sccm.

In Figure 2, the densities of the most important species are given as a function of air inlet flow (0.01 – 0.5 sccm).

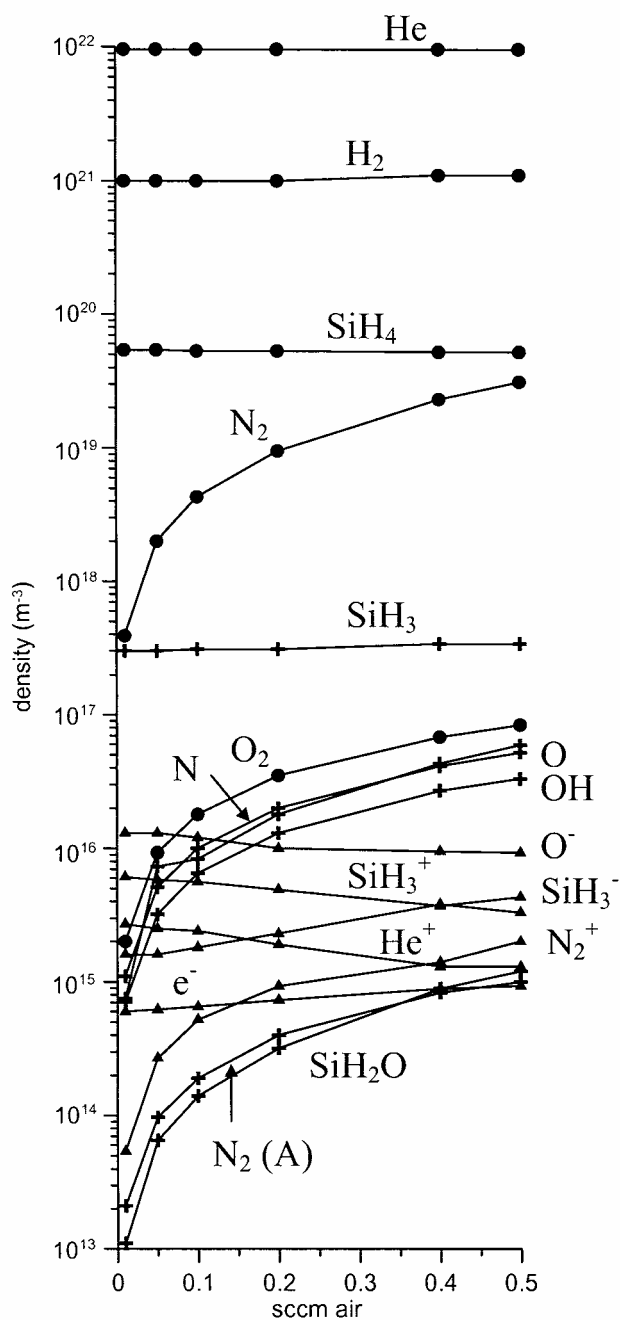


Figure 2: Calculated densities (m^{-3}) of the non-radical neutrals, radicals, ions and electrons, as a function of air input gas flow at 25 W, 13.56 MHz, 0.45 Torr, total gas flow: 20 sccm.

It appears that the neutral species (He, H₂ and SiH₄) are present at high densities, comparable to the results obtained with a SiH₄/He discharge (section 3.2.). As can be seen from figure 2, the density of SiH₄ remains more or less constant in the range of

simulations. Note that a large fraction of SiH_4 is consumed in the formation of higher order silane molecules (Si_3H_8 , Si_4H_{10} and others) and further, a large number of silane rich species stick to the wall contributing to the growth of the layer. As expected: when more air is introduced, the densities of the neutral species N_2 and O_2 become higher. Also the species, created from the electron- N_2 and electron- O_2 reactions (i.e., the ions N_2^+ , O_2^+ , O^+ , and the radicals N and O), and from the neutral-neutral reactions (i.e., SiH_2O , SiO_2 and others) show a similar increasing behavior. The most important oxygen-containing species are the radicals O and OH , while the radical N is the most important nitrogen-containing species. It is worth to mention that not so many nitrogen-containing species are formed. Indeed, the N_2 species are not consumed to a large extent in the neutral-neutral and electron- N_2 reactions. This is in contrast with O_2 , which plays a rather important role in the neutral-neutral chemistry, creating a large number of different oxygen rich species (SiH_2O , SiO_2 , OH), which also are lost in the plasma by sticking to the substrate. Hence in contrast to N_2 , a large amount of O_2 is consumed in the plasma-chemistry. When more air (i.e., also more O_2) is introduced, it can be seen that the O^- density decreases slightly. This can be explained as follows: when adding more O_2 , more O^- is consumed in the ion-neutral reactions with oxygen species (O_2^+ , O and O^+ , see Table VII). Finally, the excited species N_2 (A) and O_2 ($^1\Sigma$ and $^1\Delta$, not shown on figure) have densities in the order of $10^{14} - 10^{15} \text{ m}^{-3}$ and $10^{12} - 10^{13} \text{ m}^{-3}$ respectively.

In Figure 3, the fluxes ($\text{m}^{-2}\text{s}^{-1}$) of the most important radicals and ions towards the electrodes are given, also as a function of air inlet flow (0.1 – 0.5 sccm).

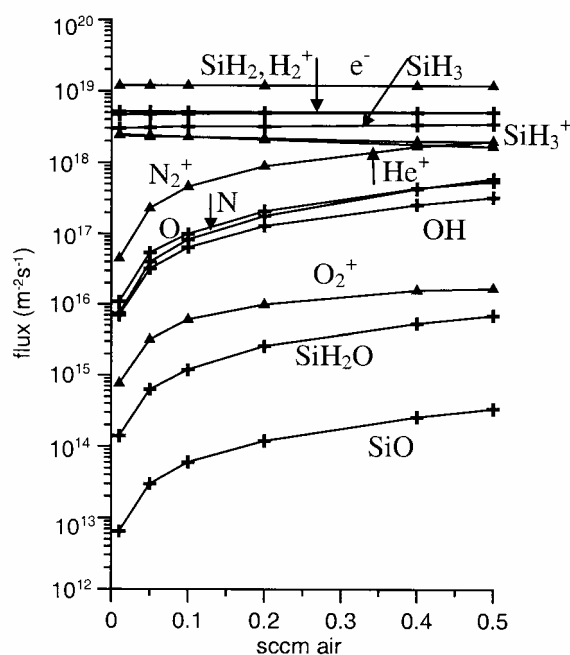


Figure 3: Calculated radical and ion fluxes ($\text{m}^{-2}\text{s}^{-1}$) towards the electrodes, as a function of air flow at 25 W, 13.56 MHz, 0.45 Torr.

Note that the fluxes to the powered and grounded electrode are equal here, due to the limitations of the one-dimensional model (no bias voltage is applied). The electron flux to the electrodes appears to be constant for the whole range of simulations. A similar behavior is also observed for the ionic species SiH_3^+ and He^+ . The fluxes of the species SiH_3 and SiH_2 have comparable densities as in the silane/helium case (i.e., in the order of $10^{18} \text{ m}^{-2}\text{s}^{-1}$). The fluxes of the species containing oxygen and/or nitrogen are found to increase, when more air is added to the plasma, which is logical. The N_2^+ flux is about two orders higher than the O_2^+ flux. The most important oxygen and nitrogen radical fluxes are O, N and OH, while the fluxes of the species SiH_2O and SiO are some orders lower. Finally, the fluxes of the other ions and radicals taken into account in our model (see Tables I and V) are still lower (not shown in this figure). Finally, it is worth mentioning that the total electron and ion fluxes towards both electrodes, averaged over 1 rf-cycle, are equal to each other.

In Figure 3, only the fluxes of the most important ions (He^+ , SiH_3^+ and H_2^+) are given. From the fluxes, we can obtain a rough estimation of the impurities included in the deposited silicium layer. We will focus only on the concentration of oxygen in the layer because it is generally known that this affects the quality of the deposited silicium layer. From the product of the fluxes with the surface sticking coefficients of

the most important silicium (SiH_3 and SiH_2) and oxygen species (O, OH), we can obtain some information of the ratio O/Si in the layer. Note that the fluxes of the SiH_3 and SiH_2 are in the order of $10^{18} \text{ m}^{-2}\text{s}^{-1}$ (for the whole range of simulations), whereas the O flux is in the order of $10^{16} \text{ m}^{-2}\text{s}^{-1}$ for 0.01 sccm air input, and it reaches a value of $5 \times 10^{17} \text{ m}^{-2}\text{s}^{-1}$ when 0.5 sccm air is introduced. As mentioned before (section 2.3), the sticking coefficients of the oxygen rich species are assumed to be 0.1, whereas the sticking coefficients of SiH_2 and SiH_3 are respectively 0.8 and 0.1 [4].

The deposition ratio for 0.01 sccm air input can be estimated in a simple way as follows:

Si: $\text{flux}(\text{SiH}_2) * \text{sticking coefficient}(\text{SiH}_2) + \text{flux}(\text{SiH}_3) * \text{sticking coefficient}(\text{SiH}_2)$

$$5 \times 10^{18} * 0.8 + 3 \times 10^{18} * 0.1 = 4.1 \times 10^{18}$$

O: $\text{flux}(\text{O}) * \text{sticking coefficient}(\text{O}) + \text{flux}(\text{OH}) * \text{sticking coefficient}(\text{OH})$

$$10^{16} * 0.1 + 8 \times 10^{15} * 0.1 = 1.8 \times 10^{15}$$

From this, it follows that the ratio O/Si becomes $1.8 \times 10^{15} / 4.1 \times 10^{18}$, giving a value of 0.05 %. For an input air flow of 0.5 sccm, similar estimations yield a ratio O/Si in the order of 2%. Because of the uncertainties in the sticking coefficients, this is only a rough estimation, and also not yet validated. However, it gives at least some idea on the order of magnitude of the amount of oxygen in the layers.

6.4. Conclusions

A 1D fluid model was presented for the modelling of silane/helium plasmas, including also impurities of oxygen and nitrogen. In the pure silane plasma, SiH_3^+ is found to be the dominant ion, because SiH_2^+ can react further in several ion-neutral reactions to form other ionic species. For the silane/helium mixture, it is found that helium does not affect drastically the silane chemistry. The addition of small amounts of oxygen and nitrogen, however, changes the plasma chemistry to a large extent. The simulations show that, for an input gas flow of air (containing 18 % oxygen and 82 % nitrogen) in the region of 0.01 – 0.5 sccm, a number of oxygen and nitrogen-containing species (i.e., O, OH, N,...) are present in the plasma at relatively high densities, and can hence be incorporated in the deposited silicon layer.

Finally, the product of the calculated fluxes of the most important oxygen and silicium containing species with their sticking coefficients gives some preliminary information of the amount of oxygen introduced in the layer.

6.5. References

- [1] G. J. Nienhuis, W. J. Goedheer, E. Hamers, W. Van Sark en J. Bezemer, *J. Appl. Phys.* **82**, 2060 (1997)
- [2] G. J. Nienhuis, W. J. Goedheer, *Plasma Sources Sc. Techn.*, **8**, 295 (1999)
- [3] G. J. Nienhuis, Ph. D. thesis, University of Utrecht (1998)
- [4] M. Kurachi en Y. Nakamura, *J. Phys. D: Appl. Phys.*, **22**, 107 (1989)
- [5] H. Chatham, *J. Chem. Phys.*, **81**, 1770 (1984)
- [6] J. Perrin, J. P. M. Schmitt, G. De Rosny, *Chemical Physics* , **73**, 383 (1982)
- [7] P. Haaland, *J. Chem. Phys.*, **93**, 4066 (1990)
- [8] H. Ehrhardt en L. Langhans, *Phys. Rev.*, **173**, 222 (1968)
- [9] A. G. Engelhardt en A. V. Phelps, *Phys. Rev.*, **131**, 2215 (1963)
- [10] H. Tawara en t. Kato, *At. Data and Nucl. Data Tables*, **36**, 167 (1987)
- [11] E. Krishnakumar, *Contrib. Plasma Physics*, **35**, 395 (1995)
- [12] A. V. Phelps: ftp://jila.colorado.edu/collision_data
- [13] M. J. Kushner, *J. Appl. Phys.*, **71**, 4173 (1992)
- [14] A. P. Hickman, *J. Chem. Phys.*, **70**, 4872 (1979)
- [15] J. M. Henis, G. W. Stewart, M. K. Tripodi, *J. Chem. Phys.*, **57**, 389 (1972)
- [16] H. Chatham, A. Gallagher, *J. Appl. Phys.*, **58**, 159(1985)
- [17] E. R. Austin, F. Lampe, *J. Phys. Chem.*, **81**, 1134 (1977)
- [18] J. Perrin, O. Leroy, M. C. Bordage, *Contrib. Plasma Phys.*, **36**, 3 (1996)
- [19] N. Itabashi, K. Kato, N. Nishiwaki, *Jpn. J. Appl. Phys.*, **28**, L325 (1989)
- [20] H. Yoshida, Y. Moishima, M. Ukai, K. Shinsaka, N. Kouchi, *Chem. Phys. Letters*, **176**, 173 (1993)
- [21] Y. Watanabe, M. Shiratani, T. Fukuzawa, H. Kawasaki, *Plasma Sources Sci. Technologies*, **3**, 355 (1994)
- [22] M. Shiratani, H. Kawasaki, T. Fukuzawa, H. Tsuruoka, T. Yoshioka, Y. watanabe, *Appl. Phys. Letters*, **65**, 1900 (1994)
- [23] J. C. Knights, R. A. Lujan, M. P. Rosenblum, R. A. Street, D. K. Biegleson, J. A. Reimer, *Appl. Phys. Letters*, **38**, 331 (1981)
- [24] M. J. Kushner, *IEEE Transactions on plasma science*, **14**, 188 (1986)
- [25] E. Hamers, Ph. D. thesis, University of Utrecht
- [26] A. V. Phelps, *Joint Institute for Laboratory Astrophysics Report No. 28* (1985)
- [27] A. V. Phelps, L. C. Pitchford, *Phys. Rev.*, **31**, 2932 (1985)
- [28] J. M. Pouvelse, A. Khacef, *J. Chem. Phys.*, **88**, 3061 (1989)

- [29] D. Albitron, *At. Data. Nucl. Data tables*, **22**, 22 (1978)
- [30] M. J. Kushner, *J. Appl. Phys.*, **71**, 6538 (1993)
- [31] J. T. Moseley, R. E. Olson, *Case studies At. Phys.*, **5**, 1 (1975)
- [32] E. W. McDaniel, V. Cernak, *Ion Molecule Reactions* (Wiley, New York, 1970)
- [33] H. Koizumi, M. Ukai, *J. Chem. Phys.*, **85**, 1931 (1986)
- [34] S. Hadj-Ziane, B. Held, P. Pignolet, *J. Phys. D*, **25**, 677 (1992)
- [35] W. B. Demore, S. P. Sander, D. M. Golden, M. J. Molina, *Chemical Kinetics and Photochemical Database for Atmospheric Modeling*, JPL Publication 90-1, 1990
- [36] W. Tsang, R. F. Hampson, *J. Phys. Chem. Ref. Data*, **15**, 1087 (1986)
- [37] K. Tokuhashi, S. Horiguchi, Y. Urano, M. Iwasaka, *Combust. Flame*, **82**, 40 (1990)
- [38] P. Dagaut, M. Cathonnet, J. C. Boettner, *Combust. Flame*, **70**, 295 (1988)
- [39] G. R. A. Johnson, *Radiation Chemistry of Nitrous Oxide Gas*, NSRDS-NBS 45, 1973
- [40] J. O. Chu, D. B. Beach, J. M. Jasinski, *Chem. Phys. Lett.*, **143**, 135 (1988)
- [41] M. Petitjean, N. Proust, J. F. Chapeanblanc, *Appl. Surf. Sci.*, **46**, 189 (1990)
- [42] R. Atkinson, J. N. Pitts, *Int. J. Chem. Kin.*, **10**, 1151 (1978)
- [43] L. G. Piper, G. E. Caledonia, *J. Phys. Chem.*, **95**, 698 (1991)
- [44] L. E. Kline, W. D. Parlow, R. M. Young, R. R. Mitchell, *Trans. Plasma Sci.*, **19**, 278 (1991)
- [45] C. DeJoseph, Report WRDC-TR-90-200, Wright Patterson Aero Laboratories, January 1990
- [46] L. G. Piper, *J. Chem. Phys.* **88**, 231 (1988)
- [47] A. Bouchoule, *Dusty Plasmas: Physics, Chemistry and Technical impacts in Plasma Processing*, John Wiley & Sons (UK), 1999
- [48] W. W. Stoffels, E. Stoffels, *Physics and application of dusty low pressure plasma*, *Trends in Vacuum Science & Technology*, **1**, **4** (2001)
- [49] G.M.W. Kroesen, E. Stoffels, W.W. Stoffels, G.H.P.M. Swinkels, A Bouchoule, Ch. Hollenstein, P. Roca I Cabarrocas, J.C. Bertolini, G.S. Selweyn, F.J. de Hoog, *Dusty Plasmas: Fundamental aspects and industrial applications*, 175, published in: *Advanced Technologies Based on Wave and Beam Generated Plasmas* (NATO Science Series), Kluwer academic Publishers, 1998 (The Netherlands)

Chapter 7: Comparison of a Boltzmann model and a Monte Carlo model for the calculation of the electron reaction rate coefficients

7.1. Introduction

In this chapter, a comparison is made between two different types of models which calculate the reaction rate coefficients of the electron methane reactions. The first type of model, i.e., the simplified Boltzmann model, is described in detail in chapter 2. The results of this Boltzmann model are used as input in the fluid models, described in the previous chapters. In the second type of model, the electron-neutral reaction rate coefficients were obtained from a one-dimensional Monte Carlo (MC) model, which considers the transport and collisions of the electrons. The Monte Carlo Model itself is taken from a particle-in-cell/Monte Carlo model (PIC/MC) [1, 2].

As mentioned in chapter 1, the PIC/MC approach is known as the most accurate method to model glow discharge plasmas, because it simulates the behavior of the individual particles in an explicit way. The trajectory is calculated with Newton's laws: the collisions between the plasma species depend on the cross sections and are determined by random numbers. However, the main disadvantage of the particle-in-cell/Monte Carlo model is the requirement of a large amount of computer time, because one needs to follow a large number of particles for statistically valid results. This means that the number of different plasma species taken into account in the model should be limited, in order to keep the calculation time reasonable. Although the fluid model is in principle not as accurate as the PIC/MC model, its great advantage is that it requires less computation time compared to the PIC/MC method, and that a large number of plasma species can be considered without significantly increasing the calculation time.

A compromise between a pure fluid model and a PIC/MC model is found when a fluid model is used with input from an electron Monte Carlo model. In this way, the main advantage of the fluid model (less computation effort) and the main advantage of the Monte Carlo model (more accurate) are combined, and the disadvantages of both individual models are reduced. The results obtained with this fluid model using Monte Carlo input will be presented in this paper, and compared to the results of a fluid model, using input from the simplified Boltzmann model. In both model

approaches, the fluid model and the Boltzmann or Monte Carlo model were run iteratively until convergence was reached.

It is, however, worth mentioning that in both cases described below, the electron energy equation is maintained in the fluid model, in order to calculate the average electron energy as a function of time and space. This average electron energy is necessary to obtain the corresponding reaction rate coefficients from the look-up tables (average reaction rate coefficients versus average electron energy). A more sophisticated hybrid fluid-Monte Carlo approach would involve that the Monte Carlo model produces the reaction rates as a function of time and space, which can directly be used in the fluid model. In this way, the calculation of the average electron energy should not be necessary anymore in the fluid model. However, despite the fact that this hybrid approach is developed successfully for the modelling of capacitively coupled rf argon plasmas in previous years [3 - 5], we were not able to convert this approach for the modelling of plasmas using molecular gases like silane or methane.

7.2. Description of the one-dimensional fluid model

The fluid model used here is the same as the one used in the previous chapters, and is described in detail in chapter 2. In the models described before, the input data (reaction rate coefficients of the electron-neutral reactions) used for the fluid model were taken from a simplified Boltzmann model.

7.3. The one-dimensional Monte Carlo model

The electron Monte Carlo model is developed for a methane plasma. Hence, in order to compare the results of the methane fluid model, which uses input from the Boltzmann model, with the results of the fluid model coupled to a Monte Carlo model, the same electron reactions were considered in both models. Whereas in the first case, the Boltzmann model produces the look-up tables (reaction rate coefficient versus average electron energy) for the electron-neutral reactions, these tables are now obtained from the Monte Carlo model for electrons.

To run the Monte Carlo model, the electric field (as a function of space (i.e., distance between the electrodes) and time) and electron density (at the start of an rf cycle) are needed as input. The Monte Carlo method is based on following a large number of electrons. The trajectory of every electron is calculated by Newton's laws in a given electric field. In order to obtain the reaction rate coefficients of the different electron

reactions, the different electron collisions (mentioned in chapter 3) are considered in the Monte Carlo model.

Because the Monte Carlo model uses the total electric field calculated from the fluid model (i.e., as a function of space and time), a more realistic EEDF (electron energy distribution function) is calculated, compared to the Boltzmann case. This leads to more accurate reaction rate coefficients for the different electron-neutral reactions.

The Monte Carlo model is run for 10 rf-cycles and follows normally 50000 electrons per rf-cycle, in order to obtain statistically good results. As mentioned above, the look-up tables produced with the Monte Carlo model are now used as input for the fluid model to calculate the source terms. The present simulations (25 Watt, 13.56 MHz, pressure region: 0.14 - 0.5 Torr) are carried out in the alpha-regime [6, 7]. Hence, secondary electrons emitted at the electrodes have no important influence on the discharge characteristics, and can therefore be neglected.

Running the fluid model with input from the Monte Carlo model proceeds as follows. First, a simulation with the fluid model is carried out using the look-up tables from the Boltzmann model. This yields, among others, an electric field and electron density. The electric field (as a function of position and time) and electron density (at the beginning of the rf-cycle, as a function of position) are then used as input for the Monte Carlo model. The distance between the electrodes (3 cm) is divided in 64 zones, while the rf cycle is divided in 80 time steps. This leads to 5200 values for the average electron energy and corresponding reaction rate coefficients (one for every reaction) as output from the Monte Carlo model.

The average electron energy (as a function of space x and time t) is calculated in the Monte Carlo code as:

$$\langle \varepsilon(x, t) \rangle = \langle m_e v^2 / 2 \rangle$$

where m_e stands for the electron mass and v is the velocity of the electron. The reaction rate coefficient k (also as a function of space x and time t), corresponding to the average electron energy, can be obtained from the product of the cross section $\sigma(v)$ (of the electron reaction) and the electron velocity:

$$\langle k(x, t) \rangle = \langle \sigma(v)v \rangle$$

From these 5200 points, the look-up tables with electron reaction rate coefficients versus the average electron energy are produced (by mathematical averaging), and they are then used as an input for the fluid model. The process of running the fluid

and Monte Carlo model iteratively is continued until convergence is reached, i.e., when the differences in species densities calculated in two successive fluid runs are less than 1%. Typically, 4 or 5 fluid-MC runs are necessary before convergence is reached.

7. 4. Comparison of the results obtained with a fluid model using input of a Boltzmann and a Monte Carlo model.

The simulations are carried out in one dimension (distance of 3 cm between the two electrodes), assuming a small capacitively coupled rf PACVD-reactor. A comparison between both models has been carried out for 2 different pressure conditions, i.e., 0.14 and 0.5 Torr. The rf frequency is 13.56 MHz and the power is kept constant at 25 Watt. The gas flow inlet is set to 20 sccm CH₄, no H₂ is pumped in.

7.4.1. Condition 1: 0.14 Torr

In order to give an idea about the differences between the electron reaction rate coefficients k , produced by the simplified Boltzmann model and by the Monte Carlo model, Figure 1 presents the electron reaction rate coefficients, as a function of average electron energy, of the electron-methane reactions given in table 1 (i.e., one vibrational excitation, one dissociation and one ionisation reaction, both for methane and hydrogen).

Electron-neutral reaction	Threshold energy (eV)	Reaction
$\text{CH}_4 + e^- \rightarrow \text{CH}_4^* + e^-$	0.16	vibr.excitation
$\text{CH}_4 + e^- \rightarrow \text{CH}_3 + \text{H} + e^-$	8.0	dissociation
$\text{CH}_4 + e^- \rightarrow \text{CH}_3^+ + \text{H} + 2 e^-$	12.6	ionisation
$\text{H}_2 + e^- \rightarrow \text{H}_2^* + e^-$	1.62	vibr.excitation
$\text{H}_2 + e^- \rightarrow \text{H} + \text{H} + e^-$	8.9	dissociation
$\text{H}_2 + e^- \rightarrow \text{H}_2^+ + 2 e^-$	15.4	ionisation

Table 1: Electron-neutral reactions occurring in a methane/hydrogen plasma for which the calculated electron reaction rate coefficients k are given as a function of average electron energy in figures 1 and 2.

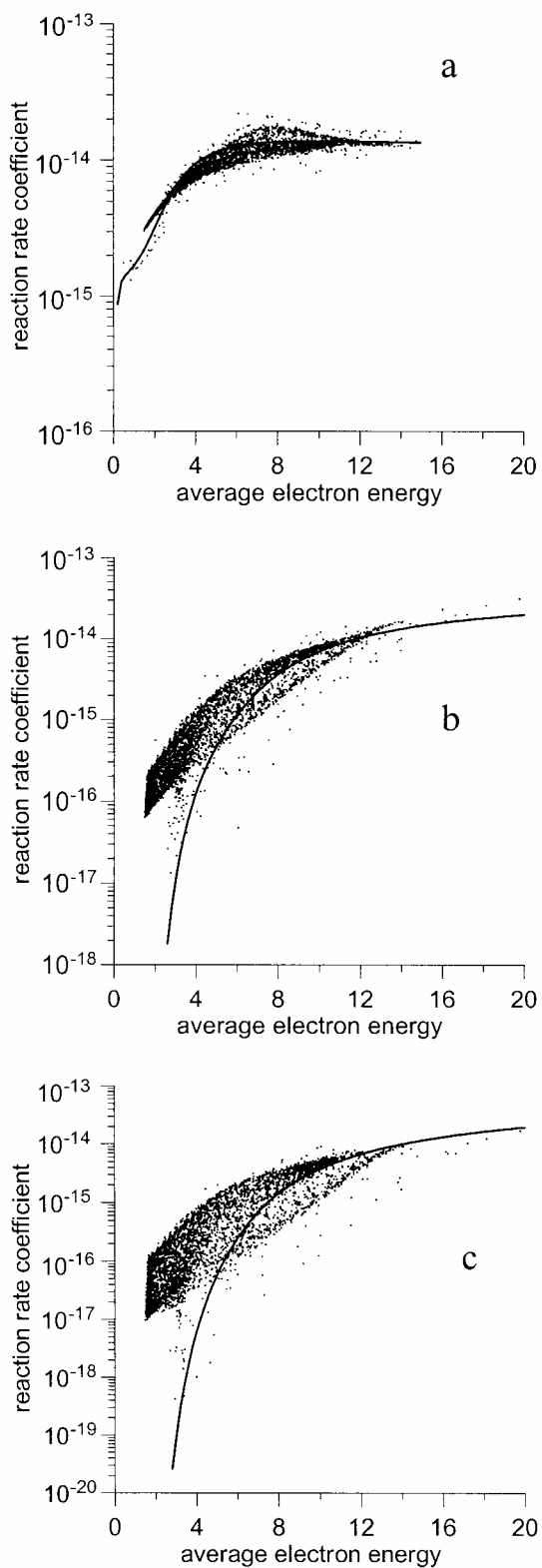


Figure 1: Reaction rate coefficients k of the electron-methane reactions given in Table 1, calculated with the Boltzmann model (curve) and the Monte Carlo model (points). a: vibrational excitation; b: dissociation; c: ionisation.

Figure 1a shows the reaction rate coefficients of the vibrational excitation reaction of methane, with a threshold energy of 0.16 eV, obtained with both models. It can be seen that the results obtained with the Boltzmann model (smooth line) and the Monte Carlo model (5200 points) are in good agreement. In the average electron energy range between 4 and 10 eV of the Monte Carlo values, a small “hill of points” (above the Boltzmann curve) can be seen. A detailed study showed that the points corresponding to this “hill” originate from the whole rf cycle: this means that these points are not created at a certain period of the rf-cycle.

Figure 1b presents the reaction rate coefficient of the dissociation reaction of methane into CH_3 and H (threshold energy: 8 eV). It can be seen that, for lower average electron energies, the Monte Carlo values give higher reaction rate coefficients compared to the Boltzmann curve. The same tendency can also be found for the reaction rate coefficients of the ionisation reaction of CH_4 which forms CH_4^+ (see figure 1c). The difference between the results of both model can be explained from the fact that the Monte Carlo model uses a more correct electric field, compared to the Boltzmann model.

Figure 2 gives information about the reaction rate coefficients of the electron-hydrogen reactions (vibrational excitation, ionisation and dissociation), also presented in Table 1. As can be seen from figure 2a, the values for the vibrational excitation reaction of H_2 with a threshold energy of 1.62 eV obtained with the Boltzmann model and the Monte Carlo model are again in good agreement. For an average electron energy between 4 and 8 eV, similar like for the vibrational excitation reaction of CH_4 , again some points are obtained above the Boltzmann curve.

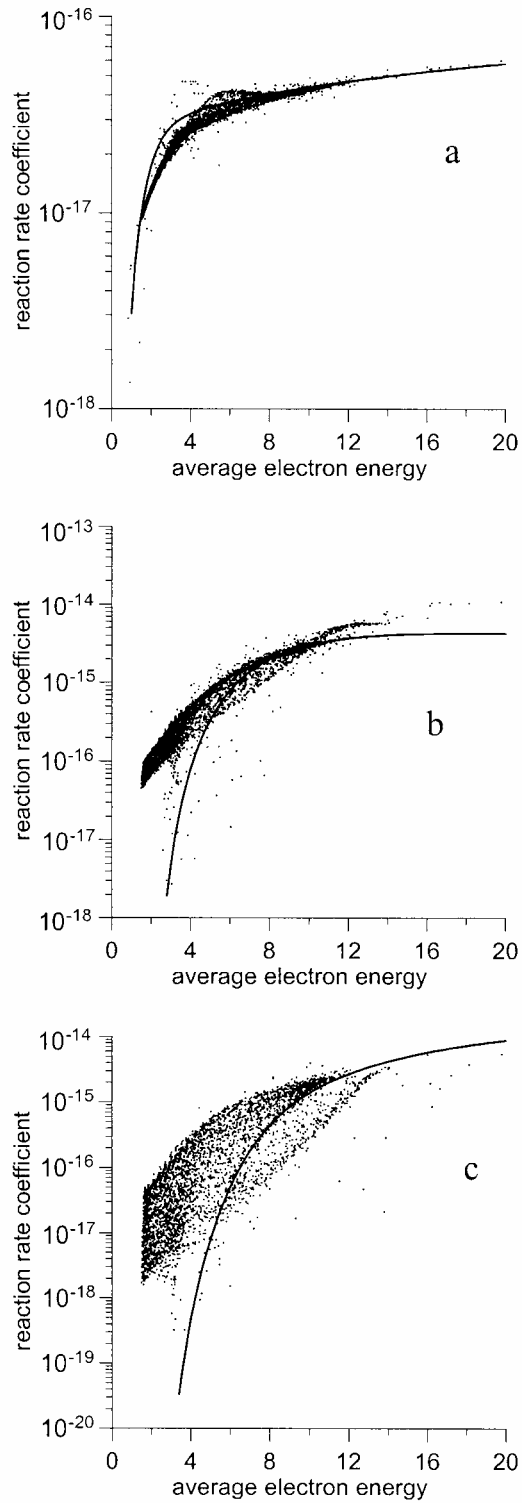


Figure 2: Reaction rate coefficients k of the electron-hydrogen reactions given in Table 1, calculated with the Boltzmann model (curve) and the Monte Carlo model (points). a: vibrational excitation; b: dissociation; c: ionisation.

For the ionisation and dissociation reaction of H₂, the same conclusions can be drawn as for CH₄, i.e., for lower average electron energies, the Monte Carlo model gives higher reaction rate coefficient values than the Boltzmann model (see figures 2b and 2c). It is worth mentioning that for the other electron-neutral reactions taken into account in the methane/hydrogen model, the same conclusions can be drawn as for the reactions described above.

In Table 2, the densities, in the middle of the plasma, of the most important plasma species are given as calculated by the fluid/Boltzmann and the fluid/Monte Carlo model. It can be seen that the differences in the charged species densities calculated with both models are considerable.

Species	Fluid/Boltzmann	fluid/Monte Carlo
Electrons	1.1x10 ¹⁵	2.1x10 ¹⁵
CH ₄ ⁺	1.8x10 ¹⁴	2.4x10 ¹⁴
CH ₃ ⁺	9.0x10 ¹³	1.5x10 ¹⁴
CH ₅ ⁺	3.6x10 ¹⁴	7.4x10 ¹⁴
C ₂ H ₅ ⁺	2.2x10 ¹⁴	5.7x10 ¹⁴
CH ₄	2.1x10 ²¹	2.3x10 ²¹
H ₂	5.8x10 ²⁰	5.8x10 ²⁰
C ₂ H ₆	2.7x10 ²⁰	2.0x10 ²⁰
CH ₃	5.4x10 ¹⁸	4.8x10 ¹⁸
CH ₂	4.1x10 ¹⁶	2.4x10 ¹⁶
H	8.8x10 ¹⁷	6.5x10 ¹⁷

Table 2: Comparison of the densities (species/m³), in the middle of the plasma, of the various plasma species calculated with the fluid models using input from a Boltzmann and a Monte Carlo model at 0.14 Torr.

The electron density calculated in the fluid/Boltzmann model is 1.1x10¹⁵ m⁻³, while this is 2.1x10¹⁵ m⁻³ in the fluid/Monte Carlo model. The higher electron density, as calculated in the fluid/Monte Carlo model, can be explained from the higher ionisation rate coefficients (see figure 1c). A rise in electron density leads also to more positive ions. It appears that the increase is most pronounced for the CH₅⁺ and

C_2H_5^+ ion densities. These ions are mainly formed in the ion-neutral reactions (i.e., for example: $\text{CH}_4^+ + \text{CH}_4 \rightarrow \text{CH}_5^+ + \text{CH}_3$). A small increase of the reactants (i.e., the densities of CH_4 and CH_4^+ are higher in the fluid/Monte Carlo model), will lead to a higher production term of this ion, and hence also a higher ion density. It should be noted that in total 8 different ions are considered in the plasma model, hence the total sum of the positive ion density equals the total electron density.

It is also worth mentioning that the neutral species densities (i.e., radicals and background molecules) calculated in both models are somewhat different. Because the production and loss terms of the species are different in both models, other species densities are obtained. This will also affect the plasma chemistry and hence, lead to other species densities.

Differences in species densities between the two models at 0.14 Torr, can be explained as follows. At this low pressure, the electrons can penetrate further into the discharge before they cause ionisation or dissociation reactions, i.e., their energy is not lost locally. Hence at low pressure, the Monte Carlo model, which uses the real electric field as a function of time and space, gives a better description of the electron behaviour than the Boltzmann model not using this “total” electric field, which produces less accurate results at low pressures. Nevertheless one can notice that both models produce results (species densities) in the same order of magnitude.

7.4.2. Condition 2: 0.5 Torr

The comparison of the reaction rate coefficients k at 0.5 Torr, obtained with the Boltzmann model and the Monte Carlo model, for the different electron-neutral reactions, gives analogous results as obtained for the low pressure case (see figures 1 and 2), and is therefore not shown here. However, the differences between the reaction rate coefficients obtained with both models (especially in the lower average electron energy range) are somewhat smaller than in the case of 0.14 Torr. An overview of the species densities (in the middle of the plasma) obtained with the two models is given in Table 3.

Species	fluid/Boltzmann	Fluid/Monte Carlo
Electrons	2.4×10^{15}	3.6×10^{15}
CH_4^+	1.1×10^{12}	1.0×10^{12}
CH_3^+	2.4×10^{13}	2.3×10^{13}
CH_5^+	1.6×10^{13}	1.8×10^{13}
C_2H_5^+	1.6×10^{15}	2.7×10^{15}
CH_4	7.2×10^{21}	7.8×10^{21}
H_2	1.4×10^{21}	1.4×10^{21}
C_2H_6	1.6×10^{21}	1.3×10^{21}
CH_3	6.4×10^{18}	5.9×10^{18}
CH_2	3.5×10^{15}	2.8×10^{15}
H	3.0×10^{18}	2.5×10^{18}

Table 3: Comparison of the densities (species/m³), in the middle of the plasma, of the various plasma species calculated with the fluid/Boltzmann and the fluid/Monte Carlo model at 0.5 Torr.

It can be seen that the differences in species densities between the two models at 0.5 Torr are smaller compared to the case studied at 0.14 Torr (section 7.4.1.). The electron density increases from $2.4 \times 10^{15} \text{ m}^{-3}$ in the fluid/Boltzmann model to $3.6 \times 10^{15} \text{ m}^{-3}$ in the fluid/Monte Carlo model (for the same reason as explained in 7.4.1.). The increase of the electron density in the fluid/Monte Carlo model, compared to the fluid/Boltzmann model, is again accompanied with an increase in ion densities. At 0.5

Torr, the largest difference in ion density is obtained for $C_2H_5^+$ (i.e., $1.6 \times 10^{15} \text{ m}^{-3}$ in the fluid/Boltzmann model and $2.7 \times 10^{15} \text{ m}^{-3}$ in the fluid/Monte Carlo model). It is worth mentioning that all other ion densities are somewhat lower in density compared to the $C_2H_5^+$ density. This can be explained as follows. At higher pressures, the ion-neutral reactions become more important. Because $C_2H_5^+$ is mainly formed in these ion-neutral reactions, it will also be present at the highest density. The neutral densities calculated in the fluid/Monte Carlo model also differ somewhat from the values obtained with the fluid/Boltzmann model. It is also worth mentioning that at higher pressures, the neutral-neutral reactions become more important. This will also affect the plasma chemistry, and hence lead to somewhat other species densities (although the differences in neutral species densities, calculated by the two approaches, are less than in the case of 0.14 Torr)

In general, it can be concluded that for 0.5 Torr, the densities of the charged and neutral particles calculated with the two models are more or less the same. Indeed, at the relatively high pressure under study here, the mean free path of the electrons is short, hence the electrons lose their energy locally, due to the many electron collisions. The reaction rate coefficients obtained with the Monte Carlo model are thus determined to a large extent by the local electric field. This local electric field is also used in the Boltzmann model to calculate the reaction rate coefficients. Hence, the use of the local electric field value in the Boltzmann model, appears to be a very good approximation for this higher pressure condition.

7.5. Conclusions

A fluid model using input from 2 different models (a Boltzmann and a Monte Carlo model) is used to simulate rf plasmas in methane, at two different pressure conditions. For the simulations at 0.5 Torr, a relatively good agreement is obtained between the results (species densities) of both models, because the electrons lose their energy locally at these relatively high pressures. Hence, the “local” electric field used in the Boltzmann model is a good approximation and gives analogous results as the fluid model with input from a Monte Carlo model. At lower pressure (0.14 Torr), the Boltzmann model becomes less accurate because the local electric field approximation used in this model is not so valid anymore. Indeed, the electrons do not lose their energy locally to a great extent. Hence, the species densities (especially the charged species densities) obtained with the fluid/Boltzmann model and the more accurate fluid/Monte Carlo model show larger differences.

However, in both pressure cases, the differences between the two models are rather small, i.e. the species densities remain in the same order of magnitude. Since we wanted to investigate the main physics and the qualitative trends (effect of power, gas flow, ...), the fluid-Boltzmann model, described in chapter 2, is good enough for the conditions used in this work. It is, however, worth mentioning that the small differences obtained for the two cases, also can be explained due to the fact that the results of the Monte Carlo model are not directly introduced in the fluid model, as is done in a real hybrid fluid/Monte Carlo model.

Finally, it is necessary to realize that when modelling plasmas in a lower pressure range (under 0.1 Torr), one should consider using a PIC/MC model.

7.6. References

- [1] M. Yan, W.J. Goedheer, 1999, IEEE Trans Plasma Science, **27**, 1399
- [2] M. Yan, W.J. Goedheer, 1999, Plasma Sources Sci. Technol., **8**, 349
- [3] A. Bogaerts, R. Gijbels, W.J. Goedheer, Jpn. J. Appl. Phys, **38**, 4404 (1999)
- [4] A. Bogaerts, R. Gijbels, W.J. Goedheer, Spectrochimica Acta, **54**, 1335 (1999)
- [5] A. Bogaerts, R. Gijbels, W.J. Goedheer, J. Anal. At. Spectrom., **16**, 750 (2001)
- [6] M. Surendra, D. B. Graves, IEEE Transactions on Plasma Science, **19**, 144 (1991)
- [7] Ph. Belenguer, J. P. Boeuf, Physical Review A, **41**, 4447 (1990)

Samenvatting

De afzetting van dunne koolstof en siliciumlagen, op verschillende substraten, is de voorbije jaren gebruikt in tal van toepassingsgebieden. Zo worden amorfe, diamantachtige lagen (diamond-like carbon layers) veelal afgezet op materialen als beschermlaag, met als doel de slijtage van het materiaal te verminderen. Het afzetten van amorfe siliciumlagen vindt dan weer zijn toepassing in de microelectronica en in de productie van zonnecellen.

Een vrij courante techniek om zulke dunne lagen te produceren is “Plasma Geassisteerde Chemische Dampafzetting” (Plasma Assisted Chemical Vapour Deposition, PACVD). In een reactorvat wordt, bij lage druk, tussen twee platen (elektroden) een plasma (geïoniseerd gas) opgewekt. In dit plasma worden tal van deeltjes gevormd, waarvan enkele zich zullen afzetten op het substraat, en zo bijdragen tot de groei van de laag. Naargelang de af te zetten laag worden verschillende precursor gassen in de reactor ingebracht. Meestal wordt methaan (CH_4) of acetyleen (C_2H_2) gebruikt voor de afzetting van diamantachtige lagen, terwijl vertrokken wordt van silaan (SiH_4) voor de productie van siliciumlagen.

Wanneer één van de twee elektroden verbonden wordt met een radio frequente voeding, terwijl de andere elektrode geaard is, wordt er tussen die twee platen een plasma gecreëerd. Dit plasma wordt opgewekt doordat de elektronen, afkomstig van de aangedreven elektrode, botsingen ondergaan met het ingebrachte gas, waardoor geladen deeltjes (ionen en elektronen) en neutrale deeltjes (al dan niet reactief) worden gecreëerd. Met andere woorden: het plasma bestaat uit een mix van geladen deeltjes (elektronen en ionen (positief en/of negatief)) en ongeladen deeltjes (radicalen en neutralen), waarbij de positieve deeltjesdichtheid (de som van de dichtheden van de positieve ionen) vrijwel gelijk is aan de som van de negatieve deeltjes dichtheden, opgeteld bij de elektronendichtheid. De elektronendichtheid in de bovenvermelde plasma's is in de orde van 10^{15} m^{-3} (druk gebied: 10 – 100 Pa, rf frekwentie: 13.56 MHz, vermogen gebied: 0 – 100 W).

De reacties die plaatsvinden in een plasma kunnen verdeeld worden in twee grote categorieën. Vooreerst zijn er de reacties waarin een elektron botst met een gas deeltje, waarbij er één (of meer) nieuwe deeltjes gevormd worden. Al naargelang er een ion of een radicaal gevormd wordt, spreekt men van een elektron-ionisatie of

dissociatie reactie. Verder zijn er nog elektron excitatie reacties (die leiden tot de productie van een geëxciteerd deeltje) en elektron aanhechtingsreacties, waarbij het elektron aan het gasdeeltje wordt gehecht, met vorming van een negatief geladen deeltje.

Een tweede groep van reacties die plaatsgrijpen in een plasma zijn de ion-neutraal en neutraal-neutraal (of radicaal) reacties: de deeltjes geproduceerd in de elektron-reacties reageren onderling tot vorming van allerlei andere deeltjes. Deze laatste groep van reacties kunnen enkel plaatsvinden wanneer gebruik gemaakt wordt van een *moleculair* precursor gas, dat radicalen kan produceren in elektron reacties.

Om een beter inzicht te krijgen in de plasma's, die gebruikt worden voor de afzettingsprocessen, wordt er gebruik gemaakt van wiskundige modellen: het plasma (en de reacties die erin plaats vinden) worden beschreven aan de hand van een combinatie van wiskundige vergelijkingen. In een eerste fase dient een model te worden ontwikkeld, om het vervolgens te valideren: de resultaten die uit het wiskundig model komen, dienen vergeleken te worden met experimentele gegevens. Vervolgens kan het gevalideerde model worden gebruikt om simulaties uit te voeren voor tal van depositie voorwaarden: op deze manier kan men een voorspelling doen van wat er in het plasma gebeurt (deeltjesdichtheden, fluxen naar de substraten,...), en kan men concluderen bij welke voorwaarden het beste resultaat (depositieproces) behaald wordt.

Dit proefschrift behandelt de wiskundige modellen ontworpen voor het beschrijven (modelleren) van methaan, acetyleen en silaan plasma's, deze laatste met onzuiverheden. Voornamelijk wordt gewerkt met een één-dimensionaal vloeistofmodel ('fluid model') dat de plasma deeltjes beschrijft aanwezig tussen de twee elektrodes. Dit vloeistofmodel werd reeds ontwikkeld door Goedheer en medewerkers. Voor elk deeltje wordt er een massabalansvergelijking opgesteld, waarbij er rekening mee wordt gehouden dat de deeltjes kunnen diffunderen (door concentratieverschillen) en migreren (onder invloed van een elektrisch veld, enkel voor geladen deeltjes). Verder wordt het elektrisch veld in het model berekend uit de Poisson vergelijking. Tenslotte zijn er ook nog de nodige randvoorwaarden die in rekening moeten gebracht worden (bijvoorbeeld: de potentiaal opgelegd aan de aangedreven elektrode). Wanneer men gedetailleerde informatie dient te bekomen

over de variatie van de plasma eigenschappen in functie van de radiale afstand (veronderstellende een cilindrische symmetrische reactor), dan dient uiteraard een twee-dimensionaal plasma model te worden gebruikt. Dit is in feite een uitbreiding van het één-dimensionale model, waar alle vergelijkingen worden opgelost, zowel in functie van de afstand tussen de elektroden als in functie van de radiale afstand.

Naast het vloeistofmodel, zijn ook nog andere gegevens nodig om een dergelijk plasma op een juiste manier te beschrijven. Voor de elektronenreacties is het belangrijk dat men de reactiesnelheidsconstanten voor de verschillende elektron-neutraal reacties kent, als een functie van de gemiddelde elektronen energie. Hiervoor maakt men gebruik van een vereenvoudigd Boltzmann model. Het gebruik van dit model vereist de kennis van de werkzame doorsneden (cross sections) van de verschillende elektron reacties. Voor de beschrijving van de radicaal chemie is ook de kennis vereist van de reactie snelheidsconstanten van de verschillende radicaal reacties, beschouwd in het plasma model.

In een eerste instantie werd een één-dimensioneel vloeistofmodel (dat reeds beschikbaar was bij het begin van dit doctoraat) gebruikt voor de numerieke simulatie van een methaan plasma. Het model zelf neemt 20 deeltjes in rekening (waaronder elektronen, verschillende neutralen, radicalen en ionen), en verder een groot aantal elektron en radicaal reacties, om de plasma chemie zo nauwkeurig mogelijk in beeld te brengen. Daar waar het niet anders kon, zijn er benaderingen gebruikt (bijvoorbeeld: voor werkzame doorsneden van bepaalde reacties, die nodig waren maar niet voorhanden). Het methaan plasma model is getest voor een hele reeks plasma parameters (druk, gas inlaat debiet, vermogen,...) en de resultaten (vooral de berekende deeltjes dichtheden) van het plasma model zijn, waar mogelijk, vergeleken met experimentele gemeten deeltjes dichtheden gehaald uit de literatuur, dit om het model te valideren. Uit de resultaten blijkt dat, vertrekkende van een methaan (CH_4) precursor gas, een hele groep van neutralen (en radicalen) gevormd worden in het plasma. Zo blijkt dat de deeltjes H_2 , C_2H_6 , C_2H_2 en C_2H_4 aanwezig zijn in het plasma, met een vrij hoge dichtheid (orde 10^{20} m^{-3}). De radicalen CH_3 , C_2H_5 en H zijn aanwezig in het plasma in lagere dichtheden (orde $10^{17} - 10^{18} \text{ m}^{-3}$), terwijl de dichtheden van de aanwezige ionen (CH_5^+ , C_2H_5^+ en CH_4^+) liggen in de orde van 10^{14} m^{-3} . Verder is de totale positieve ionendichtheid gelijk aan de elektronendichtheid

(ongeveer 10^{15} m^{-3}). Tenslotte worden de verschillende deeltjes fluxen naar de elektroden toe (substraatoppervlak) kort besproken.

In een volgende fase is vertrokken van exact hetzelfde methaan model (dezelfde deeltjes en reacties) voor het ontwerp van een twee-dimensionaal vloeistofmodel, ter beschrijving van methaan plasma's. Op deze manier verkrijgt men informatie van de deeltjes dichtheden, als een functie van afstand tussen de platen (net zoals bij het 1D model) en als functie van de radiale afstand. De resultaten van het 2D model zijn naderhand vergeleken met deze van het 1D model. Hieruit blijkt dat - en dat is ook logisch - vrijwel analoge resultaten worden bekomen in beide modellen. Wel dient er vermeld te worden dat het 2D model een grotere elektronen (en dus ook ionen) dichtheid berekent aan de uiteinden van de elektrodes, hetgeen het 1D model niet kan voorspellen. Dit heeft zijn invloed op de verschillende deeltjes fluxen (elektronen, ionen en radicalen) naar beide elektrodes toe. Een verschil in deeltjesflux in het midden en het uiteinde van de elektroden geeft een verschil in groeisnelheid, en zal dus leiden tot een niet-uniforme afgezette laag, hetgeen uiteraard niet wenselijk is. Een volgende stap in het ontwikkelingsproces van het 2D plasma model zal de inbreng zijn van de invloed van gas stromingen (convectie) doorheen de reactor. Dit valt echter buiten het werk van dit doctoraatsonderzoek.

Een alternatieve methode om diamantachtige lagen af te zetten bestaat erin acetyleen (C_2H_2) te gebruiken als precursor gas (in plaats van methaan gas). Uit het ontworpen plasma model blijkt dat de chemie van een acetyleen plasma compleet verschilt van deze in een methaan plasma. Vooreerst zijn de deeltjes die voorkomen in een acetyleen plasma verschillend van diegene in een methaan plasma. Daarenboven verschilt ook de radicaalchemie vrijwel compleet. Een belangrijk proces in een acetyleen plasma zijn de radicaal reacties met het C_2H radicaal, met vorming van de deeltjes C_4H_2 , C_6H_2 en C_8H_2 (aanwezig in het plasma in grote dichtheid (orde $10^{19} - 10^{20} \text{ m}^{-3}$)). Verder zijn ook de radicalen H , C_2H_3 , C_4H_3 en CH_2 aanwezig in het plasma met dichtheden in de orde van de $10^{15} - 10^{17} \text{ m}^{-3}$. De belangrijkste ionen zijn C_4H_2^+ en C_2H_2^+ (orde 10^{14} m^{-3}). De validatie van de bekomen gegevens (berekende deeltjes dichtheden) verliep hier moeilijker, daar er slechts weinig experimentele gegevens omtrent een acetyleen plasma beschikbaar zijn. Daar de plasma chemie danig verschilt tussen een methaan en een acetyleen plasma, zullen ook de deeltjes fluxen

naar de elektroden anders zijn. Met andere woorden: het groeiproces zal op een andere manier gebeuren. Er werd reeds een zeer eenvoudig groeimodel in het vloeistofmodel ingebouwd: een gedetailleerde studie van het groeiproces was echter niet het doel van dit onderzoek. Binnen onze onderzoeksgroep wordt hieraan momenteel wel gewerkt, met behulp van een “Molecular Dynamics” model.

Vervolgens is de invloed nagegaan van onzuiverheden (lucht, bestaande uit zuurstof en stikstof) aanwezig in een silaan/helium plasma, gebruikt voor het aanmaken van zonnecellen. Hiervoor dienden een hele reeks van nieuwe deeltjes en reacties in het plasma model te worden ingebracht. Stikstof (N_2) heeft vrijwel geen of nauwelijks invloed heeft op de plasma chemie (is weinig betrokken in chemische reacties), terwijl zuurstof (O_2) reageert in een hele reeks van reacties, die leiden tot nieuwe deeltjes die zuurstof bevatten. Ook is er reeds een eenvoudige schatting gemaakt van het zuurstofgehalte in de afgezette laag bij verschillende toevoer debieten van lucht in het plasma.

De studie eindigt met een vergelijking tussen de resultaten bekomen uit het vloeistofmodel, met enerzijds de elektron reactie snelheidscoëfficiënten berekend uit het Boltzmann model en anderzijds uit een Monte Carlo model. Hieruit blijkt dat voor een zeer lage druk (0.14 Torr) het Monte Carlo model betere resultaten geeft, terwijl bij een hogere druk (0.5 Torr), de resultaten berekend met een Monte Carlo en een Boltzmann model vrijwel aan elkaar gelijk zijn.

Summary

In recent years, the industrial use of amorphous carbon and silicon layers has shown a significant expansion. Amorphous carbon layers, also called diamond-like carbon (dlc) layers, are commonly applied as protective layers on a variety of substrates, whereas amorphous silicon layers are widely used in the microelectronics industry, and in the production of solar cells. Normally, plasma-assisted chemical vapour deposition (PACVD) is the method of choice to coat substrates with these kinds of thin amorphous layers. For that purpose, a plasma is generated between two electrodes (parallel plates), in which a large number of reactive species is created (radicals, ions and electrons from the gas molecules). Some of these reactive species (radicals and ions) will stick to the substrate and hence contribute to the growth of the layer. For the production of amorphous carbon layers, methane (CH_4) or acetylene (C_2H_2) is normally taken as input gas, while for the production of amorphous thin silicon layers, silane (SiH_4) is typically used as precursor gas.

The plasma situated between the two electrodes, is actually created when one of the electrodes is powered, i.e. connected with a radio frequent power supply, while the other is grounded. In this way, an oscillating electric field is generated between the two electrodes, which will provide the electrons with energy, leading to a large number of different electron-neutral reactions. In the reactions, a variety of plasma species is created (electrons, ions, radicals and neutrals): the sum of the negative species is nearly equal to that of the positive species densities in the plasma. Plasmas used for deposition purposes have an electron density is in the order of 10^{15} m^{-3} (pressure region: 10 - 100 Pa, rf frequency: 13.56 MHz, power region: 0 –100 W).

The reactions occurring in a plasma can be divided in two large categories. A first group are the electron-neutral reactions, yielding excited, radical or ionic species. The second group concerns the ion-neutral and neutral-neutral (or radical) reactions: the radicals produced in the electron-neutral reactions react further, and create in this way new species. Note that the second group of reactions is only present in a plasma, when a *molecular* precursor gas is used.

Numerical modelling is an interesting tool to obtain a better understanding of the plasmas used for deposition (and other) purposes. The plasma, and the reactions in the

plasma, are described by a number of mathematical equations. First, such a numerical model needs to be developed, but then it should be validated: the results obtained with the model (e.g. calculated species densities and other quantities) should be compared with experimental data. Afterwards, the validated model can be used to perform a variety of simulations, in order to look under which conditions the best plasma conditions are obtained. An important parameter is here the uniformity of the plasma: a uniform plasma will give more uniform deposited layers.

In this work, plasma models are described for methane, acetylene and silane plasmas. In a first approximation, a one-dimensional fluid model was used, already available by Goedheer and co-workers. In this model, the plasma species are described between the two electrodes with balance equations (one for every species), considering the movement of the species by diffusion (concentration gradient) and migration (potential gradient or electric field). This electric field is calculated in the model by means of the Poisson equation. Finally, a number of boundary conditions have to be specified (e.g., voltage applied at the powered electrode). When more detailed information is necessary, e.g. the plasma species distributions as a function of radial distance, a two-dimensional fluid model is required (with a cylindrical reactor symmetry). In this way, information of the plasma species is obtained as a function of distance between the electrodes (as in the one-dimensional model) and as a function of the radial distance. Generally speaking, the 2D fluid model is an extension of the 1D model in space.

For the fluid modelling of plasmas, some other input data are necessary. For the electron-neutral reactions, it is important to know the reaction rate coefficients, as a function of average electron energy. These data are generated from a simplified Boltzmann model, using the cross sections of the different electron reactions considered. Further, the description of the radical chemistry requires the knowledge of the reaction rate coefficients of the different reactions.

We modelled methane plasmas first with a 1D fluid model. A methane model was developed considering 20 species (electrons, ions, radicals and neutrals), and a large number of electron and radical reactions to describe the plasma chemistry (in an accurate way). Afterwards, the methane model was applied in a number of

simulations at different plasma conditions (pressure, gas flow, power). The results of these simulations (calculated species densities) were then compared with experimental data to validate the methane model. From the model, it follows that the densities of the plasma species H_2 , C_2H_6 , C_2H_2 and C_2H_4 are present in the discharge at high densities (order of 10^{20} m^{-3}) together with the precursor gas CH_4 . The radicals CH_3 , C_2H_5 and H are present in the discharge at somewhat lower densities (order of 10^{17} - 10^{18} m^{-3}), while the densities of the ions are in the order of 10^{14} m^{-3} . Note that the sum of the positive ion densities equals the sum of the negative species densities (electrons and negative ions). Finally, also some information is obtained on the different species fluxes towards the electrodes.

In a further stage, the methane model (species & reactions) is used in the development of a 2D fluid model of methane plasmas. In this way, information is also obtained of the plasma species, as a function of radial distance. It follows that the results obtained with the 2D fluid model are in good agreement with these obtained from the 1D model. However, the 2D fluid model calculates a higher electron density at the end of the electrodes (a result which can not be obtained with the 1D fluid model), leading to different other species fluxes in the middle and at the outer end of both electrodes. This difference as a function of radial position will affect the uniformity of the deposited layer. Finally, it is worth mentioning that a next step in the development of the 2D fluid model will be the incorporation of gas flow, in order to model larger plasma reactors in an adequate way. However, this study is beyond the scope of the Ph. D. work.

An alternative way to deposit dlc layers is by means of acetylene (C_2H_2) as precursor gas, instead of methane gas. From the developed acetylene plasma model, it follows that the plasma chemistry in an acetylene plasma is completely different from a methane plasma: different plasma species are created in the acetylene plasma, leading to other radical reactions. An important process in an acetylene plasma, is the production of the species C_4H_2 , C_6H_2 and C_8H_2 , present in the discharge at high densities (order $10^{19} - 10^{20} \text{ m}^{-3}$). Further the radicals H , C_2H_3 , C_4H_3 and C_2H are also present in the discharge at densities in the order of $10^{15} - 10^{17} \text{ m}^{-3}$. The most important ions are found to be C_4H_2^+ and C_2H_2^+ (order 10^{14} m^{-3}). The validation of the acetylene model was somewhat more difficult (compared to the methane model), due to the lack

of experimental data. A different chemistry in acetylene and methane plasmas will also lead to other species fluxes, and hence also to other growth processes. However, a detailed discussion of the growth of the layer is beyond the scope of this work, but is at the moment investigated in our group by means of Molecular Dynamics calculations.

In a further stage, the influence of small amounts of air in a silane/helium plasma reactor is modelled, used for the production of solar cells. For this, a large number of oxygen and nitrogen containing species had to be considered in the model. It is found that, while nitrogen does not affect drastically the plasma chemistry, oxygen is very reactive and creates a large number of oxygen containing species. Also a rough estimation is made of the amount of oxygen incorporated in the deposited layer.

Finally, a comparison is made between the results obtained from the fluid model, using the reaction rate coefficients obtained from the Boltzmann model, and a Monte Carlo model. We found that at relatively low pressures (0.14 Torr), the Monte Carlo model describes the electrons in a more accurate way, while at higher pressures (0.5 Torr), the results obtained with a Boltzmann model are in satisfactory agreement with the results of the Monte Carlo model.

Published articles

1. D. Herrebout, A. Bogaerts, M. Yan, R. Gijbels, W. Goedheer, E. Dekempeneer, One-dimensional fluid model for an rf methane plasma of interest in deposition of diamond-like carbon layers, *Journal of Applied Physics*, **90**, 570 (2001)
2. D. Herrebout, A. Bogaerts, M. Yan, R. Gijbels, W. Goedheer, A. Vanhulsel, Modelling of a capacitively coupled radio-frequency methane plasma: comparison between a one-dimensional and a two-dimensional fluid model, *Journal of Applied Physics*, **92**, 2290 (2002)
3. V. Ivanov, O. Proshina, T. Rhakimova, A. Rhakimov, D. Herrebout, A. Bogaerts, Comparison of a one-dimensional particle-in-cell – Monte Carlo model and a fluid model for a methane/hydrogen capacitively coupled radio frequency discharge, *Journal of Applied Physics*, **91**, 6296 (2002)
4. K. De Bleecker, D. Herrebout, A. Bogaerts, R. Gijbels, P. Descamps, One-dimensional modeling of a capacitively coupled rf plasma in silane/helium including small concentrations of O₂ and N₂, *Journal of Physics D*, accepted, to be published (2003)
5. D. Herrebout, A. Bogaerts, R. Gijbels, W. Goedheer, A. Vanhulsel, A one-dimensional fluid model for an acetylene rf discharge: a study of the plasma chemistry, Special issue on the modeling of collisional or Near-Collisionless Low Temperature Plasmas, accepted, to be published (2003)

Contribution to International Congresses

XVth Europhysics Conference on Atomic and Molecular Physics of Ionized Gases, 26 – 30 August 2000, Miskolc (Hungary). Poster: one-dimensional fluid model for a capacitively coupled rf plasma in methane.